



UNIL | Université de Lausanne

Unicentre

CH-1015 Lausanne

<http://serval.unil.ch>

Year : 2017

WNThigh colon cancer stem cells drive résistance to standard anti-angiogenic therapies

Cisarovsky Christophe

Cisarovsky Christophe, 2017, WNThigh colon cancer stem cells drive résistance to standard anti-angiogenic therapies

Originally published at : Thesis, University of Lausanne

Posted at the University of Lausanne Open Archive <http://serval.unil.ch>

Document URN : urn:nbn:ch:serval-BIB_E367D5D12DF32

Droits d'auteur

L'Université de Lausanne attire expressément l'attention des utilisateurs sur le fait que tous les documents publiés dans l'Archive SERVAL sont protégés par le droit d'auteur, conformément à la loi fédérale sur le droit d'auteur et les droits voisins (LDA). A ce titre, il est indispensable d'obtenir le consentement préalable de l'auteur et/ou de l'éditeur avant toute utilisation d'une oeuvre ou d'une partie d'une oeuvre ne relevant pas d'une utilisation à des fins personnelles au sens de la LDA (art. 19, al. 1 lettre a). A défaut, tout contrevenant s'expose aux sanctions prévues par cette loi. Nous déclinons toute responsabilité en la matière.

Copyright

The University of Lausanne expressly draws the attention of users to the fact that all documents published in the SERVAL Archive are protected by copyright in accordance with federal law on copyright and similar rights (LDA). Accordingly it is indispensable to obtain prior consent from the author and/or publisher before any use of a work or part of a work for purposes other than personal use within the meaning of LDA (art. 19, para. 1 letter a). Failure to do so will expose offenders to the sanctions laid down by this law. We accept no liability in this respect.



UNIL | Université de Lausanne

Faculté de biologie
et de médecine

Département d'Oncologie Fondamentale

**WNT^{high} colon cancer stem cells drive resistance to standard
anti-angiogenic therapies**

Thèse de doctorat

MD-PhD

Présentée à la

Faculté de Biologie et de Médecine
de l'Université de Lausanne

par

Christophe CISAROVSKY

Médecine diplômé de la Confédération Helvétique

Jury

Prof. Ivan STAMENKOVIC, président et répondant MD-PhD

Prof. Tatiana PETROVA, directrice de thèse

Prof. Monika HEGI, expert

Prof. Curzio RUEGG, expert

Lausanne 2017

Table of Contents

List of Figures.....	4
List of Tables.....	4
List of Hyperlinks	5
Acknowledgement	7
Summary.....	9
Résumé.....	10
Acronyms and Abbreviations.....	11
A. Introduction.....	14
A.1. A dedication to Cancer.....	14
A.2. Cancer Epidemic.....	15
A.3. Colorectal cancer.....	16
A.3.1 Normal intestine.....	16
A.3.2 Epidemiology.....	18
A.3.3 Molecular mechanisms and subtypes.....	20
A.3.4 Cancer stem cells and the tumor microenvironment.....	25
A.3.5. CRC prevention, treatment strategies and targeted therapies	28
A.4. Blood vessel development	31
A.4.1 Introduction.....	31
A.4.2 Vasculogenesis.....	32
A.4.3. Angiogenesis	33
A.4.4. Matrix Metalloproteases.....	35
A.4.5. VEGF signaling.....	36
A.4.6 Arterio-venous differentiation.....	37
A.4.7. Vascular maturation	38
A.4.8. Angiopoietins	39
A.4.9. Hypoxia	40
A.4.10. Apelin	41
A.4.11. Semaphorins	42
A.4.12. Pathological angiogenesis	42
A.5. Tumor Angiogenesis.....	43
A.5.1 Introduction.....	43
A.5.2. VEGF-VEGFR system in tumors.....	44
A.5.2. Myeloid cells in tumor angiogenesis.....	44
A.5.3. Cancer-associated fibroblasts.....	46
A.6. Anti-Angiogenic therapies	47
A.6.1. Classes of anti-angiogenic agents and treatment response.....	47
A.6.2. Vascular normalization hypothesis.	49
A.6.3. Intrinsic and acquired resistance.....	50
B. RESULTS.....	53
B.1. The mouse small intestinal vasculature comprises phenotypically and physiologically distinct crypt- and villus-associated blood vessels	53
B.2. Crypt-associated blood vessels remain resistant to anti-Vegf treatment in <i>Apc</i> deleted precancerous lesions	56
B.3. Blood vessels in advanced models of Wnt^{high} intestinal tumors are intrinsically Vegf-independent	59
B.4. Wnt^{high} cancer stem cells remain unaffected by anti-angiogenic therapy	62

B.5. Decreased VEGF signaling in human WNT ^{hi} colon cancer	64
B.6. Co-culture of AKP organoids and endothelial cells shows anti-angiogenic effect and non-responsiveness to VEGF treatment <i>in vitro</i>	67
B.7. Cancer stem cell- and endothelial cell- derived Sema3f and Apelin reduce vessel outgrowth and induce anti-angiogenic resistance.....	69
3. Discussion.....	72
D. Materials & Methods	82
D.1. Cell lines and culture conditions	82
D.2. Intestinal organoid culture.....	82
D.3. Human fibroblast isolation and purification.....	83
D.4. Vectors and Infection.....	83
D.5. 3D angiogenic assay in a microfluidic device	84
D.6. Animals and tumor xenografts	85
D.7. Mouse tissue and tumor xenografts collection, staining procedures and image acquisition	87
D.8. Human tissue collection, staining procedures and image acquisition.....	89
D.9. Blood endothelial and intestinal epithelial cells isolation.....	91
D.10. RNA isolation and RT-qPCR	91
D.11. Primer design.....	92
D.12. Quantifications.....	92
D.13. Statistical analyses.....	93
D.14. Study approval	93
D.15. Human tumors approval.....	94
E. Bibliography	100

List of Figures

Figure 1: Histology of the small intestine and cell types ⁶	17
Figure 2: Mismatch repair (MMR) machinery ³⁴	22
Figure 3: Classical adenoma to carcinoma sequence with APC mutation in crypt stem cells ⁶²	25
Figure 4: Treatment strategies in metastatic colorectal cancer ³⁶	31
Figure 5: Embryologic development and maturation of the blood and lymphatic vascular network ⁸⁹	33
Figure 6: Signaling pathways in tip and stalk cells ⁹¹	34
Figure 7: VEGFR2 structure and receptor signaling complexes ¹⁰⁵	37
Figure 8: Myeloid cell regulation of tumor angiogenesis ¹⁴⁵	46
Figure 9: Tumor vascular normalization in response to anti-angiogenic treatment ¹⁶⁷ ...	50
Figure 10: Summary of intrinsic and acquired resistance mechanism after anti-VEGF therapies ¹⁷⁸	52

List of Tables

Table 1: Clinico-pathological patient characteristics (part 1)	95
Table 2: Clinico-pathological patient characteristics (part 2)	96
Table 3: Detailed human tumor characteristics	97
Table 4: List of primers	98
Table 5: List of primary antibodies	99

List of Hyperlinks

1. http://www.who.int/healthinfo/global_burden_disease/projections/en/
2. http://globocan.iarc.fr/Pages/fact_sheets_cancer.aspx
3. <http://publications.iarc.fr/Non-Series-Publications/World-Cancer-Reports/World-Cancer-Report-2014>
4. <https://www.bfs.admin.ch/bfs/en/home/statistics/national-economy.html>
5. <https://globocan.iarc.fr>
6. <https://www.bfs.admin.ch/bfsstatic/dam/assets/350146/master>
7. <https://www.bfs.admin.ch/bfs/fr/home/statistiques/sante/etat-sante/maladies/cancer/specifiques.html>
8. <https://www.fda.gov/downloads/NewsEvents/Newsroom/UCM280546.pdf>
9. <https://pga.mgh.harvard.edu/primerbank/>
10. <https://blast.ncbi.nlm.nih.gov/Blast.cgi>

*To my Mother, who dedicated her life on the education of my brother
and myself. May she be proud of us.*

...

*To my Father, who ironically enough was born with the Zodiac sign of
Cancer, yet beat the disease not only once, but twice. A true example for
the expression: "what doesn't kill you makes you stronger". He probably
guided me towards the field of medical Oncology.*

...

*To my Grandmother who continuously supported me towards my studies
and decisions in life.*

...

I Love you

"There is no point of living, if you can't feel alive."

Elektra King, James Bond 007: The World is not enough

Acknowledgement

I would like to take to opportunity to thank my thesis supervisor, Prof. Tatiana Petrova. Despite the difficulties I experienced during my PhD travel, she kept patience and understanding towards me, which was very helpful to keep me motivated. Her door was always open.

I also would like to thank my direct supervisor, Dr. Jeremiah Bernier-Latmani, a talented scientist that started the project and went through with me during these three and a half years. He helped me for experiment planification, technical skills and data analysis. He also performed the initial intestinal blood endothelial cells isolation by FACS and acquired a substantial proportion of results that builds our upcoming publication.

All human samples analyses were realized thanks to a collaboration with Prof. Christine Sempoux from the Institute of Pathology in CHUV. A special message to her as we struggled finding an opportunity to add human significance in our project and thus some clinical validation.

I further wanted to thank my former Master's direct supervisor, Dr. Simone Ragusa, a dedicated post-doc in our lab who helped me handling the cell culture, especially for organoid culture. He is responsible for the AKP stem cell isolation and the AKP organoid tumor xenografts treated with IgG or DC101.

Of course a big thank you to all members of Tatiana's lab for their help and support when I needed it, to Janine Horlbeck and Jean-Christophe Stehle from the mouse pathology facility, as well as everybody in the Ludwig Institute or the EPFL who took part in this project.

I don't think I would have had the courage to keep going on my MD-PhD without the constant support of my family, my girlfriend and my dear good friends and future colleagues. I deeply express them all my gratitude and wish them in return health, success and happiness.

Finally, I would like to thank the University of Lausanne for allowing me the MD-PhD Kummer's Grant and the Alfred and Anneliese Sutter-Stöttner Foundation that helped me financially for the end of my MD-PhD.

Summary

Although chemotherapy combined with the anti-angiogenic, VEGF-blocking antibody bevacizumab is a first-line treatment for metastatic colorectal cancer (CRC) it provides only a modest survival benefit. In this work, we examined potential mechanisms driving bevacizumab resistance in tumors with high levels of Wnt signaling (Wnt^{hi}), which make up 37% of CRC cases. We showed that both normal and transformed intestinal stem cells are localized in normoxic zones surrounded by a stable vasculature, while more differentiated intestinal cells are hypoxic and associated with actively sprouting and angiogenic blood vessels. Furthermore, while anti-Vegf treatment efficiently prunes such sprouting blood vessels in Wnt^{hi} tumors, stem cell-associated vessels are highly resistant to Vegf deprivation. Analysis of tumors from colon cancer patients confirmed that vessels in WNT^{hi} tumors were anti-correlated with active VEGF-signaling. Finally, assessment of transcriptomes from endothelial cell sorted after epithelial activation of Wnt signaling demonstrated increased expression of *Sema3F* and *Apelin*. Overexpression of either gene in MC38 cancer cells, normally highly sensitive to Vegfa blockade, switched tumor sensitivity towards resistance. Our work suggests that CRC stem cells actively remodel blood vessels and identifies one of the mechanisms for intrinsic or acquired resistance to anti-VEGF therapies in CRC. Additional studies would enable the development of novel treatments and potential diagnostic tools. Indeed, high WNT activity might represent a negative predictive marker of bevacizumab response.

Résumé

Dans 20% des cas de cancer colorectaux (CCR), des métastases sont déjà présentes et justifient un traitement par bevacizumab, un anticorps bloquant le VEGF-A. Ce médicament n'augmente cependant que modestement la survie globale des patients. Nous avons investigué les mécanismes potentiels de résistance au bevacizumab dans des modèles de CCR où la voie de signalisation Wnt est fortement activée (Wnt^{hi}) et qui représente 37% des cas. Nous avons observé que les cellules souches intestinales ou cancéreuses sont associées à une vascularisation peu dense et un environnement normoxique. Par contre, les cellules intestinales ou cancéreuses bien différenciées sont hypoxiques et proches de vaisseaux en constant remaniement et fortement angiogéniques. Après traitement par anti-Vegf, la présence de cellules souches rendait les vaisseaux sanguins résistants, annulant ainsi l'effet global sur la croissance tumorale. Ces résultats ont été confirmés dans des échantillons de patients. L'analyse transcriptomique de cellules endothéliales isolées après l'activation épithéliale de la voie Wnt dans l'intestin a démontré que l'expression de *Sema3F* et *Apelin* étaient fortement augmentées. La surexpression de *Sema3F* et *Apelin* dans des tumeurs MC38 préalablement sensibles aux anti-Vegf a induit un mécanisme de résistance au traitement. Ce travail suggère donc que les cellules souches cancéreuses dans le CCR régulent activement le développement des vaisseaux sanguins et représentent un des mécanismes de résistance aux thérapies anti-angiogéniques. Il propose d'utiliser la signature WNT comme biomarqueur prédictif pour ce type de traitement.

Acronyms and Abbreviations

AKP : Apc Kras and p53

Ang1/2 : Angipoinetin 1 and 2

APC: adenomatous polyposis colitis

BEC : blood endothelial cell

BMI1 : B-lymphoma MO-MLV insertion region 1 homolog

BRAF : rapidly accelerated fibrosarcoma homolog B proto-oncogene

CC : colon cancer

CD31: cluster of differentiation 31

CD44: cluster of differentiation 44

CIMP: CpG island methylator phenotype

CIN : chromosomal instability

CMS: consensus molecular subtypes

CRC : colorectal cancer

CSC : cancer stem cell

CSF-1 : colony-stimulating factor 1

G-CSF : granulocyte colony-stimulating factor

DLL4 : Delta-like ligand 4

EC : endothelial cell

ECM : extracellular matrix

EGF(R) : epidermal growth factor (receptor)

FACS : Fluorescent-activated cell sorting

FOXO1: forkhead box 1

HER2 : Human epidermal growth factor receptor 2

ISC : intestinal stem cell

KRAS: Kirsten-rat sarcoma oncogen

LGR5: leucine-rich repeat-containing G-protein coupled receptor 5

MCR : mutation cluster region

MET or c-MET : mesenchymal epithelial transition receptor tyrosine kinase (also known as hepatocyte growth factor receptor, HGFR)

MIN : microsatellite instability

MLH1/6 : MutL Homolog 1/6

MMP : matrix metalloprotease

MMR: mismatch repair machinery

MSH2 : MutS protein Homolog 1

MSI/MSS : microsatellite instability/stability

NG-2 : Neural/Glial antigen-2

NRAS : neuroblastoma RAS viral oncogene homolog

NRP1/2 : Neuropilin-1/2

NSG: Nod scid gamma

OS : overall survival

PFS : progression-free survival

PIK3CA: Phosphatidylinositol-4,5-Bisphosphate 3-Kinase Catalytic Subunit Alpha

PMS2 : postmeiotic segregation increased *S. cerevisiae* 2

POLE /POLD1: polymerase E or D1

PROX1: prospero homeobox gene 1

PTEN: phosphatase and tensin homolog

RTK : receptor tyrosine kinase

SEMA3F : Class 3 Semaphorin member F

SMAD4 : SMAD family member 4

TCF/LEF : T-cell factor/lymphoid enhancer binding factor

TCGA: the cancer genome atlas

TGFBRII: transforming growth factor beta receptor II

TNM: tumor node metastasis

TP53: tumor protein p53

VEGF(R): vascular endothelial growth factor (receptor)

GR-1 : granzyme-1

BV8 : prokineticin 2

A. Introduction

A.1. A dedication to Cancer

The paradoxical interest I have discovered years ago and fostered since then for **Cancer** can be illustrated and metaphorized by the 1991 Walt Disney Pictures cartoon film: the Beauty **of** the Beast.

Cancer is, as would Siddhartha Mukherjee call it in his thrilling book *The Emperor of All Maladies*: “the king of terrors” or “the pathology of excess”. He emphasizes a very important fact that “the diagnosis of cancer, but not the disease itself, becomes a death sentence” (Siddhartha Mukherjee, *the Emperor of all Maladies*, a biography of cancer, Thorndike Press 2010).

Cancer is anchored in human history since 1.7 million years¹, if not more. As a genetic disorder, cancer can arise from any type of cells, any type of organs. Likewise, not only would it affect the functions of the system where it takes origin, expand and from where it will propagate, but would eventually influence the patient’s emotions and behaviors. Like Siddhartha Mukherjee implied, the diagnosis of cancer can elicit a profound sensation of depression where patients can get locked. On the other hand, it might trigger a complete life paradigm shift, where patients start to think about the meaning of their disease and actively contribute to the treatment strategy to fight against one of the most feared illness of the 21st century.

This global therapeutic approach towards the patients gave me so much personal interest at first in Cancer. In addition, the accelerated Darwinism occurring in cancer cells that elicit extraordinary mechanisms to escape cell death, immune surveillance and treatment effects demonstrate how such a dreadful disease can bring such medical and scientific interest and motivated me to do an MD-PhD.

A.2. Cancer Epidemic

What we nowadays call “the epidemic of cancer”, started already at the beginning of the 20th century, where cancer-related mortality increased by 29.8% between 1900 and 1916. Soon after, cancer had become the second most common killer in the United States of America (USA), right after cardiovascular diseases. Today, the World Health Organization (WHO) predicts in its report about global mortality causes by 2030 that cancer would keep its second place. However, unlike cardiovascular diseases that would reach a steady state (32% of total deaths), cancer is predicted to rise from 15% to 18% of the world population (8.7mio vs. 12.6mio people will die of cancer in 2015 vs. 2030, respectively). Cancer will cause more deaths than hypertensive and ischemic heart diseases combined (www.who.int¹). According to GLOBOCAN 2012, there were 14.1 million new cancer cases and 32.6 million people living with cancer (within 5 years of diagnosis) in 2012, worldwide, from where 57% (8 million) of new cancer cases, 65% (5.3 million) of the cancer deaths and 48% (15.6 million) of the 5-year prevalent cancer cases occurred in the less developed region (<http://globocan.iarc.fr>²). Globally, the number of cancer patients would grow from 12.7 million in 2008 to 22.2 million in 2030 and cancer rates worldwide are expected to increase by 75% towards 2030. That would mean cancer cases nearly doubling over the course of 22 years, especially in fast developing countries².

Indeed, in lower-to-middle income countries, cancer incidence is exploding. By 2020, 70% of the cancer patients will be in poor countries³, creating gargantuan challenges for health systems, as advances in care allows patients to live longer and with higher quality. Increased survival is a result of better knowledge of the biology and etiology of cancer, allowing the possibilities of personalized medicine. Nonetheless, these medical revolutions come with a price which put the cancer patients, the health-care systems and the society in front of the dilemma: to pay or not to treat⁴. It is indeed known that the economic impact of

cancer is more than significant and is constantly increasing. The total annual economic cost of cancer in 2010 was estimated by the International Agency for Research in Cancer (IARC) to reach US\$ 1.16 trillion (<http://publications.iarc.fr>³) which represents approximately twice the gross domestic product (GDP) of Switzerland in 2016 (www.bfs.admin.ch⁴).

Among the top four most common killing types of cancer, which account for more than half of all cases of the disease and include trachea-bronchus-lung cancers, liver cancer, and stomach cancer, colorectal cancer (CRC) occupies the 4th place². CRC is predicted to cause more deaths than breast cancer, Alzheimer's disease, tuberculosis or asthma in 2030, affecting not less than 1.5% (0.75 mio to 1.1 mio people in 2015 vs. 2030, respectively) of the global population. This makes CRC the 15th cause of all deaths worldwide (www.who.int¹)

A.3. Colorectal cancer

A.3.1 Normal intestine

Cancer is defined by uncontrolled cell proliferation and the ability to invade adjacent tissue and spread to distant organs. Better understanding of the normal tissue homeostasis is essential to unravel pathological processes. I therefore will introduce first intestinal physiology.

The gut is divided into the small intestine and the large intestine, or colon. The small intestine directly follows the stomach and is further subdivided into duodenum, jejunum and ileum. It is composed of billions of crypt/villus units, digests food and absorbs nutrients and water through the intestinal villi. Indeed, specific lymphatic vessels called lacteals protrude inside the small intestinal villus, collect dietary fat in the form of chylomicrons and regulate gut immune responses⁵. On the other side, small intestinal capillaries are highly fenestrated allowing entry of nutrients and water into the blood circulation where they will be transported

to distant organs for further processing and use. The intestinal epithelium is composed of fully differentiated epithelial cells that are located in the villus compartment where they eventually shed into the intestinal lumen. Intestinal stem cells (ISCs) are slowly proliferating cells that reside in the bottom of the crypts, together with Paneth cells, and constantly renew the epithelium by migrating through the crypt-villus axis (Figure 1).

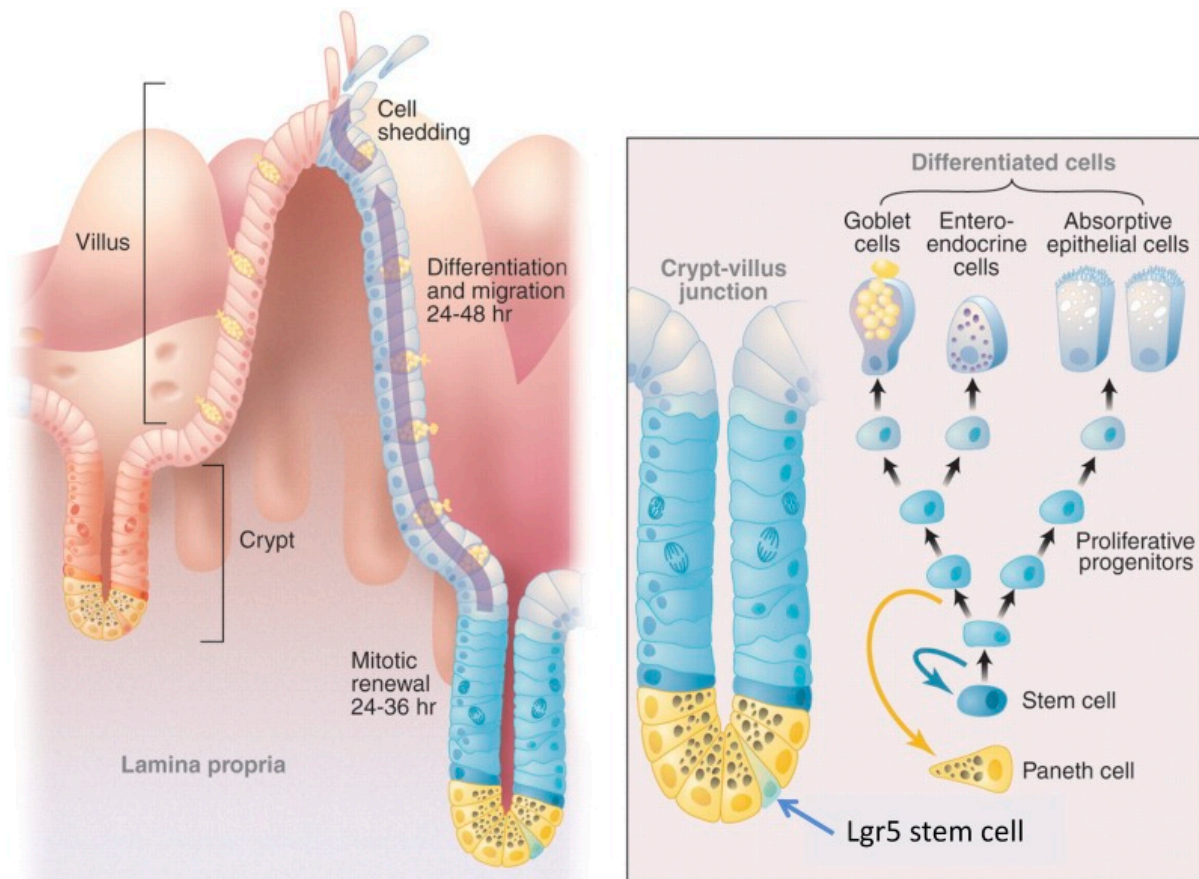


Figure 1: Histology of the small intestine and cell types⁶

ISCs are characterized by strong expression of the Lgr5 G-protein coupled receptor that binds to R-spondin and potentiates Wnt signaling⁶. Quiescent BMI+ cells are positioned just above Lgr5+ stem cells and are able to trans-differentiate into true crypt-bottom ISCs upon physiological conditions or tissue damage^{7,8}. Moreover, Paneth cells, known for their anti-microbial roles, are required for the stem cell niche and provide key factors for their survival,

such as EGF, Wnt3a and Dll4⁹. Thus, the intestinal stem cell niche is tightly regulated and highly plastic, emphasizing its importance for proper tissue homeostasis.

On the contrary, the colon which main functions are to guide feces toward the rectum, eliminate undigested foodstuffs, and absorb residual liquids, neither has villus, nor Paneth cells. Interestingly, it is the main reservoir for billions of commensal bacteria, the gut microbiota, which are essential for tissue homeostasis and short-chain fatty acid synthesis (reviewed in Ref¹⁰). Commensal bacteria can be found in the colon mucus secreted by goblet cells, which protects the intestinal mucosae from external aggressions. Defects in mucus synthesis can lead to mucosal bacteria intravasation, enhancing the risk of developing colitis and colorectal cancer^{11,12}.

A.3.2 Epidemiology

CRC is the third most common cancer in men (incidence in 2012: 746'300, 10.0% of total cancer cases) and the second in women (incidence in 2012: 614'300, 9.2% of total cancer cases) worldwide. It is also the fourth cause of cancer-associated deaths worldwide, albeit it is the second leading cause of cancer death in more developed countries (<https://globocan.iarc.fr>⁶). Indeed, 55% of CRC patients live in Western countries, especially in North America, Europe, Japan and Australia where its incidence peaks up to 44.8 and 32.2 per 100,000 in men and women, respectively. On the contrary, south and central Asia and Africa share the lowest incidences: 4.5 and 3.8 per 100,000 in men and women, respectively. This highlights wide geographical variations in incidence across the world that are commonly attributed to environmental factors such as: 1) physical activity and sedentarity, 2) body mass index (BMI), 3) energy intake, dietary and nutritional practices (especially consumption of fibers, red and processed meat), 4) diabetes, and 5) living in an urban area^{13,14}.

Despite a continuously decreasing age-specific relative risk of getting diagnosed with CRC in people born during the first half of the 20th century, it continuously increased for people born from 1990 until today. Consequently, adults born in the 1990s have a 2-4-fold increase risk of being diagnosed with colorectal cancer and eventually die from it, compared with adults born in the 1940s¹⁵. Although modest, this trend was also observed in Switzerland, with a higher incidence in people with 20-49 years of age, in comparison to a decreased incidence in other age classes in 2015 (www.bfs.admin.ch⁷). In addition, colorectal cancer has dreadfully increased over the past twenty years in some rapidly developing and expanding Asian countries, which were previously considered to be at low risk. For example, the mortality rates for colorectal cancer in Korea were four times higher in 2011 than those in 1983¹⁶. This colorectal cancer epidemic can be partly explained, as for thyroid¹⁷, breast or prostate cancer^{18,19}, by an increase of access to health care unit and better technology and screening systems to detect early tumors. However, it is also due to an increase exposure to known risk factors highlighted above and to world industrialization, urbanization and pollution²⁰.

The good news is that, on the contrary to increased colorectal cancer incidence worldwide, the 5-year survival has continuously increased in most developed countries. Indeed, in patients who received a diagnosis of CRC during the time period of 2005 –2009, survival reached 60% or more in 22 countries around the world²¹

In Switzerland, the lifelong risk of being diagnosed with colorectal cancer is 6.3% in men and 4.7% in women and the lifelong risk of dying from colorectal cancer is 2.8% in men and 2.1% in women. Around 35'000 people were estimated to live with a diagnosis of colorectal cancer, 4'100 new CRC patients were diagnosed in 2015 and 1'600 patients would have eventually

died of it, making it the second and third cause of cancer in women and men, respectively, and the third cause of cancer-related death in both sex (Federal Office for Statistics: www.bfs.admin.ch^{7,8}). Despite a stable incidence of the disease over the last thirty years (except for younger people), the relative 5-year and 10-year survival rates of CRC in Switzerland were estimated to 65% and 55%, respectively, for both sexes. Switzerland is therefore the second country in Europe with the lowest mortality rates²². Survivors of CRC now represent the third largest group of long-term cancer survivors in Western countries, ~11% of the population²³. Finally, mortality rates, as well as incidence rates increase with age. Hence the median age of CRC diagnosis is 71 and 73 in men and women, respectively (www.bfs.admin.ch⁷).

A.3.3 Molecular mechanisms and subtypes

Since CRC is a disease occurring mostly in advanced aged people, it often develops over a period of more than a decade. Following a succession of genetic mutations within the earliest premalignant lesion: the aberrant crypt foci, the latter further develops into a polyp and finally into cancer²⁴.

CIN vs. MIN: Analysis of benign and highly malignant tumors enabled to identify the sequence of mutations occurring in CRC development. As a result, CRC can be broadly classified into two distinct molecular pathways depending on the original type of genetic instability; 1) the classic sporadic adenoma to carcinoma sequence with high chromosomal instability (CIN) and 2) the sessile serrated pathway with microsatellite instability (MIN). The classic adenoma to carcinoma sequence involves mutations in the WNT pathway and >80% of them are occurring in the mutation cluster region (MCR) of *APC*, leading to a truncated protein²⁵. *APC* mutations are found in the earliest stages of the adenoma–carcinoma sequence and are at least partly responsible for the chromosomal instability²⁶. *APC* deletion

can also occur by loss of heterozygosity (LOH) in chromosomal regions such as 5q, a mechanism by which other tumor-suppressor gene region like *TP53* (17p) or *SMAD4* (18q) can be deleted²⁷. *APC* mutation induces hyperactivation of the WNT signaling through stabilization of β CATENIN that further translocates into the nucleus, engages the TCF/LEF transcription factor complex and activates its downstream target genes, such as MYC and cyclin-D1 or CD44 and LGR5 that are known to be involved in cell-cycle progression and stemness, respectively²⁸. Interestingly, increased WNT signaling is sufficient to generate pre-cancerous lesions called adenomatous polyps, which was illustrated by the work of Moser et al. and their multiple intestinal neoplasia (Min) model where *Apc* is mutated heterozygously in mice (Moser *et al.*, Science 1990). Mice spontaneously developed dozens of adenomatous polyps within the intestine. In humans, familial adenomatous polyposis (FAP) is an autosomal dominant inherited disorder that affects about 1 in 7'000 individuals. It is characterized by early-onset of hundreds to thousands of colorectal adenomas that eventually develop into cancer, as well as extra-colonic manifestations. FAP is caused by germline mutation in *APC*, leading to a non-functional truncated protein²⁵. However, even though patients carrying heterozygous *APC* mutation are at increased risk of cancer, adenomas derived from *APC* mutated stem cell need to acquire subsequent mutations in known oncogenes and tumor-suppressor genes such as *KRAS*, *PTEN*, *PIK3CA*, *TGFBR1*, *SMAD4*, *TP53*²⁹ in order to further evolve in a true cancer with metastatic potential.

On the contrary to CIN pathway, the sessile serrated pathway is initiated by mutations or epigenetic silencing of the mismatch repair machinery (MMR). Most often, the genes affected are MLH1 and MSH2 (which make up 90% of the cases), but also MLH6 or PMS2 (reviewed in Ref³⁰). These genes encode proteins involved in the recognition and repair of DNA mismatch errors (Figure 2). Inherited mutations in one of the MMR genes are the cause of Lynch syndrome, which accounts for 15-25% of families with hereditary non-polyposis colorectal cancer³¹. Recently, the molecular mechanisms of an MMR-derived

early-onset CRC were discovered. Indeed, it was found that the exonuclease activity of the genes *POLE* and *POLD1* (encoding the exonuclease domain of polymerase ϵ and δ , respectively) are impaired by mutations. It is characterized by an inherited predisposition to develop a variable number of colorectal adenocarcinomas. CRC associated with *POLE* mutations were shown to be hypermutable, even more than tumors with mutations in classic MMR genes^{32,33}.

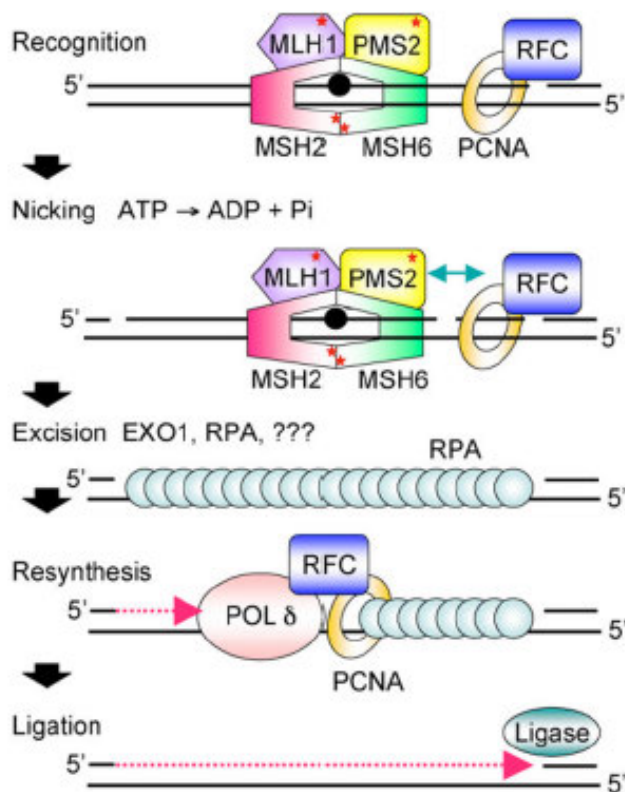


Figure 2: Mismatch repair (MMR) machinery³⁴

Tumors arising from deficient MMR accumulate short tandem DNA repeat sequences of 1-6 base pairs called “microsatellites” and are hence microsatellite unstable (MSI). MSI tumors tend to occur in younger patients, have more frequently poor differentiation (higher grades) and 45% of patients whose tumors had an MSI phenotype had stage IV disease at presentation. *BRAF*^{V600E} mutations were present in 30% of patients with MSI, and vice-versa^{35,36}. Moreover, early-stage MSI tumors have a very good prognosis and may not

progress, while advanced MSI tumors confer an usually unfavorable prognosis³⁷. Some studies also showed differential benefit of 5-FU- or oxaliplatin-based chemotherapies, however these results remain controversial^{38,39}.

It is important to note that within the MSI group, a certain subset of CRC have a high methylation phenotype known as CpG-island methylation phenotype (CIMP). Indeed epigenetic modifications, such as methylation-induced gene silencing, affect gene expression without altering the DNA (reviewed in Ref⁴⁰). CIMP is independently associated with a significantly worse prognosis⁴¹. Proto-oncogene *BRAF* mutations (nearly always V600E) are found between 8%-12% of patients with metastatic CRC (mCRC) included in clinical trials and are almost mutually exclusive to *RAS* mutations⁴². Mutations in *BRAF* are associated with poor prognosis, female gender and proximal tumors. Unfortunately, unlike for melanoma, *BRAF*-targeted therapies such as Vemurafenib are not working in case of *BRAF* mutation, and EGFR inhibitors are inefficient as well⁴³.

Primary tumor location: CRC can originate from three main anatomical part of the colon that are equally represented, depending on the population studied: the ascending colon (~35%), the descending colon (~35%) and the rectum (~30%)⁴⁴. CRC can thus be classified according to the primary tumor localization, creating an anatomical subtype. Proximal or right tumors are located from the caecum until the splenic flexure, whereas distal or left tumors are located from the splenic flexure until the rectosigmoid junction. Finally, rectal tumors arise from the rectosigmoid junction until the anorectal angle. Proximal and distal colon (including rectum) are derived from embryologically distinct origins and differ in many anatomical aspects⁴⁵. Although commonly grouped together as CRC (see A.2.1), primary tumor location has been shown to affect patient prognosis. For example, proximal tumors have been shown to be preferentially hypermutated and carry unfavorable *BRAF* mutation, unlike distal tumors. Moreover, proximal metastatic tumors have a worse prognosis

compared to their distal counterparts⁴⁶. To some extent, they derive from specific molecular pathways and thus respond differentially to standard and targeted chemotherapies^{47,48,49}

CRC molecular subtypes: In order to better understand the molecular mechanisms regulating CRC and to unravel the relationship between the previously discussed subtypes, extensive work over the past five years has been accomplished to discover common molecular signatures among CRC. Since The Cancer Genome Atlas (TCGA), it appeared clear that CRC was not a unique disease but that patients could be clustered according to their gene expression profiles and mutational status. Unbiased classification approaches have been applied to multiple CRC data sets in several studies and indicate the existence of distinct biologically homogenous subgroups. However, differences in the generation of gene-expression profiles and data processing resulted in partial overlap between the studies and the generation of 3-6 CRC subtypes^{33,50-57}. In an effort to unify the classification of CRC, a consortium was created, gene-expression profiles were processed altogether and generated four main consensus molecular subtypes (CMS)⁵⁸. The two main pathways regulating CRC development are represented; CMS1 is hypermutated and display intense immune activation (MSI pathway). On the contrary, CIN-driven CMS2-4 share most of their mutational profiles, with the exception of CMS3. Prevalence of *KRAS* mutation is indeed increased in the latter, which convey a particular enhancement of signaling in metabolic pathways. CMS4 represents a highly aggressive and desmoplastic subtype where the expression of genes involved in the epithelial to mesenchymal transition (EMT), supported by activation of the TGF- β signaling, foster tumor angiogenesis and cancer-associated fibroblasts (CAFs). Patients with CMS4 have the worst prognosis due to non-response to current therapies and tumor aggressiveness. Finally, CMS2, which represents the biggest subtype and 37% of all tumors, is characterized by canonical WNT pathway activation and thus a stem-like phenotype (see A.3.1.).

In summary, colorectal cancer is a highly heterogeneous disease in which several parameters clearly influence tumor behavior, treatment response and thus patient prognosis. Nonetheless, the interaction between those factors remains to be fully investigated. In this project, we focused on WNT-driven CMS2, which represents the majority of all CRCs and for which well-defined animal models are available.

A.3.4 Cancer stem cells and the tumor microenvironment

Physiological tissue homeostasis is maintained by cellular adaptations and by constant repopulation of fully differentiated cells derived from specific stem cells. Stem cells are defined by their self-renewal capacity and the ability to give rise to all differentiated cells of the tissue. In tumors, cancer stem cells (CSCs) have typically a deregulated self-renewal capacity and are known to be responsible for treatment resistance and disease relapse in previously successfully treated tumor⁵⁹. Indeed, cancer stem cells have a low mitotic index compared to their more differentiated counterparts and hence resist to conventional chemotherapies targeting highly proliferative cells. CSCs also actively participate in tumor heterogeneity as they hierarchically organize the tumor bulk and are able to generate a variety of subclones with specific genetic profiles⁶⁰.

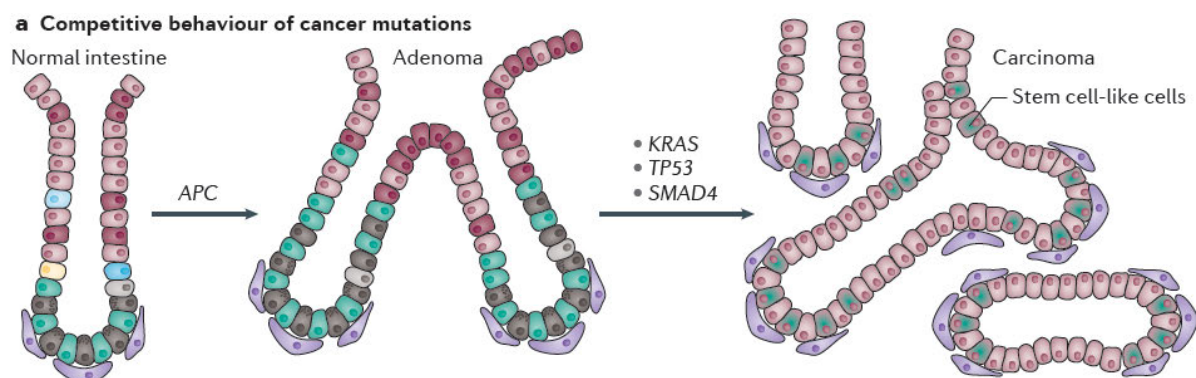


Figure 3: Classical adenoma to carcinoma sequence with APC mutation in crypt stem cells⁶²

(green: intestinal stem cells; brown: Paneth cells; purple: mesenchymal cells; light pink: enterocytes; dark pink: goblet cells; light blue: enteroendocrine cell)

Confirmation of the presence of CSCs were first described in hematopoietic malignancies and transplantation of selected acute myeloid leukemia stem cells was sufficient to generate a tumor in the recipient mouse⁶¹.

In the intestine, Lgr5+ crypt stem cells, or intestinal stem cells (ISCs), maintain high level of Wnt signaling and Wnt hyperactivation upon specific *Apc* deletion in Lgr5+ cells is sufficient to generate intestinal adenomas in mice (Figure 3 and Ref⁶³). Moreover, 5-10% of intestinal adenoma cells highly express the stem cell marker *Lgr5* and sustain tumor growth⁶⁴. CMS2 is therefore derived predominantly of cancer stem or progenitor cells. In human CRC, LGR5+ CSCs have been shown to promote liver metastasis and selective ablation of LGR5+ cells was followed by stem cell repopulation from differentiated KRT20+ cancer cells. Treatment with anti-EGFR antibodies combined with CSCs targeted therapy significantly impaired tumor growth, thus highlighting their roles in CRC development and maintenance^{65,66}

Work by Vermeulen et al. showed that WNT activity in colon cancer cells is at least partly regulated by myofibroblasts-derived hepatocyte growth factor (HGF). Indeed, *in vitro* stimulation of colon cancer stem cells with HGF was able to decrease GSK3 β activity and phosphorylation of Thr41 and Ser45 in β -catenin, hence decreasing its proteasomal degradation. HGF thus enhanced Wnt signaling and reinstalled features of stemness in more differentiated cells⁶⁷. These results highlight the importance of the tumor microenvironment (TME) in the regulation of CSCs and might explain why colorectal tumors harboring activating mutations in the WNT/ β -catenin pathway show variable levels of WNT pathway activation. Indeed only cells with the highest levels of WNT pathway activation actually display nuclear localization of β -catenin and possess stem cell properties⁶⁷. The dynamic plasticity of stem cells has potential clinical relevance and CSCs may acquire new

functional properties under the pressure of microenvironmental signals or as a consequence of genetic mutations responsible for drug resistance⁶⁸. Chemo-radiotherapy, especially alkylating agents, can also generate additional mutations further sustaining tumor growth and acquired resistance to treatment regimens.

Other cell types composing the TME have been shown to regulate CSCs functions in CRC. Endothelial cells promoted the CRC stem cell phenotype through the production of the Notch ligand DLL1 and activation of Notch signaling⁶⁹. Mesenchymal cells, CAFs and CD4 T cells have also been shown to play a role in colorectal CSC self-renewal and invasion^{70,71,72}. Chemotherapy-activated CAFs induced the expression of IL-17A, sustaining CSC self-renewal capacity and tumor growth⁷³. However, mesenchymal cells and CAFs have mostly been studied for their roles in tumor angiogenesis, which will be discussed in more details in A.4.2-3 and A.5.3.

To summarize, CRC is intimately linked with cancer stem cell plasticity and the microenvironment tightly regulates this stem cell niche through secreted factors and specialized stromal cells. Future cancer treatment strategies should therefore target both proliferating cancer cells and cancer stem cells. Moreover, therapies combining the tumor microenvironment and the niche factors could improve the effectiveness of CSC-targeted therapies in metastatic diseases⁷⁴.

In this project, I will focus on the microenvironmental regulation of endothelial cells by intestinal cancer stem cells, with emphasis on the development and maintenance of tumor-associated blood vasculature in CMS2 colorectal cancer and how treatment response might be affected by the presence of CSCs.

A.3.5. CRC prevention, treatment strategies and targeted therapies

Prevention. Colorectal cancer benefits from an efficient large-scale screening program that was shown to decrease global health costs linked to colorectal cancer and to increase early detection and hence patient prognosis^{75,76,77}. In Vaud state (Switzerland), men and women >50-69 years are asked to enter the screening program by consulting their family doctor and performing either a guaiac or immunochemical fecal occult blood test every other 2 years or a flexible sigmoidoscopy by a trained gastroenterologist every ten years^{78,23}.

Localized and locally advanced disease. Current treatment strategies for patients with CRC depends on 1) tumor stage at diagnosis (Tumor Node Metastasis - TNM staging system), 2) patient's age and performance status at diagnosis and 3) the presence of specific gene mutations at diagnosis and during tumor progression. Stages I-II defines early or local tumors and stages III-IV are classified as locally advanced or metastatic tumors, respectively. Early tumors (Stage I-II) are treated with a clear curative intention. Indeed, the goal of colorectal cancer screening is to detect these localized or even pre-cancerous lesions and to remove them endoscopically or surgically. The absence of benefit of adjuvant therapies (5-FU/Leucovorin, oxaliplatin, irinotecan) in stage I-II is well established and decreases the risk of death only by an absolute 3%–5% in stage II with the single-agent 5-FU. On the contrary, the absolute risk of death of patient with stage III CRC decreases by 10%–15% with fluoropyrimidines alone plus a further 4%–5% with oxaliplatin-containing combinations. Therefore, except for some high-risk stage II tumors, adjuvant chemotherapy will be proposed to patients with stage III or IV only. Indeed, the 5-year survival rate with surgery-only treated patients with stage I, stage II and stage III are 85-95%, 60-80% and 30-60%, respectively²³. Particular attention should be paid to MSI subset of stage II patients (10%–15% of the cases) who are at a very low risk of recurrence and in whom the benefits of chemotherapy are very unlikely²³. Clinical trials established that early stage I-II tumors do

not benefit from addition of targeted therapies, such as bevacizumab^{79,80} or cetuximab^{81,82}. Stage III tumors are usually surgically removed with complete lymph node dissection and adjuvant chemotherapy is administered to prevent cancer relapse or prolong the progression-free survival time (PFS) and thus overall survival (OS).

Differences in treatment of colon and rectal cancers. Although The Cancer Genome Atlas has shown some genomic similarities between non-hypermutated colon and rectal cancers, distinct genetic and epigenetic modifications were observed^{33,58}. Moreover, wide anatomical disparities differentiate colon and rectal cancers. Indeed, they don't share the same blood vascular supply and lymphatic drainage and the rectum is located within the pelvis (and not abdomen like the colon) wrapped in a specific fat envelop called the mesorectum. Thus the clinical assessment of rectal cancer is mostly based on rectoscopy, complete colonoscopy, Magnetic Resonance Imaging (MRI) and Endorectal Ultrasonography (ERUS). Therapeutically, rectal cancers are treated according to the circumferential resection margin (CRM) observed by the clinical assessment, as well as the presence of lymph node or distant organ involvement. On the contrary to colon cancer, which metastasizes mostly to the liver, rectal cancers more often metastasize to the lungs. Furthermore, rectal cancer may benefit from neoadjuvant chemotherapy and radiotherapy to increase the likeliness of total mesorectal excision, a strong prognostic factor. However, most metastatic rectal cancer (and primary upper rectal cancer, i.e. >12cm from the anal verge) are handled similarly to metastatic colon cancer (ESMO guidelines⁸³). On the other side, therapeutic strategies for lower rectal cancers are remarkably different.

Metastatic CRC. About 20%–25% of newly diagnosed CRC patients will present a metastatic disease (mCRC), and the same percentage of patients will develop metastases later resulting in a relatively high overall mortality rate of 40%–45%⁸⁴ (Surveillance,

Epidemiology and End results Program; SEER; <https://seer.gov.org>). The basis of mCRC chemotherapeutic treatment is a combination of fluoropyrimidine (5-FU/Leucovorin) with oxaliplatin and/or irinotecan in addition to biological targeted therapies (Figure 4).

Resection of the primary tumor lesion in asymptomatic mCRC is still a subject of debate as studies revealed conflicting results. Interestingly, Peeters et al. showed an increase vascular density in metastatic lesions after primary tumor resection and Ghiringhelli et al. showed benefits of adding bevacizumab in the context of metastatic disease only when primary tumors were resected^{85,86}.

Since 2004, new biological therapies targeting the epidermal growth factor receptor (EGFR, such as cetuximab), small tyrosine kinase inhibitors (TKIs, such as regorafenib) and anti-angiogenic treatment targeting the vascular endothelial growth factor signaling (VEGF, such as bevacizumab) were implemented in patients with metastatic CRC (Figure 4). Advances in the pathogenesis of colorectal cancer showed that tumors with mutations in *KRAS*, *NRAS* and *BRAF*, *MET*, *PIK3CA* and *PTEN* as well as amplification of *HER2* are driving intrinsic resistance to anti-EGFR treatment^{36,87}. These mutations (pan-RAS mutations) are the only predictive biomarkers for treatment response in colorectal cancer. Importantly, a retrospective analysis by Tejpar et al. showed that *KRAS* WT tumors benefit mostly from anti-EGFR therapy when the primary tumor occurred in the distal part of the colon⁴⁸. In addition to the anti-EGFR effect, cetuximab has been shown to induce immunogenic cell death in cancer cells and to elicit potent tumor response⁸⁸. Anti-angiogenic bevacizumab is the second most important targeted therapy in mCRC. In order to better understand how anti-angiogenic therapies are working and what are the basics of their use in oncology, I would like first to introduce the mechanisms regulating the development and maintenance of blood vessels.

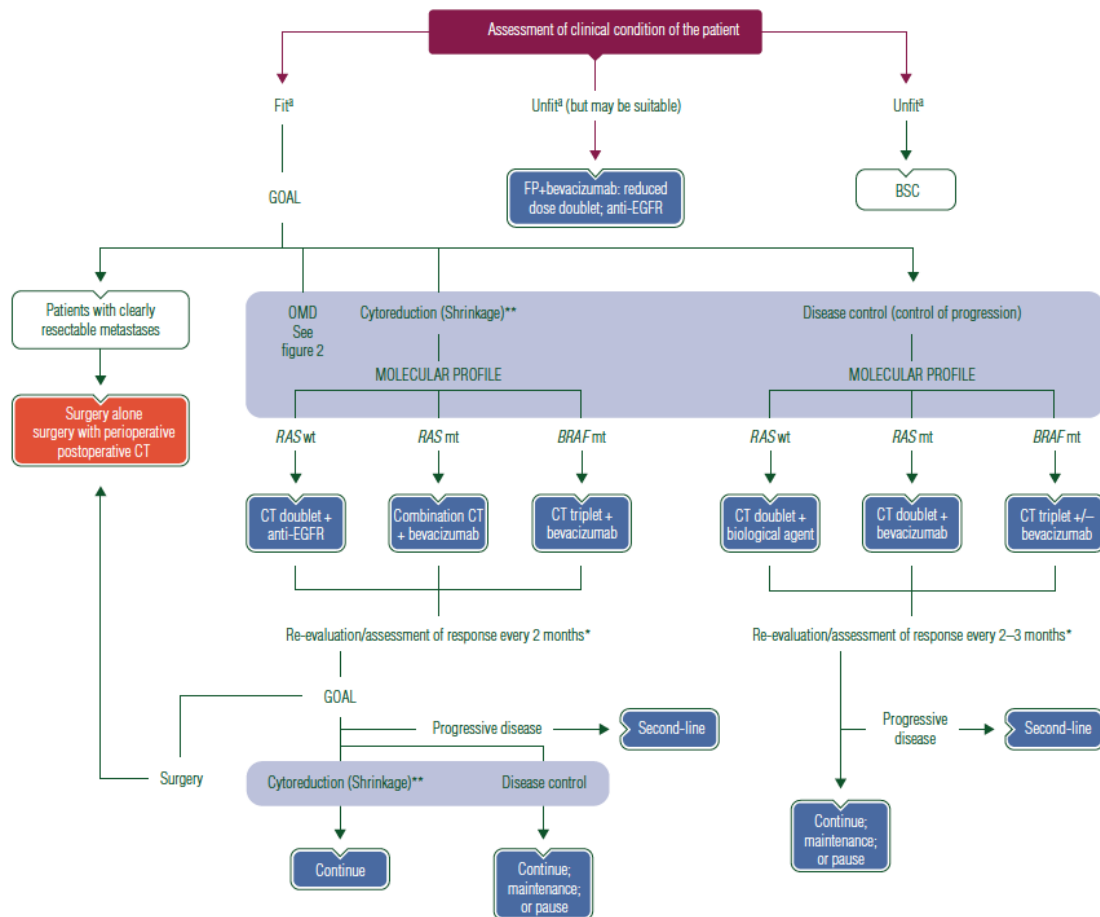


Figure 4: Treatment strategies in metastatic colorectal cancer³⁶

A.4. Blood vessel development

A.4.1 Introduction

As the diffusion distance of molecules is limited (100– 200 μm for O_2), the vasculature in any organ and tissue has to be established early in development. Actually, the cardiovascular system is the first functional organ system that develops in vertebrates, and growth and differentiation of the embryo rapidly depend on its function. The circulatory system is composed of two main networks: the blood and the lymphatic vasculatures. They comprise two interdependent vascular systems in most tissues; however, their organization and function are distinct. Altogether, they act as complementary entities necessary for the transport of gases, such as oxygen and CO_2 , nutrients, hormones and other products to cells of all tissues and organs, as well as the removal of metabolic wastes and circulation of

immune cell. The blood vascular system is divided into a low-pressure pulmonary vasculature responsible for the blood oxygenation and a high-pressure systemic vasculature that delivers oxygen throughout the body. Moreover, the circulatory system, with its lymphatic entity, is needed to uptake interstitial fluid, as well as macromolecules, such as high molecular weight proteins or triglycerides, and to bring them back to the blood circulation. The lymphatic vasculature plays important immune functions that involves immune cell trafficking and antigen presentation within the secondary lymphoid tissues, such as peripheral lymph nodes or in the intestine. The main difference of these two networks lies in the fact that the cardiovascular system forms a continuous loop around which the heart pumps blood, whereas the lymphatic system comprises a one-way, open-ended transit network without a central driving force. The circulatory system is also involved in temperature regulation.

A.4.2 Vasculogenesis

The blood vascular system is composed of blood vessels that are formed by interconnected endothelial cells (ECs) lining the interior of a vessel tube. The earliest sign of ECs and formation is the appearance of mesodermal cell clusters, the so-called haemangioblastic aggregates that are precursors for both endothelial and hematopoietic cells. They subsequently mature into blood islands in the yolk sac, and the external cells, called angioblasts, differentiate from mesodermal progenitors and migrate, acquire arterial or venous fate, and assemble into the first embryonic blood vessels to form the primitive vascular embryonic networks: the dorsal aorta and the cardinal vein. The formation of this network, called vasculogenesis, is under the direction of vascular endothelial growth factor A (VEGF-A), Fibroblast Growth Factor 2 (FGF-2) and Bone Morphogenetic Protein 4 (BMP-4)⁸⁹ (Figure 5).

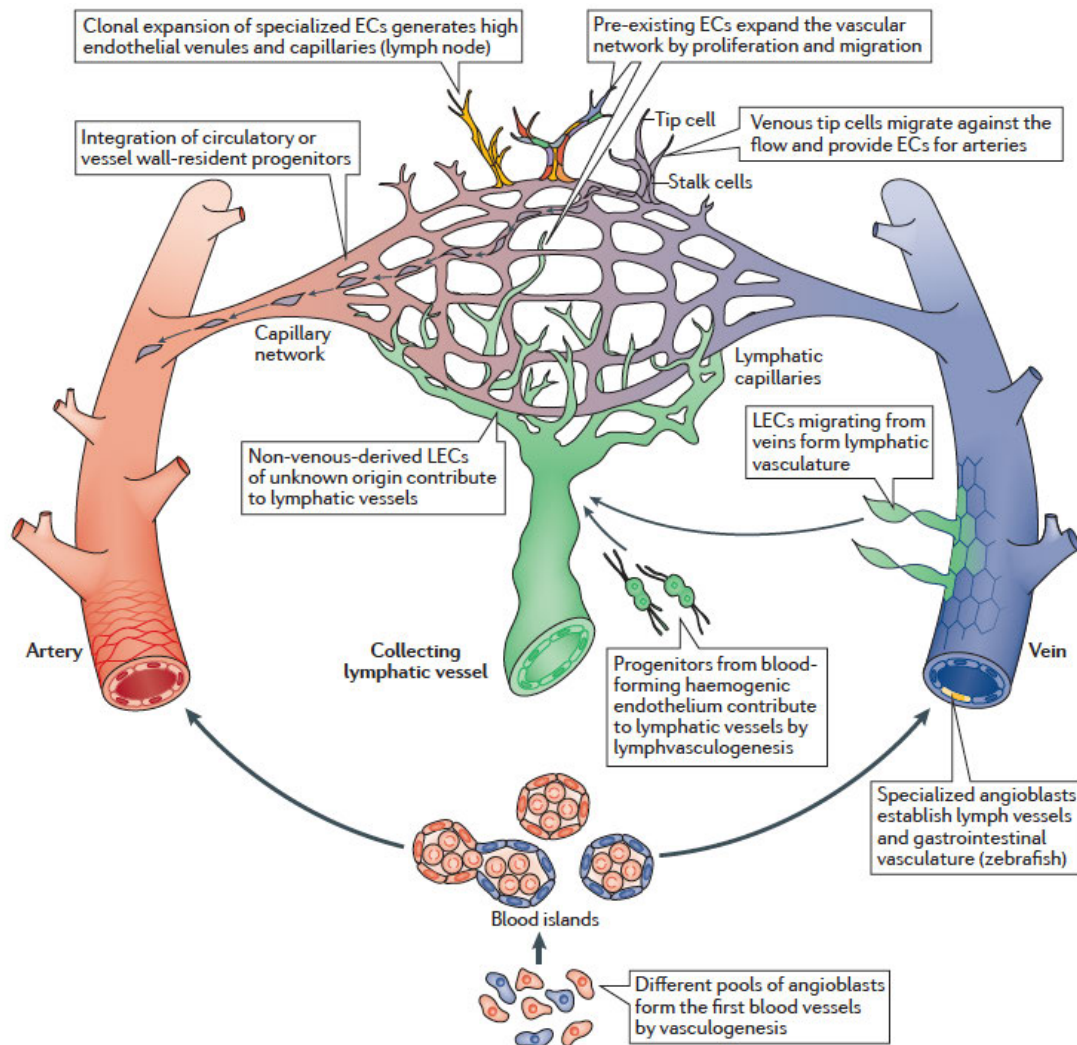


Figure 5: Embryonic development and maturation of the blood and lymphatic vascular network⁸⁹

Of note, highly branched vessels start to appear within the intestinal villi already during embryonic development and further mature after weaning of the mice with intestinal microbe colonization (Bernier-Latmani *et al.*, unpublished and Ref⁹⁰). Interestingly, small intestinal angiogenesis has been linked to the presence of Paneth cells and secretion of anti-microbial peptides⁹⁰.

A.4.3. Angiogenesis

The expansion of the primitive blood vessels is achieved by angiogenesis, the process through which new vessels arise from pre-existing ones and subsequently remodel into

functional vessel circuits. During adulthood, most blood vessels remain quiescent and angiogenesis occurs only in the cycling ovary (menstruations), in the placenta during pregnancy, wound healing and tissue repair. However, it is reactivated during specific pathological conditions, such as cancer (see section A.4.12 and A.5.)

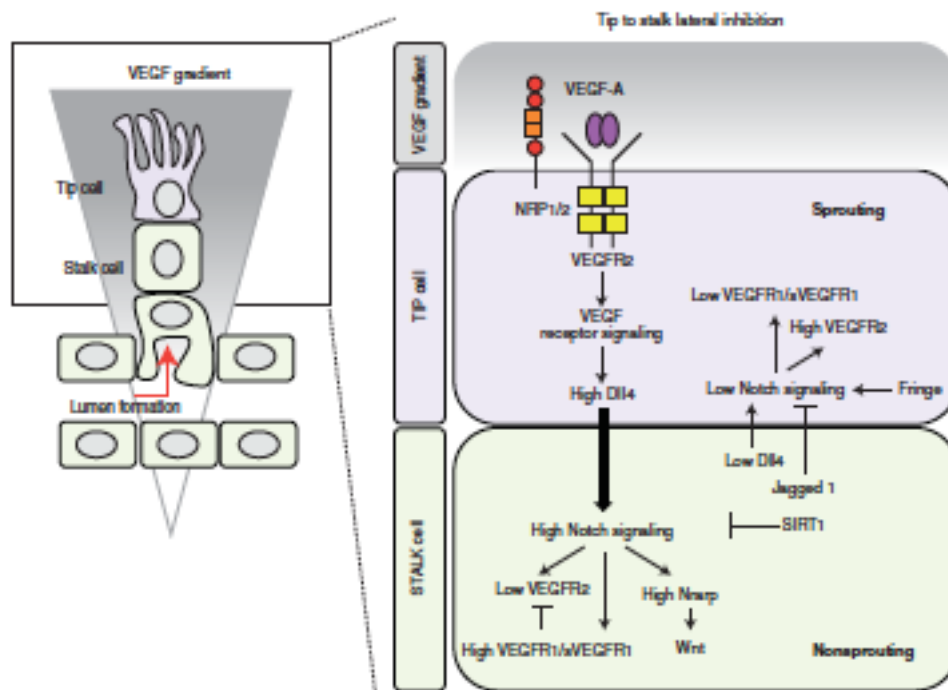


Figure 6: Signaling pathways in tip and stalk cells⁹¹.

Tip cells express high levels of VEGFR-2 and sense microenvironmental VEGF-A gradients. VEGFR-2 signaling induces DLL4 expression in tip cells that binds to its receptor NOTCH2 on the adjacent stalk cell. DLL4/NOTCH1 signaling downregulates VEGFR-2 in stalk cells, preventing tip cell differentiation (negative feedback loop).

Blood vessels arising from angiogenesis need to undergo morphological changes to be fully functional, such as pruning, branching and sprouting. Vascular branching and sprouting requires ECs to adopt specialized phenotypes and functions. ECs that participate in the stabilization of the growing vessels and proliferate are called stalk cells, whereas gradient-sensing leading ECs are called tip cells. The tip/stalk cell specification is mostly regulated by the VEGF and NOTCH signaling. Indeed, elongating tip cells activate VEGFR2 signaling pathway through VEGF gradient that further drive Notch ligand DLL4 expression in ECs.

DLL4 interact with its cognate receptor NOTCH1 on the adjacent stalk cells that inhibits expression of VEGF and VEGFR2, thus preventing the tip cell phenotype (Figure 6; reviewed in Ref⁹¹). The plasticity between tip and stalk cells is kept throughout life and can be activated by angiogenic signals. Tip cells are able to form anastomoses with neighboring sprouts to build vessel loops and further expand the vascular network. Pruning is the mechanism by which endothelial cells located in non-perfused areas migrate to neighboring vessels, thus decreasing vascular density. Alternatively, in the absence of VEGF-A, vessels regress by apoptosis or intussusception⁹². Remaining blood vessels are therefore fully functional and excessive vascular beds removed⁹³.

A.4.4. Matrix Metalloproteases

Angiogenesis and the formation of new sprouts from tip cells also require proteolytic breakdown of the basement membrane and detachment of mural cells that are associated with mature blood vessels. The basement membrane, together with the coat of mural cells, sustain ECs survival and prevent them from leaving their positions. Basement membrane degradation and extracellular matrix (ECM) digestion is mediated by matrix metalloproteases (MMPs) such as MMP1/2/9 and tissue inhibitors of metalloproteinases (TIMPs) that are expressed by tip cells⁹⁴. MMPs are a family of highly homologous zinc endopeptidases that cleave peptide bonds of ECM proteins, such as collagens, laminins, elastin, and fibronectin. The imbalance of the MMPs and TIMPs are implicated in many pathological processes such as cancer metastasis, arthritis, inflammation and cardiovascular diseases. MMPs not only generate a passage for developing vessels, but also liberate proangiogenic growth factors that are sequestered in the matrix. They alternatively may generate angiostatic molecules, for example the conversion of plasminogen into angiostatin by MMP7/9⁹⁵. Liberation of antiangiogenic molecules from the ECM is essential to prevent inappropriate sprouting and coordinate branching⁹⁶.

A.4.5. VEGF signaling

VEGF-A, also called VPF (vascular permeability factor), was discovered 30 years ago as one of the first factors related with angiogenesis and binds to both receptor tyrosine kinases (RTKs) VEGFR-1 and VEGFR-2^{97,98}. In addition, VEGF-B and Placental Growth Factor (PIGF) bind to VEGFR-1, but their functions are mostly restricted to the coronary vasculature and pathological conditions, respectively^{99,100}. VEGF-C and VEGF-D bind to VEGFR-2 and VEGFR-3 and are mostly involved in lymphangiogenesis¹⁰¹. The requirement for VEGF-A signaling in early vasculogenesis and angiogenesis is underscored by early embryonic lethality of mice lacking a single *VEGF-A* allele¹⁰². *Vegfr2*-null mice also die at early developmental stage¹⁰³. In humans, alternative splicing of the *VEGF-A* gene gives rise to isoforms of 121, 145, 165, 189 and 206 amino acids¹⁰⁴. The affinity of the isoforms to the ECM increases with their size and is important for generating a continuous gradient of VEGF. VEGF₁₂₁ is hence the most soluble isoform, but shows reduced affinity to VEGFRs. VEGFA₁₆₅ is presumably the predominant form, with potent activation of VEGFR2. VEGFs also bind with high affinity to the Neuropilin (NRP) family members NRP1, and less potently to NRP2¹⁰⁵. Neuropilins function as co-receptor for VEGFR2 with which they form complexes that potentiate VEGF signaling (Figure 7). NRP-1 and NRP-2 play important roles in the vascular differentiation as they are expressed in developing arteries and veins, respectively¹⁰⁶.

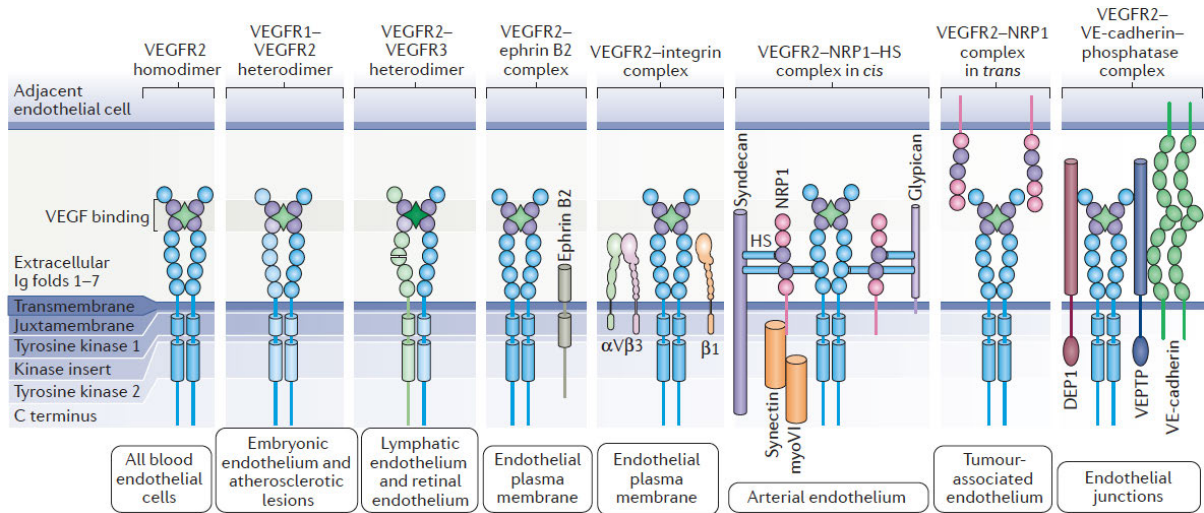


Figure 7: VEGFR2 structure and receptor signaling complexes¹⁰⁵

A.4.6 Arterio-venous differentiation

Following assembly of primitive vessels in the early embryo (such as the dorsal aorta and the cardinal vein), vascular remodeling transforms the plexus into a hierarchically organized network of arteries, capillaries, and veins. As we previously described with Neuropilins, specific factors are involved in the arterio-venous differentiation during vasculogenesis and angiogenesis. Ephrins are membrane-attached proteins and their Eph receptors are the largest subfamily of RTKs. Blocking Eph-A receptor signalling inhibits VEGF-induced cell survival, migration and sprouting *in vitro*¹⁰⁷. There is complementary expression of *ephrin-B2* in arterial ECs, and its cognate receptor *Eph-B4* in venous ECs, from early developmental stages until adulthood¹⁰⁸. Moreover, postnatal arteriogenesis is regulated by Dll1-mediated Notch activation of *ephrin-B2* expression¹⁰⁹. Disruption of Notch signaling causes loss of arterial markers and re-expression of venous signature genes, suggesting that Notch promotes arterial specification by repressing venous identity. On the contrary, COUP-TFII, an orphan receptor, regulates venous specification by repression of Notch signaling.

A.4.7. Vascular maturation

During maturation of the developing vasculature, blood vessels recruit mural cells composed of precursor vascular smooth muscle cells (VSMCs) and pericytes that derive from multiple sources, including the neural crest, perivascular mesenchymal cells and proepicardial cells^{110,111}. Pericytes establish direct cell-cell contact with ECs in capillaries and immature vessels, whereas vascular smooth muscle cells cover arteries and veins and are separated from ECs by a matrix. Unlike VSMCs, pericytes, are embedded within the endothelial basement membrane (BM). Mural cells deliver survival signals to ECs and control the diameter of medium and large blood vessels, thus regulating blood pressure, blood flow and vessel tone. Indeed, mature VSMCs express contractile proteins and are distinguished from pericytes through their separation from the vascular BM by a layer of mesenchymal cells and extracellular matrix, the intima. Pericytes from different organs are morphologically distinct, which mirrors diversity also at the molecular level. Several markers have indeed been used to identify pericytes, including smooth muscle actin (SMA), desmin, Neural/Glial antigen-2 (NG-2) and Platelet-derived growth factor receptor- β (PDGFR- β), the receptor for the best-known ligand Platelet-derived growth factor B (PDGF-B) that induces potent mitogenic signaling in both pericytes and VSMCs^{112,113}. However, none of these markers is absolutely specific for pericytes, and none of the markers recognizes all pericytes; their expression is dynamic and varies between organs and developmental stages. Mural cell induction, differentiation, proliferation, and migration as well as production and remodeling of extracellular matrix are also triggered by Transforming growth factor β (TGF β). Finally, mural cells require ephrin-B2 for their association around ECs, as mural cell-specific ephrin-B2 deficiency causes mural cell migration and vascular defects¹¹⁴.

A.4.8. Angiopoietins

Angiopoietin-1 (Ang-1), an agonistic ligand of the endothelial RTK Tie-2 is mostly expressed by pericytes, vascular smooth muscle cells and fibroblasts. Ang-1 is necessary for maintaining maximal interactions between ECs, pericytes and the ECM. It thus contributes to vascular remodeling during development and maintenance of vascular stability. Indeed, Ang-1/Tie-2 signaling promotes EC survival, integrity of the endothelial barrier and vascular quiescence. Deletion of either *Ang-1* or *Tie-2* results in embryonic lethality¹¹⁵. On the contrary, Ang-2 is a context-dependent agonist or antagonist of Tie-2 phosphorylation and signaling, and *Ang-2* overexpression causes embryonic lethality similar to deletion of *Ang-1* or *Tie-2*¹¹⁶. When combined with Vegf-a, *Ang-2* is expressed at sites of blood vessel remodeling where pericytes detach, induces endothelial cell proliferation and migration. However, in the absence of Vegf-a, Ang-2 activity leads to vascular regression¹¹⁷. In general, *Ang-1* is preferentially expressed in quiescent blood vessels, whereas Ang-2 plays important roles in inflammation and sepsis, and is rapidly released from endothelial cells by inflammatory stimuli. Indeed, endothelial Ang-2 can be stored in Weibel-Palade bodies, where it has a long half-life and can be released and secreted within minutes upon stimulation, together with the pro-coagulation von Willbrand Factor (vWF)¹¹⁸. Ang-2 constitutively forms oligomers and its activity is regulated by the state of its oligomerization. Namely, the lower oligomerization state of Ang-2 is essential for the Ang-2-specific Tie-2 cellular redistribution and vascular disruption, whereas multimeric structures of Ang-1 and Ang-2 induced similar stabilization responses¹¹⁹. Ang-2 clustering was successfully reproduced by delivering an Ang-2 binding and Tie-2 activating antibody (ABTAA) that further exerted agonistic activity on Tie-2 signaling and promoted vascular stability through endothelial function¹²⁰. Activation of Tie-2 by Ang-1 protects the blood vessels from Vegf-induced leakage by inhibiting the ability of Vegf to induce endocytosis of VE-cadherin¹²¹. VE-cadherin is a key component of EC junctions and, when complexed with Vegfr-2, maintains

EC quiescence through recruitment of phosphatases that dephosphorylate Vegfr-2, thus restraining Vegf signaling. Other transmembrane proteins sharing similar functions include occludins and members of the tight junctions, such as claudins. The ability of ECs to regulate cell-cell adhesion between them is necessary to control the exchange of fluids and the transmigration of immune cells, as well as EC quiescence¹²². Indeed, VE-cadherin is essential to maintain *Claudin5* expression in stabilized vessels, and the absence of Vegf stabilizes FoxO1 transcription factor, which translocates into the nucleus to repress myc-driven endothelial proliferation. *FoxO1* is therefore highly expressed in quiescent BECs. Finally, suppression of Tie-2 signaling is mediated by the Vascular endothelial cell-specific phosphotyrosine phosphatase (VE-PTP), a receptor tyrosine phosphatase that dephosphorylates Tie-2¹²³.

A.4.9. Hypoxia

VEGF signaling is the major pathway involved in angiogenesis and modulates as well the effect of other signaling pathways on the vascular system, like for ANG-2. Hypoxia is defined by insufficient oxygen supply within a tissue and is a strong regulator of angiogenesis predominantly through induction of *VEGF* expression in hypoxic cells. Sensing of oxygen levels is allowed by the Prolyl hydroxylase domain enzymes (PHDs) that belong to a protein family of α -ketoglutarate-dependent dioxygenases and utilize oxygen to hydroxylate their target proteins at specific proline residues¹²⁴. Upon hydroxylation, these targets may be recognized by the von Hippel-Lindau (VHL) E3 ubiquitin ligase system and subjected to proteasomal degradation. The best-known target proteins of PHDs are the Hypoxia-inducible factors 1a and 2a (HIF-1a/2a). In the absence of oxygen, PHDs fail to modulate these proteins, which hence escape proteasomal degradation, and consequently result in the induction of downstream target genes. Activity of PHDs is also regulated by nitric oxide (NO). Synthesis of NO is accomplished by the NO synthase (NOS) using L-arginine, oxygen and the cofactor NADPH. Three different NO synthase (NOS) isoforms are present and

endothelial NOS (eNOS) is primarily expressed in medium to large blood vessels and VEGF induces NO synthesis. Fluid shear stress also upregulates eNOS and the anticoagulant factor thrombomodulin. This mechanism is necessary to keep vessels dilated, perfused, and free of clots. Furthermore, NO-mediated *VEGFR2* downregulation prevents tip cell formation¹²⁵. Finally, the lack of oxygen in hypoxic environment prevents aerobic glycolysis and thus generates lactate. ECs take up lactate from the extracellular milieu via the Monocarboxylate transporter-1 (MCT1), which further activates HIF signaling. ECs exposed to lactate also increase the expression of *VEGF* and other receptor tyrosine kinase ligands, thus promoting their angiogenic behavior¹²⁶. Oxygen is therefore a major regulator of blood vessel development and maintenance.

A.4.10. Apelin

We previously exposed the most significant and better studied signaling pathways in angiogenesis. However, given the importance of the vascular system, many other factors play a role in its regulation, either by enhancing or decreasing angiogenesis. Here, I will focus on Apelin and Sema3F, two secreted proteins well known for their effect on endothelial cells and that are important for the understanding of this project.

Apelin has been identified as the endogenous ligand for the G protein-coupled receptor Apj (also known as AplnR). Apelin and Apj induce a wide variety of physiological functions, including blood pressure regulation via NO synthesis, heart contractility, appetite and drinking behavior as well as other metabolic processes^{127,128}. Interestingly, during embryonic development, *Apelin* is highly expressed in blood ECs where it has been shown to induce EC proliferation when combined with *Vegf*¹²⁹. However, on the contrary to *Vegf-null* mice, *Apelin* deficient mice are viable but have narrow blood vessels during embryologic development and after birth¹³⁰. Apelin is hence important for vascular maturation, promoting

vascular dilation and pericytes recruitment¹³¹. Moreover, *Apelin* expression by arterial cells allowed proper alignment of arteries and veins, thus regulating blood vessel patterning¹³². On the contrary, *Apelin-Cre*^{ERT2} reporter mice showed preferential *Apelin* expression in endothelial tip cells under pathological conditions¹³³. Apelin is therefore a promising angiogenic peptide whose effect on blood ECs is context-dependent and can be modulated by the presence or absence of Vegf-a.

A.4.11. Semaphorins

Semaphorins have been first identified by their role in axon guidance cues and induction of localized collapsed of neuronal growth cones through F-actin depolymerization¹³⁴. Class 3 Semaphorins are particularly interesting as they have demonstrated potent antiangiogenic functions, thus exerting similar effect on ECs as for neurons. Unlike other Semaphorins, class 3 Semaphorins are secreted molecules and they signal through Nrp1/2 and PlexinA1-4 or PlexinD1. Studies showed that Sema3A inhibited the binding of Vegf to Nrp1, thus preventing endothelial cell migration and proliferation¹³⁵. Similarly, Sema3F can elicit an antiangiogenic response in ECs by binding to Nrp2 and inhibiting Vegf-induced Erk1/2 phosphorylation and cell proliferation¹³⁶. When combined, Sema3A and Sema3F induced synergistic pro-apoptotic and anti-migratory functions *in vitro*¹³⁷. Similar findings were observed with Sema3B-E and Sema3G, demonstrating that angiogenesis is tightly regulated and Class 3 Semaphorins might exert redundant functions if produced within the same microenvironment¹³⁸.

A.4.12. Pathological angiogenesis

Angiogenesis, which is a critical process during embryonic development, occurs in specific diseases including intraocular neovascular disorders, immunogenic rheumatoid arthritis, psoriasis, and tumorigenesis. Defective vascular supply can also lead to specific medical conditions such as myocardial infarction or limb ischemia. The next chapter will summarize

major difference between physiological and tumor angiogenesis.

A.5. Tumor Angiogenesis

A.5.1 Introduction

Once a tumor lesion exceeds a few millimeters, passive diffusion throughout the tumor is no longer possible and hypoxia and nutrients deprivation trigger an “angiogenic switch”. Tumor vessels have abnormal organization and functions. Vessel appearance varies from abnormally wide, irregular and tortuous to thin channels with small or compressed lumens preventing efficient blood flow. Histologically, tumor ECs are poorly assembled, protrude outside the vessel and are occasionally multilayered. Unbalanced regulation between arterio-venous factors compromises flow and generates shunting. The basement membrane is irregular in thickness and composition, and fewer, more loosely attached mural cells cover tumor vessels¹³⁹. The resulting irregular perfusion impairs oxygen, nutrient, and drug delivery, and compromises the responses to chemo- and radiotherapy because of poor perfusion and inadequate tissue oxygenation. Vessel leakiness due to unstable endothelial cell layer together with the expansion of a dense tumor mass and lymphatic vessel compression increases the interstitial fluid pressure (IFD) and further impedes nutrient and drug distribution while increasing oncotic pressure. The loosely assembled vessel wall also facilitates tumor cell intravasation and distant dissemination. As a consequence of poor oxygen, nutrient, and growth factor supply, tumor cells further sustain angiogenesis by increasing the release of VEGF and other pro-angiogenic signals in an effort to compensate for the poor functioning of the existing ones. However, excessive proangiogenic factors are not balanced by antiangiogenic molecules, hence the ultimate response is poor, leading to additional chaotic vascular organization and tumor hypoperfusion. The presence of a hypoxic and consequently acidic tumor milieu constitutes a hostile microenvironment that is believed to drive selection of more malignant subclones and further promotes tumor cell

dissemination. In addition, hypoxia and low pH also compromise the cytotoxic functions of immune cells that infiltrate a tumor¹⁴⁰.

In summary, the tumor microenvironment comprises multiple signaling molecules and pathways that influence and promote tumor angiogenesis. It is therefore important to understand the key players involved in the regulation of the stromal remodeling in order to potentiate current anti-angiogenic drugs targeting tumor vessels.

A.5.2. VEGF-VEGFR system in tumors

Already in the 1970s, work by Folkman et al. suggested to target tumor angiogenesis for the treatment of cancer¹⁴¹. Later on, VEGF was discovered as the major angiogenic factor in physiological conditions, and *VEGF* expression was highly increased by rapidly proliferating cancer cells¹⁴². Knowing that most of adult blood vessels remain in a quiescent state, direct inhibition of VEGF appeared a promising therapeutic approach for cancer. Indeed, injection of a monoclonal antibody specific for VEGF inhibited the growth of three aggressive tumor types *in vivo*¹⁴³. Further studies enabled the development of the well-known bevacizumab, a humanized monoclonal antibody specific for VEGF used in the clinics for the treatment of various cancers (Ref¹⁴⁴ and section A.6.). Nevertheless, *VEGF* is not only expressed by cancer cells but also by other stromal cells and signaling pathways other than the VEGF-VEGFR system are important for tumor angiogenesis. I will therefore focus in the next sections on the role of myeloid cells and fibroblasts in tumor angiogenesis.

A.5.2. Myeloid cells in tumor angiogenesis

The tumor microenvironment is composed of a variety of cells that influence the angiogenic response to a tumor and recruited leucocytes are known to increase VEGF bioavailability and signaling during angiogenic switch¹⁴⁵. Tumor infiltrating leucocytes can be divided into lymphoid and myeloid cells. Although T- and B-lymphocytes play major roles in the

development of an anti-tumor response, I will focus on monocytes, macrophages and neutrophils.

Bone-marrow-derived myeloid progenitors (BMDMPs) have been shown to promote tumor angiogenesis and monocytes attracted to the tumor quickly differentiate into macrophages upon colony-stimulating factor-1 (CSF-1) stimulation¹⁴⁶. High macrophage numbers positively correlates with vascular density in human tumors, but the definite role of macrophages depends on their activation status¹⁴⁷. Indeed, classical tumor associated macrophages (or M1 polarized) are activated by Th1 cytokine upon acute inflammation and promote anti-tumor response. On the contrary, anti-inflammatory M2-polarized macrophages are activated by Th2 cytokine like IL-4 and IL-13 and have notable pro-angiogenic functions¹⁴⁸. *Ang-2* expression is often increased in tumor-associated endothelial cells and can bind to its cognate receptor Tie-2 that is expressed on a specific Tie-2-expressing monocytes (TEMs) subpopulation¹⁴⁹. TEMs markedly increase tumor angiogenesis and promote an immunosuppressive microenvironment through secretion of IL-10¹⁵⁰ (Figure 8).

Tumor angiogenesis is also maintained by a heterogeneous population of immature myeloid progenitors (often called myeloid-derived suppressor cells, MDSCs) which comprise both mononuclear and granulocytic lineages and that are classified by their surface expression of CD11b and granzyme-1 (Gr-1)¹⁵¹. CD11b+/Gr1+ myeloid cells in turn sustain tumor angiogenesis by the synthesis of MMP-9 which increases VEGF-A bioavailability and thus significantly diminish the impact of VEGF-targeted therapies. Moreover, Tumor-secreted G-CSF attracts CD11b+/Gr1+ neutrophil and Ly6G+Ly6C+ granulocytes that in turn produce of VEGF-A¹⁵².

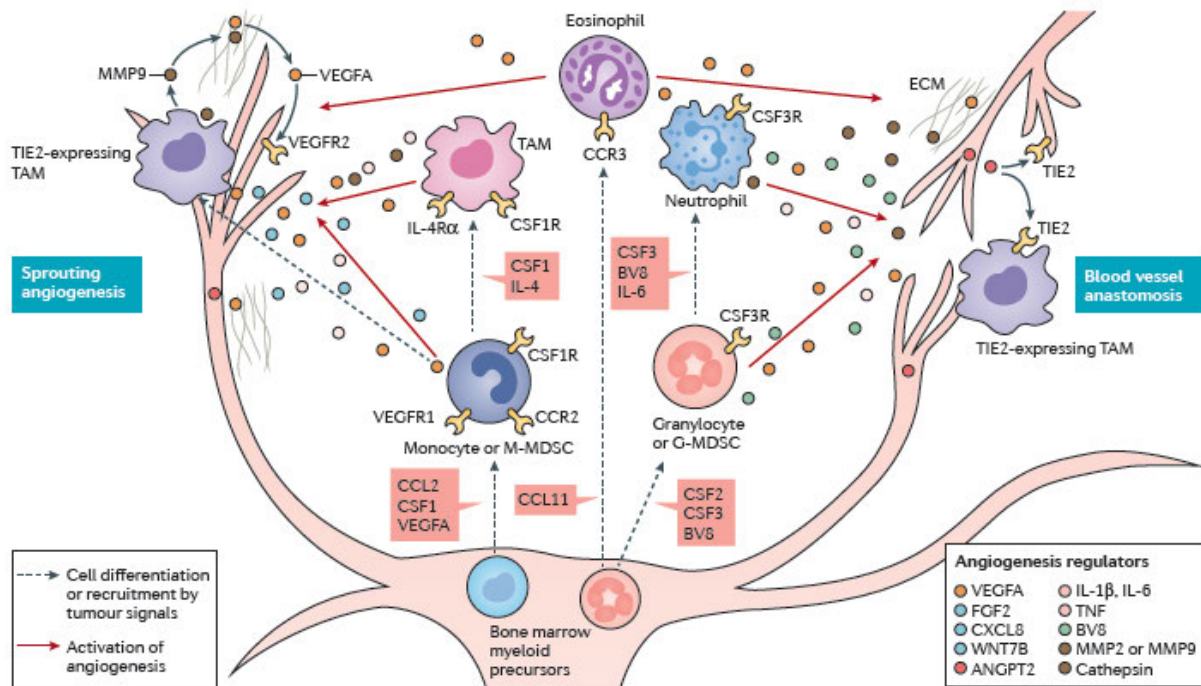


Figure 8: Myeloid cell regulation of tumor angiogenesis¹⁴⁵

The role of neutrophil, or tumor-associated neutrophils (TAN) has been demonstrated by Gr1-targeted therapy which decreased Cd11b+/Gr1+monocytes as well as neutrophils. Notably, neutrophils express Bv8 which in turn induces tumor angiogenesis by recruitment of BMDMPs. Anti-Bv8 treatment inhibited significantly tumor vascular density and myeloid cells homing to the peripheral blood and tumors¹⁵³. Leukocyte infiltration within the tumor and specific signal activation turn thus the tumor microenvironment into an independent angiogenic niche that may confer resistance to anti-angiogenic therapies.

A.5.3. Cancer-associated fibroblasts

Unlike their normal counterparts, cancer-associated fibroblasts (CAFs) adopt a new protumorigenic and proangiogenic phenotype. CAFs demonstrate a high degree of heterogeneity due to their various origins¹⁵⁴. Cancer cells indeed recruit resident fibroblasts, such as pericyptal myofibroblasts in CRC, but also from circulating mesenchymal cells or through epithelial to mesenchymal transition of cancer cells. Interestingly, CAFs isolated

from tumors resistant to angiogenic blockade with an anti-VEGF-A neutralizing antibody produced higher levels of alternative proangiogenic factors including PDGF-C, ANG-2, and Cyclooxygenase 2 (COX2)¹⁵⁵. As a result, cancer-associated fibroblasts actively participate in the tumor angiogenic process and are at least partly responsible for treatment refractoriness to anti-VEGF therapies.

A.6. Anti-Angiogenic therapies

A.6.1. Classes of anti-angiogenic agents and treatment response

Given that tumor angiogenesis is a prerequisite for continuous tumor growth, development of drugs able to target the main driving angiogenic pathways caught substantial focus in the oncologic field. VEGF-A is the major endothelial growth factor and its importance in physiological angiogenesis was emphasized by the embryonic lethality of mice carrying a single defective copy of the gene¹⁰². VEGF-A was therefore legitimately the first target of antiangiogenic treatment. Bevacizumab is a humanized monoclonal antibody binding with high affinity to VEGF-A and preventing its interaction with VEGFR-1/VEGFR-2 and thus pathway activation. Bevacizumab was approved for the first time in the treatment of metastatic colorectal in 2004 and showed modest but significant increase in the overall survival when combined with 5-FU/leucovorin and irinotecan chemotherapies¹⁵⁶. Other cancers were subsequently investigated and metastatic HER2 negative mammary tumors, relapsing or metastatic non small-cell lung cancer (NSCLC), highly advanced ovarian cancer and relapsing or metastatic renal cell carcinoma (RCC) showed significant benefit when combined with standard chemotherapies. Bevacizumab monotherapy was also approved for relapsing WHO grade IV glioblastoma (GBM) after previous Temozolomide treatment (www.swissmedicinfo.ch). Interestingly, tumor responses varied substantively according to tumor type and displayed heterogeneous benefit between patients with apparently similar tumors. Indeed metastatic colorectal showed the best overall survival benefit (5 months), followed by metastatic NSCLC (2 months) and GBM as a monotherapy (1 month). On the

contrary, HER2 negative mammary carcinoma and RCC treated by bevacizumab only improved the progression free survival (PFS)^{156–160}. Despite Food and Drug Administration (FDA) approval of bevacizumab for all of these tumors, metastatic mammary carcinoma was rejected soon after due to improper risk/benefit/costs ratios⁸.

Bevacizumab alone was mostly ineffective and when combined with chemotherapy only moderately improved patient outcome. The constellation of angiogenic molecules expressed in a tumor increases with malignant progression, rendering certain tumors less dependent on VEGF. Thus, novel therapies with broader or more specific targets needed to be tested. Aflibercept (VEGF Trap, known in the US as ziv-aflibercept), is a recombinant fusion protein with receptor components of VEGFR-1 and VEGFR-2 that binds multiple ligands in the angiogenesis network (VEGF-A, VEGF-B, and PlGF). However, clinical benefits were less pronounced in mCRC, compared to bevacizumab treatment (1.5 months vs 5 months), probably reflecting minor contributions of VEGFB and PlGF¹⁶¹. Small tyrosine kinase inhibitors (TKIs) are small molecules that specifically bind to and thus prevent phosphorylation of specific residues on one or more receptor tyrosine kinases. Common TKIs with known antiangiogenic effects are sunitinib, sorafenib and regorafenib. The latter is approved as a third line therapy for mCRC and shows activity against the VEGFR2-3, PDGFR and TIE2 RTKs, between others. We would therefore expect global antiangiogenic effect by targeting VEGF signaling and thus tumor angiogenesis, pericytes recruitment through PDGFR pathway alteration and ANG-2-mediated angiogenesis. However, despite deep antiangiogenic expectations, regorafenib showed an overall survival improvement of only 1.4 months¹⁶². Sunitinib and sorafenib are both multiple TKIs widely used for the treatment of renal cell carcinoma and hepatocellular carcinoma, among others^{163–165}. Colorectal cancer did not respond to any of the treatments, both in early and late stage tumors. Similarly to Regorafenib, specific targeting of the angiopoietin/Tie-2 signaling

pathway is a promising therapeutic approach. Indeed, Ang-2 binding and Tie-2 activating antibody (ABTAA) promoted vascular stability¹²⁰ and demonstrated sustained tumor vascular normalization with improved hypoxia and acidosis, improved vascular perfusion, drug delivery, decreased tumor growth and metastatic potential as well as increased immune cell infiltration¹⁶⁶.

Heterogeneity in antiangiogenic treatment response highlights differential molecular mechanisms regulating tumor type specific angiogenesis. Better knowledge of the critical pathways involved would lead to enhanced tumor growth inhibition.

A.6.2. Vascular normalization hypothesis.

Anti-angiogenic therapies have been developed with the hypothesis that inhibiting the vascular supply would cause nutrient and oxygen starvation of the tumors and thus decrease tumor growth. However, as discussed above, bevacizumab alone was not sufficient to elicit a proper anti-tumor response and was only beneficial in combination with conventional chemotherapy. The paradox between anti-angiogenic effect and increased efficacy of standard chemotherapy was proposed to result from vascular normalization¹⁶⁷. Through inhibition of common angiogenic signals, anti-angiogenic treatment re-established equilibrium between pro- and antiangiogenic factors (Figure 9). Normalization of the tumor vasculature further improved tumor blood perfusion by pruning of pericytes devoided vessels, by enhancing the vascular pericytes coverage, reducing vascular permeability and the interstitial fluid pressure and thus more homogeneous delivery of chemotherapeutic agents. Vessel normalization was unfortunately shown to be a transient state (“time window”), as these drugs ultimately induce excessive vessel regression, or tumor vasculature escapes VEGF blockade^{168,169}.

A.6.3. Intrinsic and acquired resistance

VEGF, or more globally anti-angiogenic treatment escape can result from intrinsic or acquired resistance (evasive). We already discussed some roles of bone marrow-derived cell recruitment by tumor cells and the surrounding microenvironment. Myeloid cells are indeed able to sustain cancer with VEGF-A, as well as other alternative pro-angiogenic factors. Another mechanism of acquired resistance is the upregulation of alternative angiogenic pathways. After treatment with an anti-Vegfr2, RIP1-TAG2-derived tumors demonstrated increased expression of Fgf1/2, ephrin A1-2 and Ang-1/2^{170,171}.

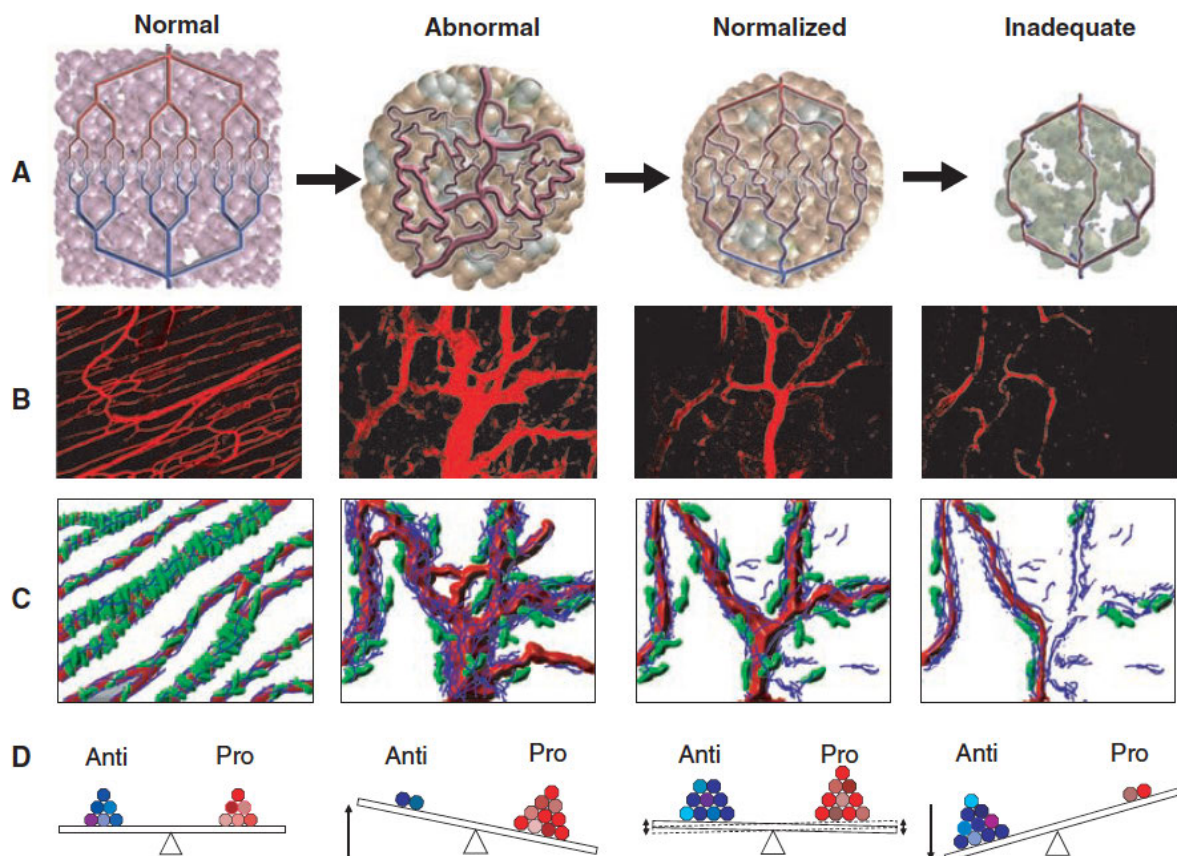


Figure 9: Tumor vascular normalization in response to anti-angiogenic treatment¹⁶⁷.

A. The normal vasculature is tightly regulated and organized, in comparison to highly abnormal tumor blood vessels. Upon antiangiogenic treatment, the organization of the tumor vasculature is normalized. However excessive antiangiogenic therapies may induce tumor resistance or inadequate chemotherapy delivery. **B.** Representative two-photon images of the normal muscle vasculature and tumor vessels at initiation or after antiangiogenic treatment. **C.** Schematic view of pericytes (green) and basement membrane (blue) modifications during antiangiogenic treatment. **D.** Changes in the balance between pro- and anti-angiogenic factors in the tissue.

Moreover, vascular normalization induces transient increase in pericytes coverage. VEGF signaling in blood vessels is hence decreased by mural cells stabilization and maintenance of pro-survival factors produced locally by pericytes¹⁷². Their sensitivity to VEGF-targeted therapies decreases (Figure 10).

As opposed to the acquired resistance mechanisms to anti-angiogenic therapies, some tumors likely possess intrinsic characteristics leading to treatment failure. The constant selective pressure occurring in the developmental stages of a tumor participates in that process. Some pathways involved in intrinsic resistance are shared with the evasive mechanisms, yet the timing with which they appear is different. Nonetheless, independent factors such as poorly vascularized pancreatic tumors or the presence of mature tumor capillaries and arterialization in hepatocellular carcinoma may reduce substantively the sensitivity to VEGF inhibitors^{173,174}.

Finally, detailed histopathological evaluation of the organization of the tumor vascular network in primary lesions or in metastasis demonstrated that distinct vascular patterns exist between tumors¹⁷⁵⁻¹⁷⁷. Frentzas et al. described the prognostic value of the desmoplastic or replacement histopathological pattern with response to current anti-VEGF therapies. High desmoplasia was associated with significant angiogenesis induction and increased sensitivity to anti-VEGF treatment. On the other hand, the replacement growth pattern of metastatic tumor cells within their host organ (liver or lung) and utilization of the already formed and functional blood vasculature, compromised significantly the effect of antiangiogenic therapies. Indeed, tumor angiogenesis was not elicited in this particular situation¹⁷⁷.

To conclude, tumor angiogenesis is a rather chaotic process involving multiple cell types, physico-mechanical forces as well as numerous signaling pathways differentially regulated

according to the tumor context. Therefore, in this project, we wanted to address the specific role of the colon cancer stem cells in the regulation of the associated blood vasculature. We also decipher the intrinsic mechanisms by which CSCs drive anti-angiogenic treatment refractoriness and suggest potential new therapeutic approaches targeting alternative angiogenic pathways.

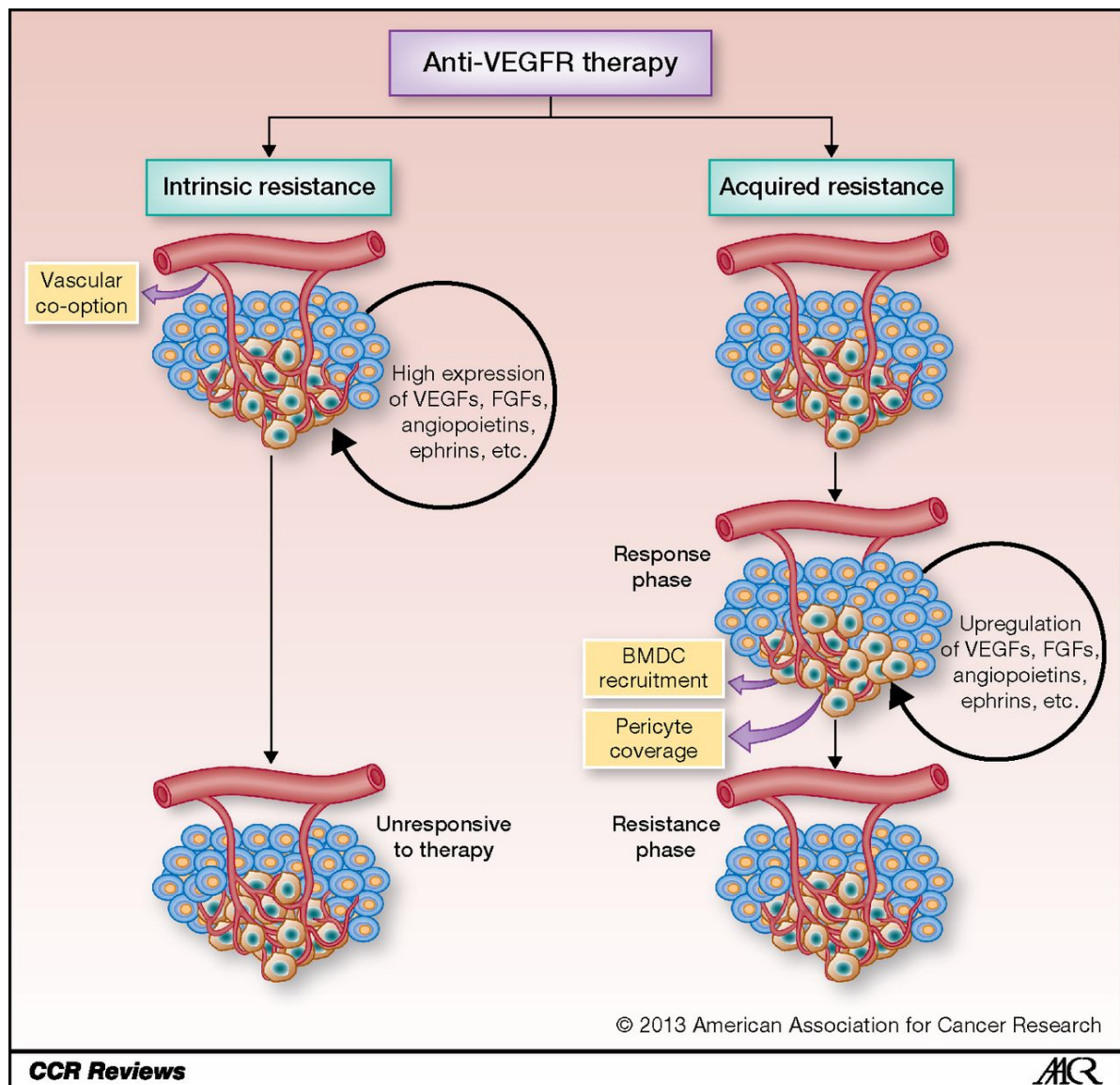


Figure 10: Summary of intrinsic and acquired resistance mechanism after anti-VEGF therapies¹⁷⁸

B. RESULTS

Jeremiah Bernier-Latmani generated images shown in Figures 1A, 1B, 2A, 2B and participated in the sample collection for the analyses of gene expression profile comparing endothelial cells isolated from WT and *Apc^{fl/fl}-Vil-Cre^{ERT2}* intestine. Transcriptome data were generated by the Swiss Institute of Bioinformatics at The University of Lausanne and the data were analysed Drs Nadine Zangger, Jeremiah Bernier-Latmani and Mauro Delorenzi. This microarray analyses (Affymetrix GeneChipTM Mouse Gene 1.0 ST Array) identified candidate molecular regulators tested at the end of my thesis. Dr Simone Ragusa performed the AKP organoid tumor experiment and treated with a control IgG or DC101 It demonstrated for the first time the resistance of such tumors to anti-Vegf treatment. These results played important roles in my project, therefore they are included in my thesis report. I used “we” when data were coming from the collaborators or with their help, and “I” when I was the main responsible providing the results.

B.1. The mouse small intestinal vasculature comprises phenotypically and physiologically distinct crypt- and villus-associated blood vessels

The small intestine is subdivided into crypts and villi and we first sought to characterize the organization of the blood vasculature in those two compartments by whole-mount and paraffin section immunostaining. We observed that villus-associated blood vessels in adult mice were more dense and branched compared to crypt vessels (Fig. 1A). Moreover, villus but not crypt blood vessels displayed cytoplasmic extension called filopodia¹⁷⁹ characteristic of angiogenic blood vessels (Fig. 1A, insert A). In order to further examine the relationship between intestinal crypts and blood vessels, we repeated the whole-mount immunostaining in the *Lgr5-eGFP-Cre^{ERT2}* mouse model, where GFP expression is under the control of the *Lgr5* promoter, highly expressed in intestinal stem cells¹⁸⁰. As expected, epithelial GFP expression was restricted to the bottom of the crypts (Fig. 1A), and we confirmed that GFP-

positive cells were associated with a sparse vascular network (Fig. 1A, insert B). Similar results were made for the colon (data not shown). These observations prompted us to think that the master regulator of endothelial cell proliferation and migration Vegf might be differentially expressed from crypts to villi.

Specific signaling pathways are active in blood endothelial cells (BECs) according to the position they occupy and the function they exert within the growing blood vessels¹⁸¹ (see A.3.3.). I was therefore interested to look at the level of expression and the localization of three proteins induced or repressed by Vegf signaling, as well as hypoxia. I performed immunostaining of the endothelial quiescence markers Claudin-5 and the transcription factor Forkhead box-O1 (FoxO1). I found that their expression was restricted to crypt-associated blood vessels (Fig. 1D-E). Moreover, as FoxO1 needs to translocate into the nucleus to be active, I confirmed that its subcellular localization in the crypt vessels was predominantly within the nucleus (Fig. 1D). Finally, while it was completely absent from villus-associated blood vessels, it was also expressed within the cytoplasm of the intestinal lacteals, as well as in the nucleus of differentiated enterocytes at the villus tip (Fig. 1D). These results confirmed previous publications showing that Vegf phosphorylates FoxO1 in endothelial cells, thus excluding it from the nucleus and preventing activation of downstream target genes¹⁸². Moreover, Vegf/Vegfr-2 signaling was shown to decrease the expression of *Claudin-5*¹⁸³. On the contrary, the tip cell marker Endothelial-specific marker-1 (Esm-1, also known as Endocan), a secreted protein increasing the bioavailability of Vegf by competing with fibronectin in the extracellular matrix (ECM), was restricted to endothelial cells at the tip of the villus and mostly absent in the crypts (Fig. 1C)^{122,184-186}. As Vegf signaling seemed to be mostly active on top of the villi and knowing that hypoxia is a potent inducer of Vegf expression¹⁸⁷, we looked at the localization of Hif-1a and pimonidazol adducts¹⁸⁸, a chemical compound that forms intracellular complexes in an hypoxic microenvironment.

Figure 1

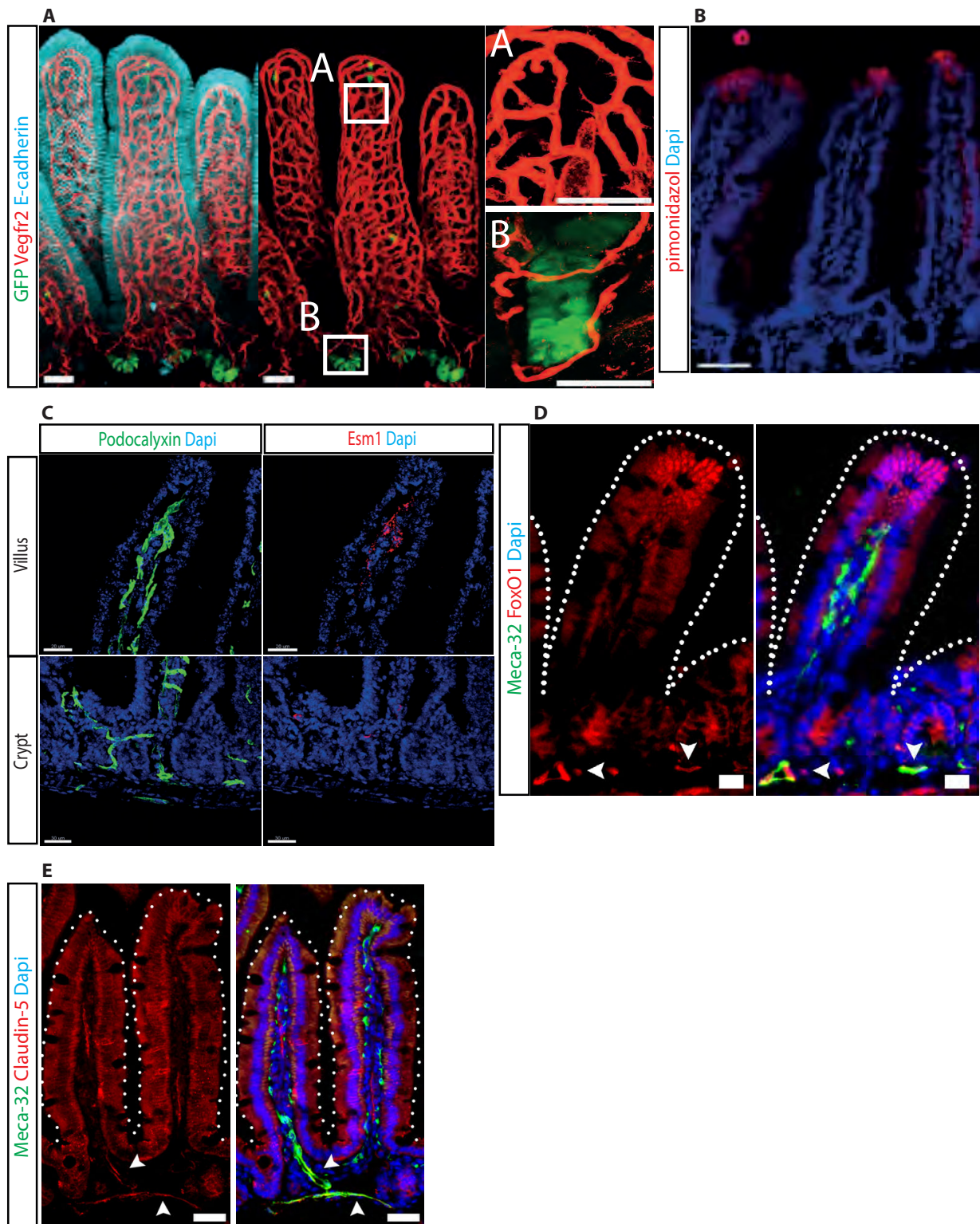


Figure 1. Mouse small intestine blood vessel characterization.

(A) Immunostaining of the *Lgr5-eGFP-Cre^{ERT2}* mouse small intestine. Dense and sprouting vasculature in the villi (insert A), while crypt-associated vessels are sparse and non sprouting (insert B). (B) Hypoxia distribution in the normal mouse intestine. (C) Esm-1 expression is restricted to villus blood vessels. (D) Markers of quiescent endothelial cells FoxO1 and (E) claudin-5 are predominantly expressed in crypt vessels (arrowheads: positive vessels). Scale bars: 20µm, A-C; 30µm, D, E. A-B: pictures by Dr. Jeremiah Bernier-Latmani.

We found that hypoxia was restricted to the top of the villus where differentiated enterocytes reside, while crypt areas were normoxic (Fig 1B). Finally, I analyzed by immunostaining the localization of proliferating BECs within the small intestine and found that few endothelial cells were proliferating (~1%) and, consistent with the above results, that the proliferation was mostly restricted to the villus (Fig. 2C and 2E).

To further investigate which of the crypt or villus blood vessels rely on active Vegf signaling, we treated adult mice with DC101, a monoclonal antibody with high affinity for Vegfr-2, which prevents binding of Vegf and thus blocks Vegf/Vegfr-2 signaling¹⁸⁹. In agreement with our previous observations, DC101 efficiently pruned and decreased the total number of sprouts in villus blood vessels, while it had no effect on crypt-associated blood vessels (Fig 2A). In line with these data, Vegf target Esm-1 was absent in the villus-associated blood vessels after DC101 treatment (Fig 2G-H). Vegf blockade also completely abolished BEC proliferation in both the crypt and villus (Fig 2C and E), demonstrating efficient antibody delivery.

We therefore concluded that intestinal blood vessels are divided into two phenotypically distinct vasculatures: a fast remodeling and angiogenic Vegf-dependent villus-associated blood vasculature and a more quiescent and stable Vegf-independent crypt vascular network.

B.2. Crypt-associated blood vessels remain resistant to anti-Vegf treatment in *Apc* deleted precancerous lesions

We previously showed that villus, but not crypt vessels, depend mostly on Vegf signaling (Fig. 2A). We therefore asked if such vessel compartmentalization was induced by intestinal stem cells. We thus used the *Apc*^{fl/fl}-*Vil-Cre*^{ERT2} (*Apc*^{ΔIEC}) mouse¹⁹⁰, where *Apc* can be

specifically deleted in all intestinal epithelial cells after intraperitoneal (i.p.) injection of tamoxifen, leading to significant crypt expansion.

Namely, *APC* is mutated in more than 80% of human colorectal cancer and was shown to be sufficient to generate benign adenomas (reviewed in Ref¹⁹¹). As expected, after epithelial *Apc* deletion, we observed expanded intestinal crypts, along with increased epithelial proliferation¹⁹². Simultaneously, crypt vessels, and, to a lesser extent villus vessels, expanded as well (Fig. 2B). Interestingly, expanded crypt vessels were phenotypically similar to normal crypt vessels, characterized by reduced branching and almost no filopodia (Fig. 2A, bottom panels, Fig. 2B). On the contrary, villus vessels were highly dense and showed numerous branchpoints and filopodias, mimicking normal villus vessels. I then analyzed the proliferation of blood endothelial cells and observed that it was markedly increased and no longer restricted to villus vessels (Fig. 2F). We also studied the effect of Vegf blockade with DC101 on intestinal blood vasculature of *Apc*^{ΔIEC}. We found the treatment reduced the length and the number of branching points of villus vessels (Fig. 2B, right panels and data not shown) while, in contrast, crypt vessels remained intact (Fig. 2B, right panels). Additionally, endothelial cells in vessels were still proliferating after DC101 treatment (Fig. 2F). Of note, Esm-1 staining was markedly reduced in mice treated with DC101 (data not shown). Therefore persistence of BEC proliferation was not due to suboptimal dosage or inefficient delivery of the treatment.

Altogether, these results show that the crypt enlargement occurring after epithelial *Apc* deletion is accompanied by a crypt vessel expansion that remains Vegf-independent. Moreover, it suggests that epithelial Wnt activation promotes endothelial proliferation.

Figure 2

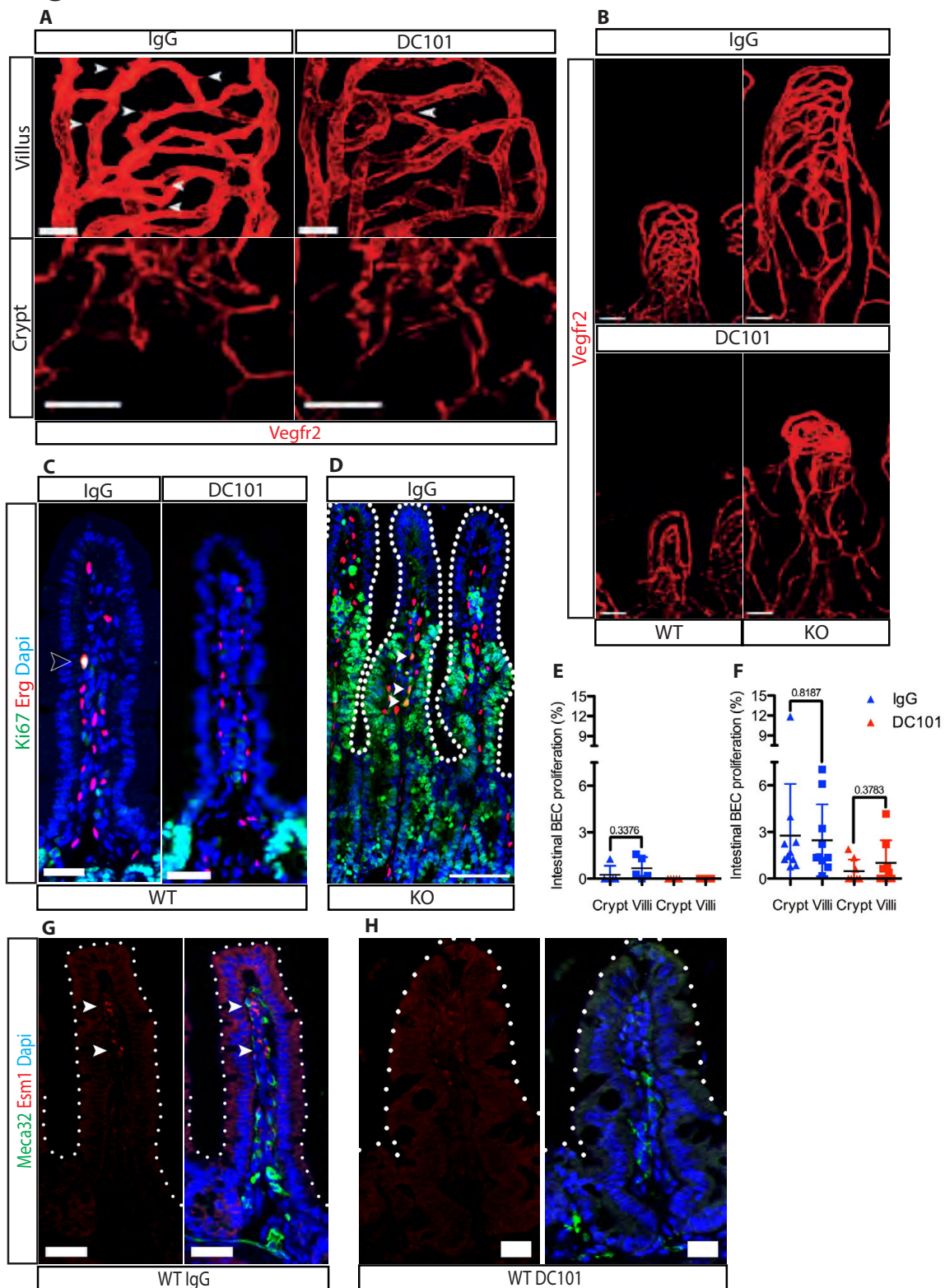


Figure 2. Vegf inhibition doesn't affect crypt-associated blood vessels in the WT and the *Apc-Vil-Cre^{ERT2}* mouse small intestine.

(A) Blood vasculature in the normal (WT) mouse small intestine treated with IgG or DC101. Numerous filipodias (arrowhead) in villus vessels compared to crypt vessels. DC101 abolishes filipodias in villus vessels (pictures by Dr Jeremiah Bernier-Latmani). (B) Vascular phenotype of the WT and *Apc-Villin-Cre^{ERT2}* (KO) mouse small intestine treated with IgG (top panels) or DC101 (bottom panels)(pictures by Dr Jeremiah Bernier-Latmani). (C) DC101 blocks endothelial cell proliferation in wild type intestine. Immunofluorescent staining of proliferation marker Ki67 (green), endothelial marker Erg (red) and DNA (blue) (arrowhead: proliferating BEC). (D) Increased BEC proliferation in the KO mice (arrowheads) . (E) Localization of proliferating BECs in the WT (n=5) and (F) KO mouse small intestine (n=8-10), treated with IgG or DC101. (G) Esm-1 expression is localized at the top of villus vessels and (H) is suppressed by DC101. Datas are presented as mean \pm SD; Student's t test. Scale bars: 20 μ m, A, B; 50 μ m, C; 100 μ m, D; 30 μ m, G-H.

B.3. Blood vessels in advanced models of Wnt^{high} intestinal tumors are intrinsically Vegf-independent

The *Apc*^{ΔIEC} mouse model recapitulates benign intestinal tumors. However, genes commonly mutated or deleted in advanced CRC include *TP53* and *KRAS*²⁷. We therefore generated the *Apc*^{fl/fl}, *Kras*^{Lsl-G12D}, *Tp53*^{fl/fl}, *Vil-Cre*^{ERT2} (AKP) mouse model where, in addition to *Apc*, *Tp53* is deleted and *Kras* is constitutively activated and addressed the relationship between intestinal stem cells and the blood vasculature. Rapid expansion of intestinal crypt cells results in early animal lethality in this model, which precluded the analyses of remodeling of the associated blood vessels *in vivo*. We therefore harvested crypt intestinal cancer cells after the short term induction of the Cre recombinase and cultured them *in vitro*¹⁹³. Normal intestinal crypt cells proliferated when cultured in 3D in Matrigel and give rise to all intestinal differentiated cells, forming so-called “intestinal organoids” or “mini-guts”¹⁹³. In case of transformed intestinal epithelium, such organoids are however predominantly composed of intestinal stem cells and their progeny and therefore represent a useful model to study the development of tumor vasculature in the context of high epithelial Wnt signaling. We injected tumor organoids subcutaneously in NOD/scid IL2-Rγ^{null} immunodeficient mice (NSG) and treated them with a control IgG or DC101. We observed that blocking Vegf signaling did not affect growth of organoid tumors (Fig. 3C-D). In contrast, tumor growth of the mouse colon adenocarcinoma cell line MC38, which has low levels of Wnt signaling (Fig. 3B and 3N), was significantly impaired (Fig. 3I-J). Moreover, a significantly larger proportion of MC38 blood vessels expressed Vegf target *Esm1* (20%), whereas only 3% of blood vessels of AKP organoid tumors were *Esm1*-positive (Fig. 3K). I therefore concluded that, in contrast to AKP tumors, MC38 tumors rely substantively on the Vegf signaling pathway for tumor angiogenesis and thus could be used as a model to assess and compare anti-angiogenic treatment efficacy.

In order to understand how the tumor-associated vasculature is regulated *in vivo*, I started analyzing by immunofluorescence the AKP organoid tumor xenografts and observed that these tumors were highly heterogeneous and displayed a significant proportion of colon cancer stem cells expressing high levels of CD44 and Prox1^{194,195}. *CD44* and *Prox1* are indeed known Wnt target genes¹⁹⁶.

In addition, unlike in MC38 tumors, the major canonical Wnt transcription co-factor β -catenin could be detected both in the cytoplasm and the nucleus (Fig. 3A, B). I next assessed the relationship between Wnt^{high} cancer stem cells (hereafter CD44^{high}), Wnt^{low} cancer stem cells (hereafter CD44^{low}) and the associated blood vessels in the presence or absence of DC101. CD44 was used as a stem cell marker as β -catenin was highly expressed throughout the tumors, hence preventing the differentiation between stem cell and more differentiated areas. Overall vascular density was decreased after DC101 treatment in both AKP organoid tumors and MC38 tumors (Fig. 3E-G)¹⁹⁷ and only a small proportion of blood vessels were expressing Vegf target Esm-1. Importantly, most of Esm-1 was found around CD44^{low} cells (Fig. 3M and 3Q) and DC101 almost abolished its expression, as mentioned earlier (Fig. 3L). On the contrary, markers of mature blood vessels FoxO1 and Claudin-5 were highly expressed in the tumor vasculature, specifically around CD44^{high} stem cells (Fig. 3P and data not shown). Unlike for Esm1, DC101 treatment didn't affected FoxO1 expression (Fig. 3O), which was predominantly found within the nucleus of endothelial cells (Fig. 3S), similarly to the normal mouse intestinal crypts.

Figure 3

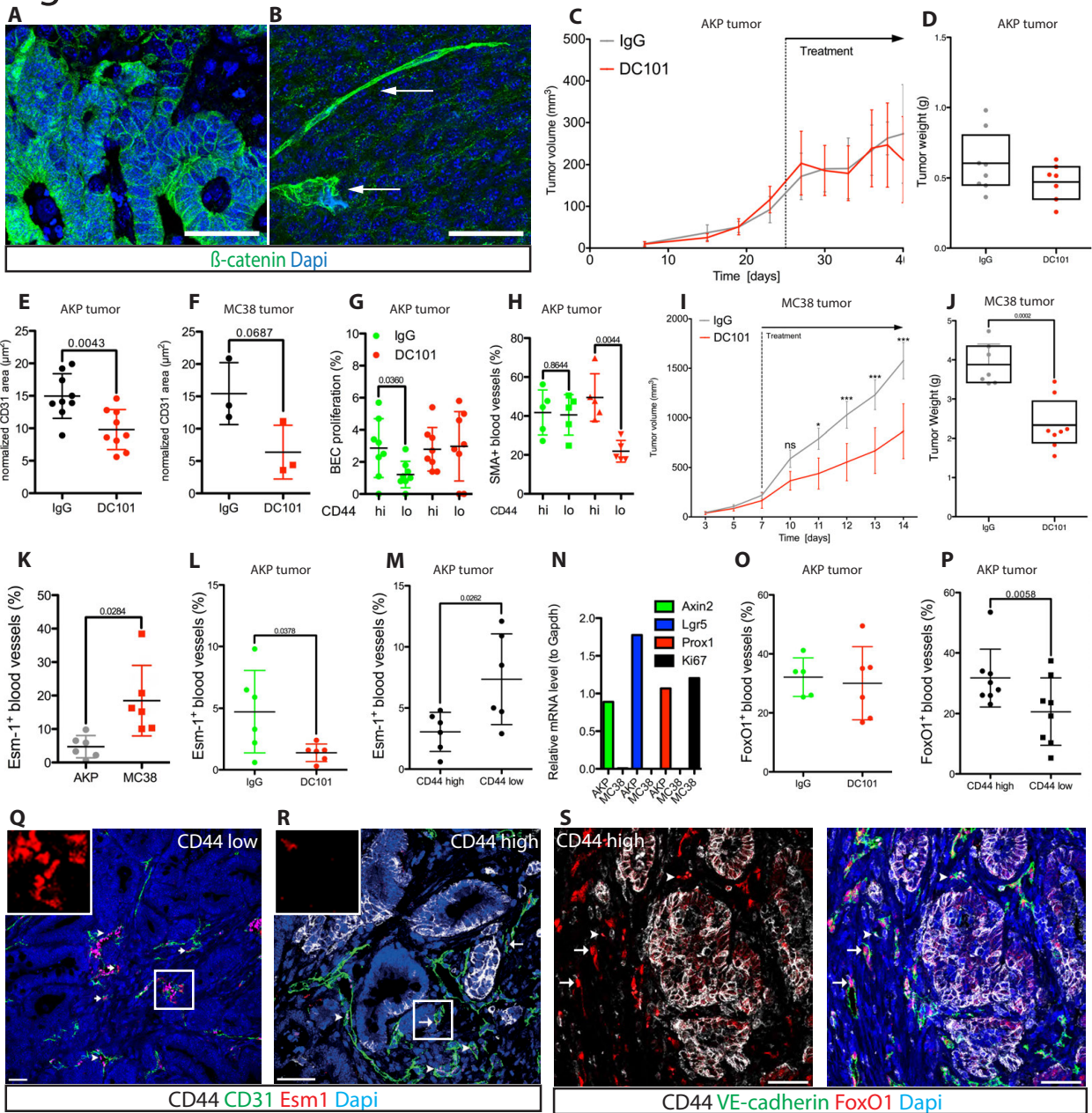


Figure 3. Wnt^{high} cancer stem cells regulate the tumor vasculature in a Vegf-independent way.

(A) Nuclear and cytoplasmic β -catenin in AKP tumor. (B) Endothelial β -catenin in MC38 tumor (arrows). (C) Tumor growth curve of AKP tumors treated with control IgG or DC101 and (D) corresponding weights (Analysis by Dr. Simone Ragusa, n=7-8/group). Vascular density in (E) AKP and (F) MC38 tumors according to IgG or DC101 treatment. (G) Percentage of BEC proliferation in AKP tumors according to CD44 status and treatment. (H) Percentage of SMA⁺ blood vessels according to CD44 status and treatment (I) Tumor growth curve of MC38 tumors treated with control IgG or DC101 (n=7-8/group) and (J) corresponding weights. (K) Percentage of Esm-1⁺ blood vessels in AKP and MC38 tumors. (L) Percentage of Esm-1⁺ blood vessels in AKP tumors treated with IgG or DC101. (M) Percentage of Esm-1⁺ blood vessels in AKP tumors treated with IgG according to CD44 status. (N) mRNA expression of Wnt target genes in AKP organoids and MC38 cells. (O) Percentage of FoxO1⁺ blood vessels in AKP tumors treated with IgG or DC101. (P) Percentage of FoxO1⁺ blood vessels in AKP tumors treated with IgG according to CD44 status. (Q) High Esm-1 staining in CD44 low areas of AKP tumor (arrows, insert) compared to (R) CD44 high areas (arrow, insert). Red blood cells are shown with arrowheads. (S) Numerous FoxO1⁺ vessels around CD44 high areas of an AKP tumor. FoxO1⁺ vessels are shown with arrows. Red blood cells are shown with arrowheads. Scale bars: 50 μ m, A, B, L, O. Statistics: C, H Data are shown with mean \pm S.D. Two-way ANOVA with repeated measures; ns p>0.05, **p <0.01, ***p <0.001. D-G, I-K, M-N Data are presented as box and whiskers; Tukey appearance or scatter plots and shown with mean \pm S.D. Student's t test if 2 groups, One-way ANOVA if >2 groups.

Given the heterogeneity of the AKP tumors, I also analyzed the vascular density specifically in the vicinity of CD44^{high} cancer stem cells and CD44^{low} differentiated cancer cells and observed that colon cancer stem cells were associated with a higher vascular density (illustrated by Fig. 3Q and 3R). Similarly to *Apc*^{ΔIEC} mouse (Fig. 2F), vascular proliferation was enhanced about 3-fold compared to the normal gut (Fig. 3G) and remained similar between stem cell- and differentiated-associated vasculature. Importantly, endothelial cell proliferation was comparable in DC101 and IgG tumors (Fig. 3G). Finally, in order to assess if cancer stem cells-associated blood vessels were functional, I analyzed hypoxia by staining for Hif1a and pimonidazole adducts and found that cancer stem cells were located in normoxic areas, independently of the treatment (Fig. 4A-C).

These results indicate that in the presence of additional mutations, blood vessels associated with Wnt^{high} cancer stem cells share common features with normal stable and quiescent blood vessels. Yet, they actively proliferate independently of Vegf signaling and thus tumors resist to anti-Vegfr-2 therapy.

B.4. Wnt^{high} cancer stem cells remain unaffected by anti-angiogenic therapy

Cancer relapse and treatment resistance are often attributed to the presence of cancer stem cells^{198,199}. As DC101 treatment did not affect AKP organoid tumor growth and had only a mild effect on CD44^{high}-associated blood vessels, I wanted to assess if the treatment affected cancer stem cells. I analyzed tumor cell proliferation and found that the majority of proliferating cells were CD44^{low} or Prox1^{low}, independently of the treatment (Fig. 4D-E). I also did not find any difference in CD44^{high} or Prox1^{high} proliferation upon the control- or DC101 treatments, suggesting that anti-angiogenic treatment was ineffective against cancer stem cells (Fig. 4E). As shown in Fig. 1B, we previously found that epithelial crypt cells remained in relative normoxia, even after crypt expansion (data not shown). I then next examined the relative pO₂ status of CD44^{high} and CD44^{low} epithelial cells after DC101 treatment. Staining

for both Hif1a and pimonidazole adducts showed that hypoxia was significantly higher in CD44^{low} cells, as well as in the surrounding stroma, compared to CD44^{high} (Fig. 4A). Additionally, even though DC101 treatment decreased overall hypoxia in our AKP model, CD44^{high} cells were more normoxic compared to CD44^{low} (Fig. 4B). Finally, the pool of CD44^{high} or Prox1^{high} expressing cells was not affected by DC101 treatment, but, surprisingly, even slightly increased (Fig. 4F).

Together, these observations suggest that tumorigenic intestinal stem cells actively organize a stable and mature blood vasculature. Therefore, therapies targeting Vegf signaling used in

Figure 4

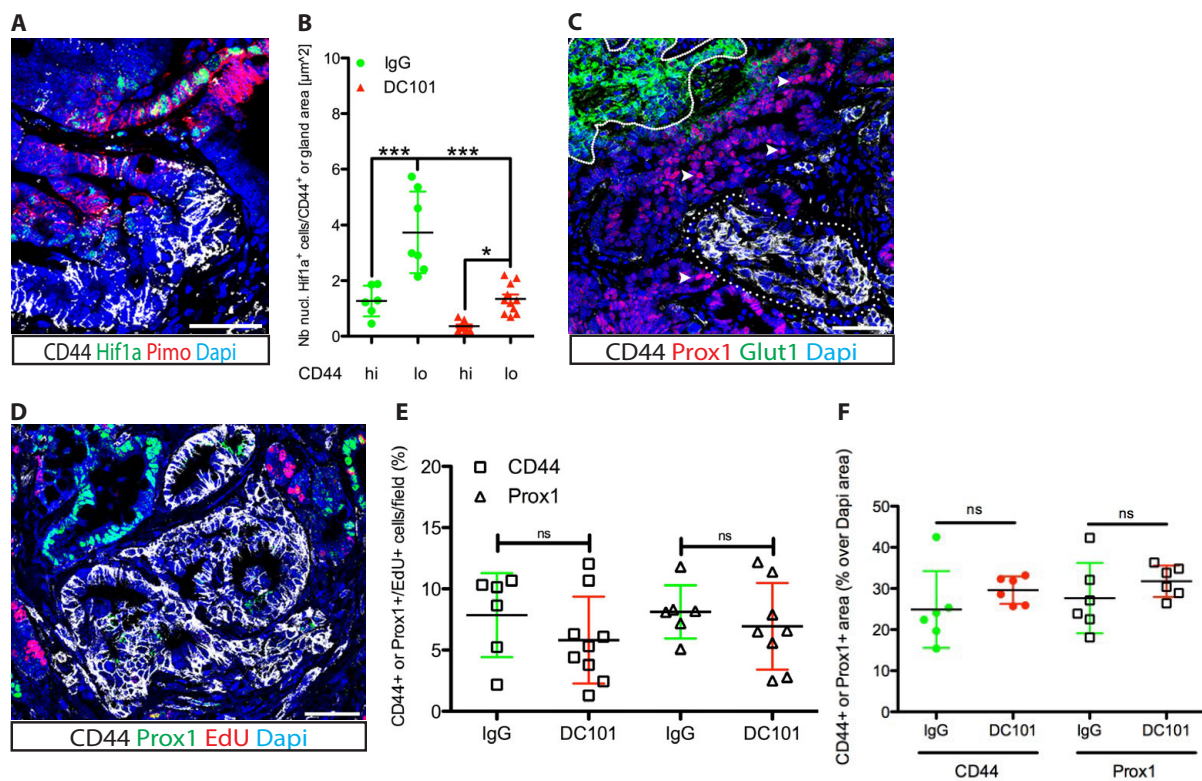


Figure 4. Wnt^{high} cancer stem cells reside in a normoxic niche and are resistant to Vegf blockade.

AKP tumors. (A) CD44⁺ cells are Hif1a⁺ and pimonidazole. (B) Number of Hif1a⁺ cells according to CD44 expression (hi=high, lo=low). Numbers are normalized to quantified area (n=6-11/group). (C) Mutual exclusivity of CD44⁺, Prox1⁺ and Glut-1⁺. (D) Low proliferation of CD44⁺ or Prox1⁺ cells compared to more differentiated cells. (E) Percentage of proliferative CD44⁺ or Prox1⁺ stem cells in IgG or DC101 treatment (n=6-9/group). (F) Normalized CD44⁺ or Prox1⁺ areas in IgG or DC101 treatment (n=6/group). Statistics: Data are shown with mean ± S.D. One-way ANOVA; ns p > 0.05, *p < 0.05, ***p < 0.001. Scale bars: 50 μm, A, C, D.

patients with Wnt^{high} CRC would eventually kill differentiated cells and their associated blood vessels, but the cancer stem cells and their vasculature would remain unaffected.

B.5. Decreased VEGF signaling in human WNT^{hi} colon cancer

The results in animal models prompted us to ask whether VEGF signaling is differentially regulated in blood vessels from human CRC, especially in WNT^{hi} tumors. Indeed, Guinney *et al.* showed that the expression of VEGF signaling-related genes was significantly downregulated in WNT^{hi} CMS2 human tumors, supporting our previous analysis⁵⁸. In collaboration with Prof. C. Sempoux (IUP), I hence analyzed by immunohistochemistry 48 human colon adenocarcinoma samples with matched normal tissue (summary Fig. 5B, patient details in Table 1 and 2). First, WNT status was determined by immunostaining for nuclear β -CATENIN and PROX1. WNT^{hi} tumors (Fig. 5A and 5G, top panels) were designated as such if both β -CATENIN and PROX1 were highly expressed throughout the tumor (correlation β -CATENIN and PROX1: Pearson score $r = 0.3301$, $p = 0.0219$; inter-observer reliability: $\kappa=0.88$ and 0.938 for β -CATENIN and PROX1, respectively). WNT^{neg} tumors were negative for both markers (Fig. 5G, bottom panels). Next, I performed immunostaining for CD31 and ESM1 to assess VEGF signaling status in WNT^{hi} and WNT^{neg} tumors. While no difference was observed in overall tumor vessel density (Fig. 5C, top panels), vascular ESM1 expression was significantly lower in WNT^{hi} compared to WNT^{neg} tumors (inter-observer reliability for ESM1: $\kappa=0.889$; Fig. 5C, bottom panels). I also confirmed previous reports demonstrating the presence of increased angiogenesis in MSI tumors, decreased β -CATENIN expression and a tendency to decreased PROX1 expression (Fig. 5D-F and Ref²⁰⁰). Indeed MSI tumors displayed higher ESM1 expression in comparison to MSS tumors (Fig. 5D). Since in our mouse models of Wnt^{hi} tumors we observed a compartmentalized tumor vessel phenotype according to the epithelial differentiation status (Figs. 1A, 2A, 3M), I next sought to investigate if such compartmentalization could be found

in human WNT^{hi} tumors. As previously reported²⁰¹, nuclear β -CATENIN and PROX1 distribution was heterogeneous within the same sample and thus WNT^{hi} tumors were subdivided into WNT^{hi} -high (WNT^{hi} -H) or WNT^{hi} -low (WNT^{hi} -L) areas based on PROX1 and nuclear β -CATENIN expression (Fig. 5A and data not shown). Consistent with the observations in WT and *Apc* ^{Δ IEC} small intestine, WNT^{hi} -H areas had significantly lower vessel density and ESM1 expression compared to WNT^{hi} -L areas (Fig. 5C, right panels). However, CD44^{high} areas in AKP tumors were associated with increased vascular density. The tumor or mouse model used or the stem cell markers selected for the analysis might explain this discrepancy.

Altogether, these results confirm our previous observations in animal models and suggest that WNT^{hi} tumors have significantly less VEGF signaling than other subtypes. Hence, we emphasize that WNT^{hi} colon cancer have low VEGF-mediated angiogenesis which make these tumors intrinsically resistant to antiangiogenic therapies and suggest the activation of alternative pathways for tumor growth.

Figure 5

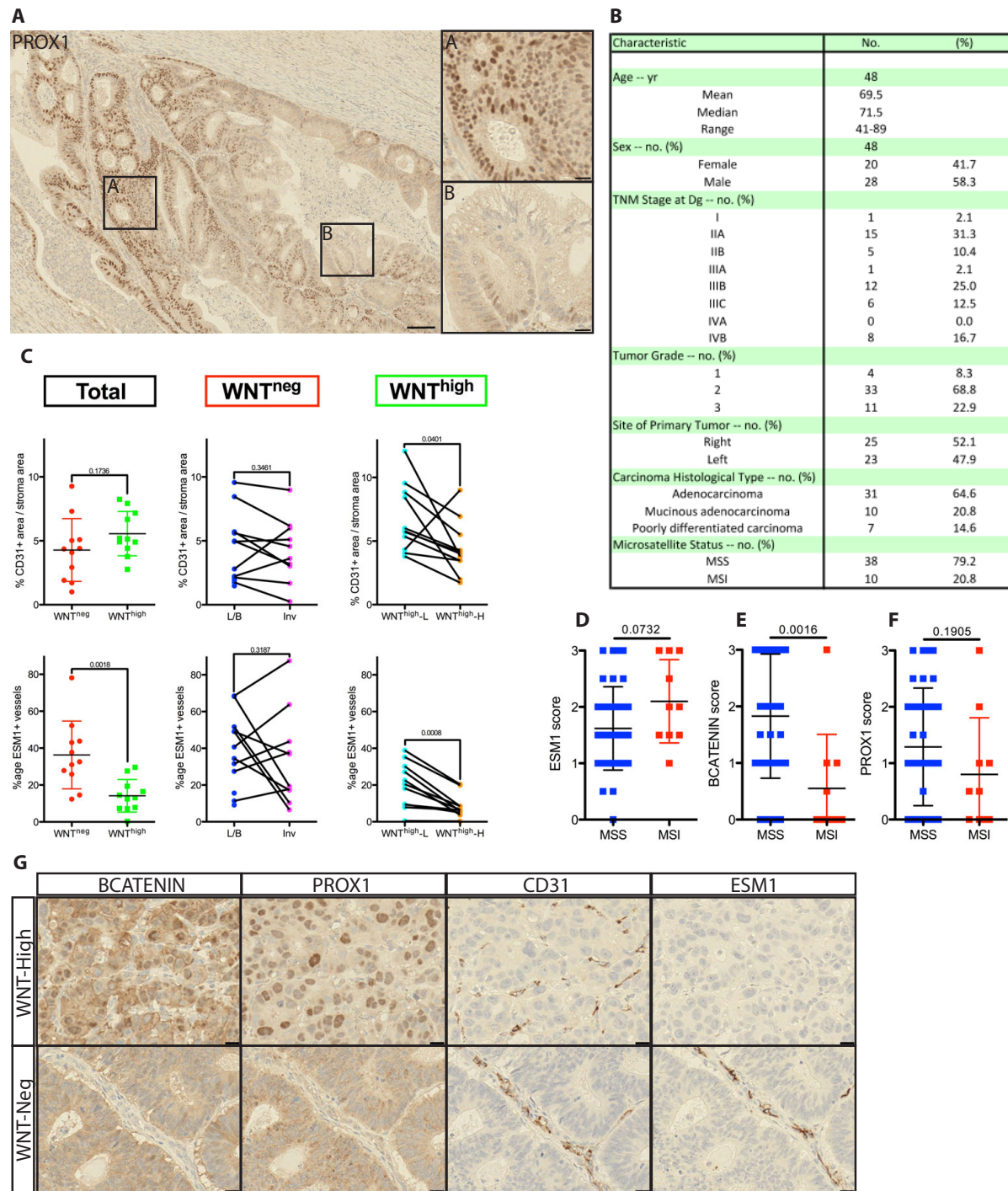


Figure 5. Reduced VEGF signaling in WNT^{high} human colon cancer

(A) Representative picture of PROX1 heterogeneous expression in a WNT^{high} tumor. High magnification in a $PROX1^{high}$ area (insert A) and high magnification in a $PROX1^{low}$ area (insert B). (B) Patients and tumors characteristics. (C) Scatter plots comparing WNT^{high} and WNT^{neg} tumors (left panel). Scatter plots with matched samples in WNT^{neg} tumors (middle) and WNT^{high} tumors (right panels). Top column represents the vascular density and bottom column the percentage of ESM1⁺ blood vessels. Tumor heterogeneity was assessed comparing luminal/bulk (L/B) vessels to vessels at the invasive front (inv) in WNT^{neg} tumors and vessels in WNT^{high} or WNT^{low} area of WNT^{high} tumors ($WNT^{high-H/L}$, resp)(n=10-11/group). (D) ESM1, (E) BCATENIN and (F) PROX1 score in tumors according to microsatellite status (MSS: n=38, MSI: n=10). (G) Representative pictures of tumors with high or low WNT signaling (shown by PROX1 and BCATENIN IHC) and the associated blood vasculature. Datas are shown with mean \pm S.D. Unpaired two-tailed Student T-test. Scale bars: 100µm, A; 20µm, inserts and G.

B.6. Co-culture of AKP organoids and endothelial cells shows anti-angiogenic effect and non-responsiveness to VEGF treatment *in vitro*

In order to study whether AKP organoid and specifically cancer stem cells can directly affect blood endothelial cell growth and patterning, I co-cultured AKP organoids with MS-1 endothelial cells that were previously transduced with a lentivirus expressing GFP²⁰² (schematic view Fig. 6A). MS-1 is an immortalized mouse blood endothelial cell line derived from pancreatic islets (hereafter: MS-1). In such device, endothelial cells, fibroblasts and organoids are seeded in three different channels, and endothelial cells sprout and expand in response to the gradient of VEGF-A and other factors produced by fibroblast and/or tumor cells. Interestingly, already in control conditions EC migration across the central channel was significantly decreased in the presence of AKP organoids (Fig. 6C). Furthermore, while addition of VEGF enhanced migration and sprouting of control ECs, such behavior was strongly attenuated in the presence of cancer cells (Fig. 6D). Finally, while control- or VEGF treated MS-1 cells were growing as a highly proliferating angiogenic front (Fig. 6B, top panel with star and Fig. 6E) with tip cells sprouting at the edge, AKP organoids suppressed this phenotype and induced formation of isolated endothelial sprouts (Fig. 6B, bottom panels and Fig. 6E).

Figure 6

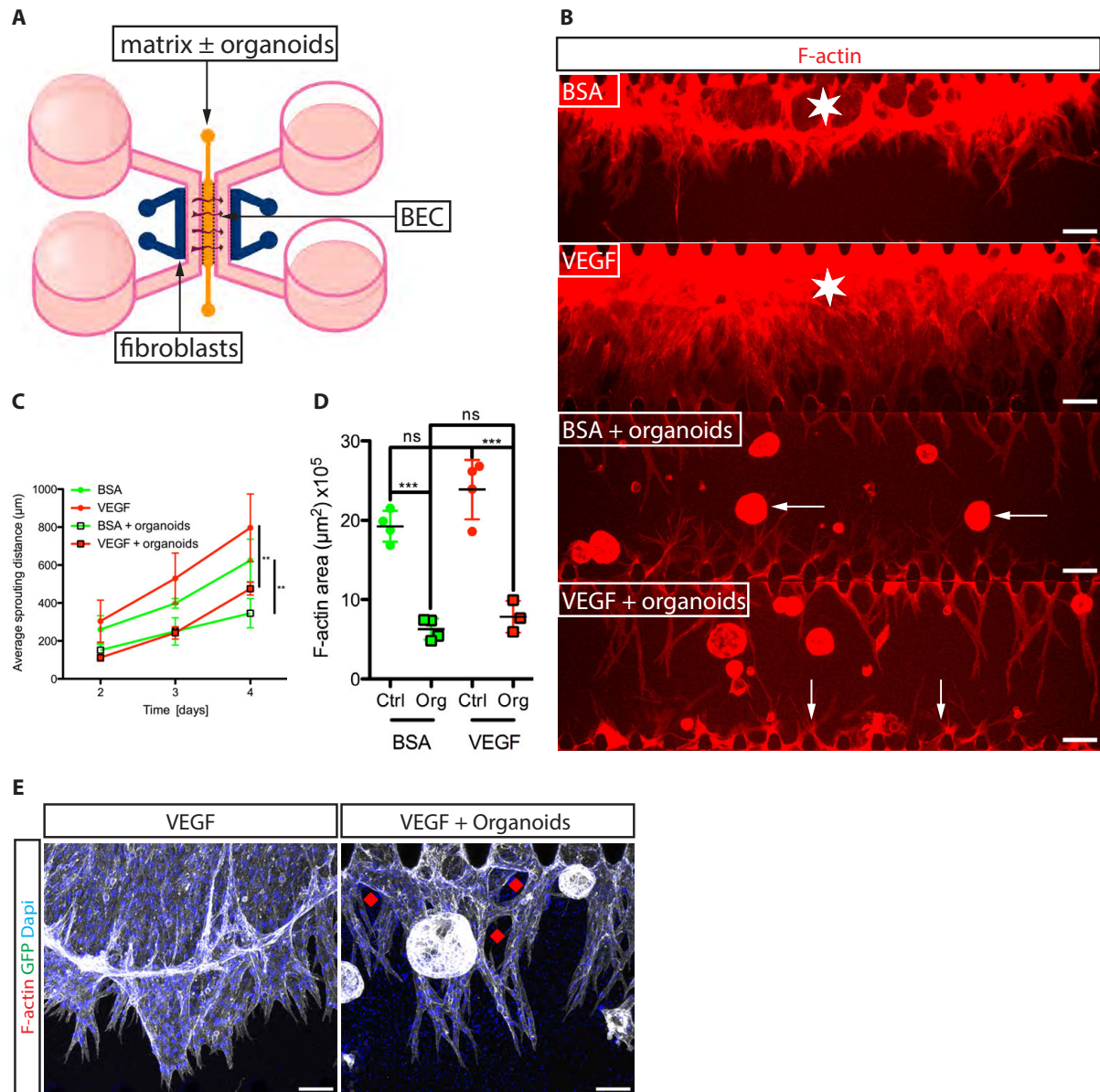


Figure 6. AKP organoids prevent BEC migration and decrease VEGF response in a 3D co-culture system.

(A) Schematic view of the 3D microfluidic co-culture system. Fibroblasts are seeded on the left channel, AKP organoids in the central channel and BECs in the right medium channel. Laminar flow (curved arrows) is applied from left to right concomitant with BSA or VEGF gradient (courtesy of Esther Bovay). (B) Representative pictures of BSA- or VEGF-stimulated BECs after 3 days. BECs (star) and AKP organoids (horizontal arrows) are stained for F-actin (vertical arrows = fibroblasts). (C) BECs migration over time upon BSA or VEGF stimulation in the presence/absence of AKP organoids. (D) BECs-specific F-actin areas within the central channel with (Org) or without (Ctrl) AKP organoids, after 3 days. (E) Cell immunofluorescent staining showing the central channel. Presence of an angiogenic front with numerous small sprouts in the absence of organoids. BECs form individual and well patterned vessel when co-cultured with organoids. Red diamonds indicate acellular space. Statistics: Data are shown as mean ± S.D. One-way ANOVA; ns $p > 0.05$, ** $p < 0.01$, *** $p < 0.001$. Scale bars: 100µm, B; 200µm, E.

Altogether, these *in vitro* results show that colon cancer cells with high Wnt signaling can directly modulate EC behavior. In particular, they prevent uncontrolled outgrowth of endothelial cells, likely by releasing soluble factors that modulate EC proliferation and patterning. These experiments still need to be completed by assessment of EC proliferation and Vegf activation by immunostaining. Moreover, assessment of EC sprouting phenotype when co-cultured with MC38 cancer cells could demonstrate the importance of Wnt^{high} cancer cells in blood vessel remodeling.

B.7. Cancer stem cell- and endothelial cell- derived Sema3f and Apelin reduce vessel outgrowth and induce anti-angiogenic resistance

As a last step, we addressed the molecular mechanisms regulating Vegf-independent vascular expansion and patterning by Wnt high tumors. Blood endothelial cells were sorted from the wild type or *Apc*^{ΔIEC} intestine and their transcriptomes were identified by Affymetrix Mouse Gene 1.0 ST Array. Bioinformatics analysis of differentially expressed genes revealed that two secreted proteins, Class 3 Semaphorin F and Apelin, were in the top 10 of the most induced genes in blood endothelial cells from *Apc*^{ΔIEC} mice (Fig. 7A). Class 3 Semaphorins bind to Neuropilin 1-2 and PlexinA1-4 receptors (see A.3.11.). They are negative regulators of sprouting angiogenesis through inhibition of the PI3K/Akt pathway and by suppression of *Vegf* expression²⁰³. In particular *Sema3F* was shown to be highly expressed in the avascular zone of the retina and to inhibit Vegf-driven vascular outgrowth and sprouting²⁰⁴. Although Sema3F is typically described as having a tumor suppressor function in range of animal models and in human malignancies²⁰⁵, surprisingly it is highly expressed in tumors derived from patients with familial adenomatous polyposis (FAP) syndrome²⁰⁶ and *Sema3F* expression was described in normal intestinal stem cells²⁰⁷. I therefore wanted to confirm by qPCR *Sema3F* expression in the FAC-sorted intestinal endothelial and epithelial cells as well as AKP organoids and found similar expression between the two cell types (Fig. 7B).

Figure 7

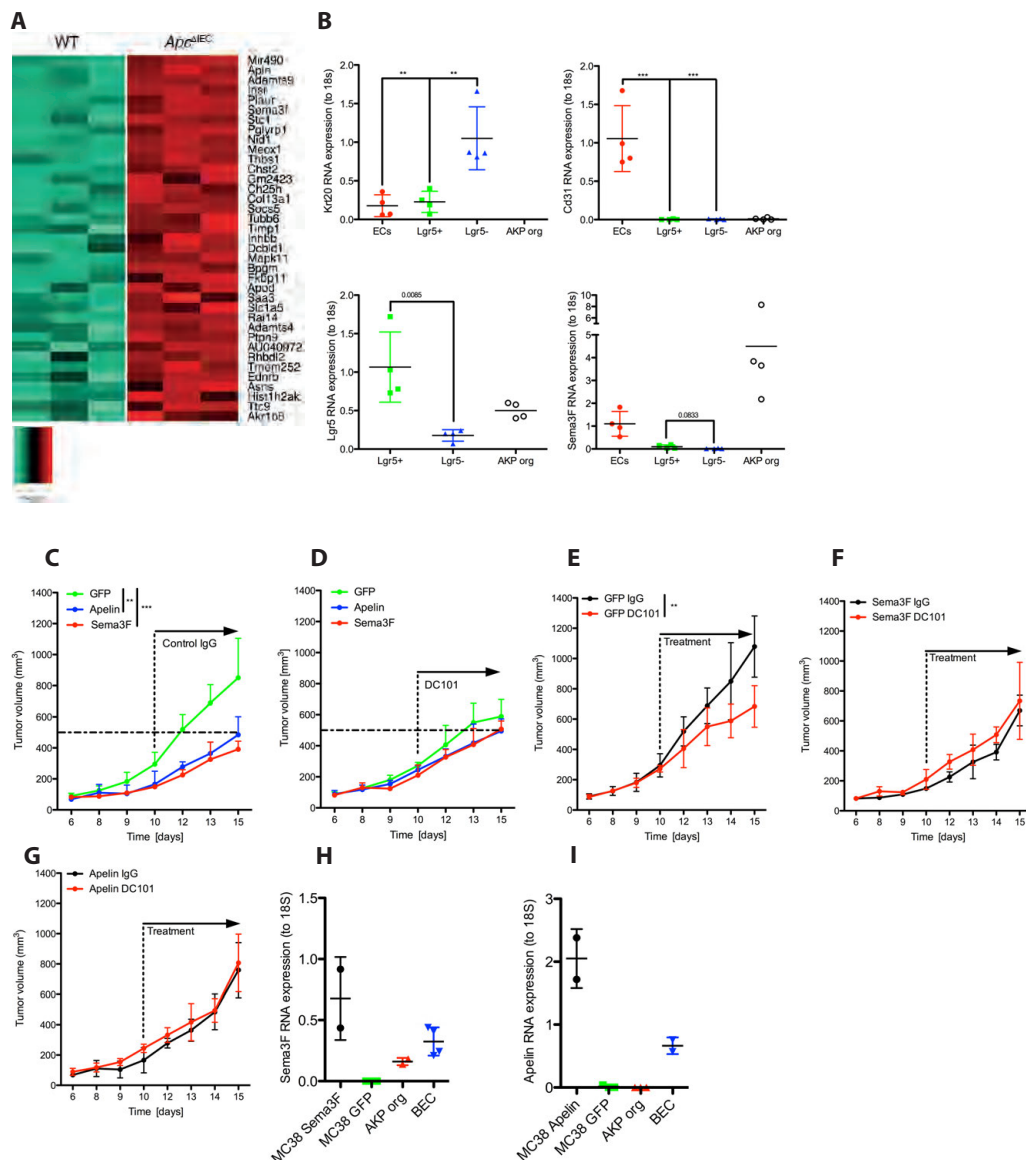


Figure 7. Apelin and Sema3F induce resistance to anti-Vegf treatment in MC38 tumors.

(A) Microarray analysis of FAC-sorted endothelial cells in control WT and in *Apc-Villin-Cre^{ERT2}* mice (data by Drs J. Bernier-Latmani and N. Zangger). (B) qPCR analysis of FAC-sorted endothelial cells, Lgr5^{+/−} cells from *Apc-Lgr5eGFP-Cre^{ERT2}* mice and AKP organoids cultured *in vitro*. RNA expressions are normalized to 18S (n=4/group). Tumor growth of (C) MC38 overexpressing GFP (control), Apelin or Sema3F treated with a control IgG (n=2-3/group). (D) MC38 overexpressing GFP (control), Apelin or Sema3F treated with a DC101. (n=2-3/group) (E) MC38 overexpressing GFP (control) treated with IgG or DC101. MC38 overexpressing (F) Sema3F or (G) Apelin treated with IgG or DC101. qPCR analysis for (H) Sema3F or (I) Apelin of transduced compared to AKP organoids cultured *in vitro* and FAC-sorted BEC from the normal mouse intestine. Statistics: Data are shown with mean ± S.D. B, Top row: One-way ANOVA; **p < 0.01, ***p < 0.001. Bottom row: Unpaired two-tailed Student t-test; C-G, Two-way ANOVA with repeated measures; **p < 0.01. C-D, Horizontal bar = 500mm³.

Interestingly, preliminary qPCR results suggest that other class 3 Semaphorins are expressed in AKP organoids, as well as in FAC-sorted Lgr5 intestinal stem cells (data not shown). Although these findings still need to be confirmed with more samples, they globally

indicate that rather paradoxically colon cancer endothelial cells as well stem cells produce high levels of *Sema3F*, and other class 3 Semaphorins, which are usually associated with angiogenesis suppression and inhibition of tumor growth²⁰⁸.

In order to assess if *Sema3F* is sufficient to inhibit Vegf-a driven angiogenesis in tumors, I overexpressed *Sema3F* in MC38 cells using lentiviral transduction (Fig. 7H) and injected them subcutaneously in immunocompetent mice (Fig. 7C and 7F). As described for other models, overexpression of *Sema3F* reduced but did not completely abolished growth of MC38 tumors (Fig. 7C). Most importantly, while the control MC38-GFP tumors were highly sensitive to Vegf inhibition with DC101, the growth of MC38-*Sema3F* tumors was not affected (Fig. 7E and 7F).

Our microarray analysis between control and *Apc*^{ΔIEC} intestinal FAC-sorted BECs also revealed *Apelin* as the second most induced gene (Fig. 7A). As discussed previously (see A.4.10.), *Apelin* is an endothelial-specific peptide, which previously was shown to promote BEC proliferation and survival after binding to its G protein-coupled receptor *Apj* and to induce a “normalized” phenotype when overexpressed in tumors cells^{209,210}. I first confirmed absence of expression in MC38 and transformed intestinal stem cells (Fig. 7I). Then, overexpression of *Apelin* in MC38 tumors resulted in comparable tumor growth impairment as for MC38 tumors overexpressing *Sema3F* (Fig. 7C). Additionally, *Apelin* overexpression suppressed DC101-induced tumor inhibition (Fig. 7G).

Altogether, these results show that *Sema3F* is expressed both in intestinal blood endothelial cells and normal and transformed intestinal stem cells. Likewise, *Apelin* is induced in endothelial cells after epithelial *Apc* deletion. Both secreted proteins were able to induce resistance to anti-Vegf treatment in previously sensitive MC38 tumors, thus confirming their

roles in colon cancer angiogenesis. Nevertheless, given the small number of animals used for this pilot study (n=2-3/group), further confirmation with a larger cohort is required. Moreover, histologic analysis of tumor vascular density, EC proliferation and hypoxia would allow for better understanding of the mechanisms of action of Apelin and Sema3F in tumors.

To summarize, we propose that Wnt^{high} colon cancer stem cells produce Sema3F to actively prune and repress Vegf signaling in the surrounding blood endothelial cells. Moreover, they induce high levels of *Apelin* expression in endothelial cells, promoting vascular proliferation and expansion (Fig. 8). However, what triggers *Sema3F* expression in colon cancer stem cells and what signaling pathways leads to *Apelin* expression remain unknown.

Figure 8

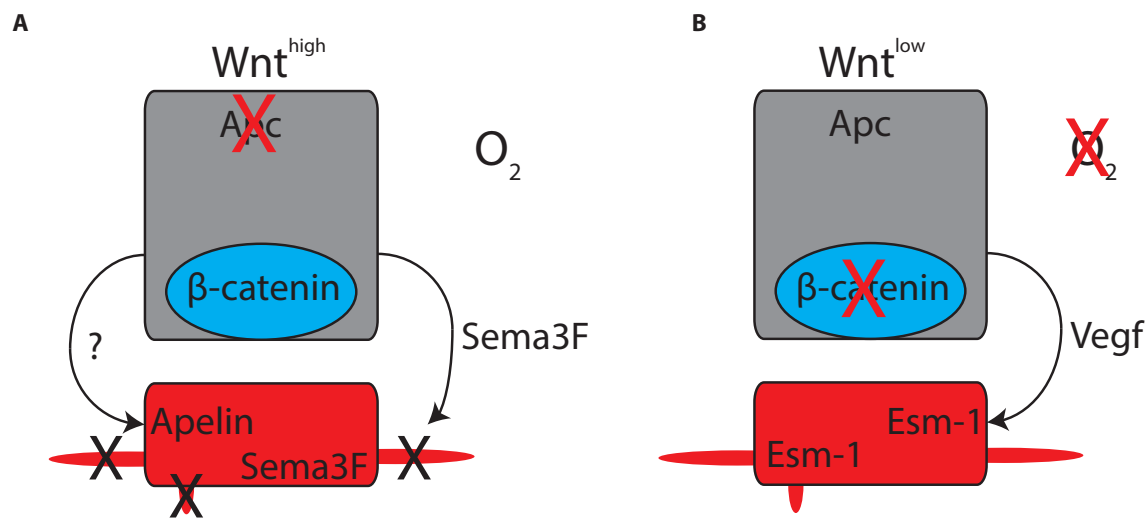


Figure 8. Proposed mechanism of vascular remodeling by Wnt^{high} colon cancer stem cells.

(A) Normoxic Wnt^{high} colon cancer stem cells produce and secrete Sema3F, preventing Vegf-mediated sprouting angiogenesis. Moreover, *Sema3F* expression is also induced in endothelial cells. Additionally, Wnt^{high} colon cancer cells induce endothelial *Apelin* expression which enable expansion of the tumor vasculature. ?: unknown factor inducing *Apelin* expression in endothelial cells. (B) On the contrary, Wnt^{low} cells reside in hypoxia, which induces the expression of *Vegf* and Vegf-driven endothelial cell proliferation and sprouting, as demonstrated by *Esm-1* expression.

3. Discussion

Here, we report that in multiple pre-clinical mouse models of Wnt^{hi} colon cancer, intestinal (cancer) stem cells actively regulate their surrounding microenvironment, orchestrating a

stable vascular network to maintain a normoxic niche. Moreover, we uncovered a Vegf-independent mechanism of blood vessel remodeling within crypt- and cancer stem cells that relies on the pro-angiogenic Apelin and the chemorepulsive Sema3F. These results highlight the need to study tissue- and tissue compartment-specific blood vessel formation and expansion. The molecular mechanisms exposed in that study have three main outcomes: 1) multiple pro-angiogenic and anti-angiogenic factors acts simultaneously in physiological and pathological conditions and influence together the final vascular phenotype. We therefore need to investigate these angiogenic factors together, and in the context of the local microenvironment. 2) Cancers arising from the same organ display different molecular signatures that influence the surrounding stroma and hence the vascular system. Distinct molecular pathways thus differentially regulate the tumor vasculature and modulate the potential response to antiangiogenic therapies. 3) Despite >10 years of the anti-VEGF blocking antibody bevacizumab approval for the treatment of metastatic colorectal cancer and the extraordinary advances in the field of angiogenesis and tumor angiogenesis, markers that predict response or resistance to anti-VEGF remain elusive. Here we suggest that patients with metastatic colon cancer where the primary tumor, or its corresponding metastases, carry a stem cell signature with active WNT signaling (CMS2⁵⁸), would not benefit from bevacizumab treatment, or any VEGF-targeting agents.

To understand how intestinal stem cells actively regulate their vascular supply, we first observed that blood vessels were differently organized (Fig. 1A) and expressed different markers within the two physiologically distinct intestinal compartments, crypt and villus (Fig. 1C-E). The intestinal stem cell niche was indeed associated with a sparse but stable vascular network maintaining a normoxic microenvironment in the crypts. Interestingly, vascular heterogeneity have been observed in the murine bones, where CD31^{high} and Endomucin^{high} blood vessels (type H vessels) have been associated with osteoprogenitors,

on the contrary to sinusoidal vessels expressing low levels of both markers²¹¹. Moreover, hematopoietic stem cells (HSCs) have been described in close relationship with blood vessels. However, unlike intestinal stem cells, the HSCs niche was found in a hypoxic microenvironment^{212,213}. Similar observations of proximity between blood vessels and progenitor cells were made in the testis and in the central nervous system^{214,215}. Organ-specific blood vessels are therefore important regulators of the maintenance of tissue stem cells, as a source of oxygen and nutrients. Indeed, it was recently shown that Lgr5+ intestinal stem cells rely on mitochondrial metabolism and disruption of oxidative phosphorylation strongly affected stem cell functions²¹⁶.

We further investigated the role of Vegf signaling between crypt and villus and found that crypt vessels, but not villus vessels, were resistant to Vegf blockade in wildtype and precancerous intestinal lesions after specific epithelial *Apc* deletion with the intestine (Fig. 2B). These results confirmed previous reports where vascular density in villus vessels was decreased after administration of a soluble decoy receptor for VEGF, a small molecule VEGFR tyrosine kinase inhibitor or an antibody to Vegfr2^{217,218}. Moreover, Yamasaki *et al.* described the need of fenestrated endothelia in a renal cell carcinoma model for anti-Vegf optimal response, and Vegf induces and maintain fenestrations in endothelial cells *in vitro*^{117,219,220}. Yet, intestinal capillaries are highly fenestrated, therefore Vegf activity is differently regulated in the crypt-villus axis.

However, while previous studies focused on which vessels were sensitive to Vegf blockade, e.g. the intestinal villus, none addressed the mechanisms of resistance in non-responding crypt vessels. Here we show the direct relationship between crypt expansion upon activation of the Wnt signaling and the corresponding vascular network enlargement. Interestingly, we found that expanded crypt vessels didn't depend on Vegf signaling but rather on alternative angiogenic pathways. Additionally, increased number of stem or progenitor cells induced

endothelial cell proliferation (Fig. 2F). We therefore concluded that stem cells actively induced vascular remodeling by fine-tuning pro- and anti-angiogenic factors. Our study highlights the active role of stem cells in vascular regulation, where most previous studies focused on the roles of (myo-) fibroblasts or immune cells, such as macrophages, neutrophils or mast cells^{145,221–223}.

In vitro culture of intestinal organoids is a powerful tool to study stem cell/niche functions and tissue response to mutations and physical damage²²⁴. Here, we used tumorigenic intestinal organoids, which recapitulate advanced CRC and form moderately differentiated tumors composed of glands with high nuclear β -catenin and little stroma. We first demonstrated that Wnt activation in advanced tumors conferred resistance to anti-Vegf treatment (Fig. 3C-D). However, Wnt signaling in tumor cells was heterogeneous, which affected the surrounding blood vasculature. We found that, in Wnt^{high} areas, the blood vascular network displayed low Vegf signaling (Fig. 3K-M) and that both cancer stem cells and the surrounding microenvironment were located in normoxia (Fig. 4A-B). We hypothesized that despite the fact that anti-Vegf treatment reduced globally vascular density (Fig. 3E), remaining blood vessels were capable of maintaining normoxia and provide nutrients to stem cells. Indeed, Vegf-a blockade did not affect tumor growth (Fig. 3C-D). We even found a tendency towards increased relative proportion of Cd44^{high} and Prox1^{high} cells after DC101 treatment (Fig. 4F), and β -catenin nuclear localization remained unchanged (data not shown). Definitive suppression of Vegf signaling in Wnt^{high} tumors could thus paradoxically favors stem cell phenotype.

To assess the clinical relevance of our observations in animal models, we analyzed human colon cancer samples. We found that when both canonical WNT markers nuclear β -CATENIN and PROX1 are present (WNT^{high}), tumor vascular density remained similar

compared to WNT^{low} tumors. However, VEGF signaling was decreased, demonstrated by significantly reduced *ESM1* expression (Fig. 5C and 5G). These results confirm at the protein level previous transcriptome analysis of the consensus molecular subtypes (CMS) in CRC⁵⁸. Indeed, 37% of all CRC were associated with high levels of WNT signaling and so-called CMS2 tumors had low activation of the VEGF pathway. Interestingly, 52% of primary left tumors are CMS2 (Ref⁵⁸ and Dienstmann ASCO meeting 2015) and retrospective analysis assessing the role of primary tumor localization on patient prognosis and treatment response suggested worse outcome when patients with left tumors were treated with bevacizumab. On the contrary, patients with right tumors benefited from the addition of anti-VEGF treatment⁴⁸. MMR-deficient CRC are predominantly observed in the right colon and microsatellite instability was associated with increased serum VEGF-A concentrations, increased angiogenesis and significant survival benefit when bevacizumab was added to conventional chemotherapies, as compared to patients with microsatellite stable (MSS) tumors^{200,225}. We confirmed that *ESM1* expression was higher in MSI tumors (denoted by loss of MLH1 expression in IHC) and that both β -CATENIN and PROX1 were downregulated (Fig. 5D-F).

Other cancer types demonstrated global non-responsiveness to antiangiogenic treatment, such as glioblastoma (GBM), ovarian cancer or breast cancer⁸⁰. Nonetheless, Sandmann et al. showed that the specific proneural GBM subtype led to patient improvement with the treatment²²⁶. Similarly, a VEGF-dependent gene signature has been described to positively correlate with mesenchymal subtype and BRCA mutations in ovarian cancer, which suggests potential benefit from bevacizumab treatment²²⁷. However, Wnt-driven mammary carcinoma express progenitor cell markers and are resistant to Vegf blockade²²⁸. Importantly, Wnt/ β -catenin signaling was associated with the poor prognosis triple-negative breast cancer which does not benefit from bevacizumab treatment^{229,230}. WNT signaling, stem cell

phenotype and antiangiogenic response might therefore not be unique characteristics of CRC.

Gene expression profiling and mutational status of cancer cells have been associated with differential response to antiangiogenic therapies. Nevertheless, little is known about the organization of the primary tumor and metastatic vasculature and their relationship with anti-VEGF treatments. Interestingly, Reynolds et al., described vascular patterns of colorectal cancer metastasis in the liver, lung metastasis of tumors from various origins and their impact on bevacizumab treatment response^{176,177}. These so-called histopathological growth patterns (HGFs) were divided into desmoplastic, pushing and replacement patterns. The desmoplastic growth pattern, in which tumors are well encapsulated and “independent” from the metastatic site, demonstrated good pathological response to bevacizumab treatment. On the other hand, the replacement HGP, also known as vascular co-option, where metastases profit from the local vasculature, was mostly resistant to the anti-VEGF therapy. These studies confirmed previous observation that replacement growth pattern of CRC liver metastases were mostly non-angiogenic²³¹. Finally, blood vessel architecture and localization within the tumor has also been described as an important factor predicting response to Vegf blockade. Tumors with a dense vascular network throughout cancer cells have been shown to respond to antiangiogenic therapies, whereas tumors with an apparent distance between blood vessels and cancer cells were resistant²³². In fact, we did observe similar vascular patterns between AKP organoid tumors and MC38 tumors. MC38 tumors displayed homogeneous and spread blood vessels in between cancer cells, whereas blood vessels in AKP tumors were restricted to tumor stroma and delimited from cancer cells. It is thus conceivable that in metastatic WNT^{high} CRC, either primary or secondary lesions, display the replacement HGP and are not angiogenic. Instead, they might take advantage of the pre-existing vasculature. Alternatively, WNT^{high} CRC tightly regulate blood vessel development generating a favorable microenvironment for the survival⁵⁸ of cancer stem cells.

Consequently, tumors might be more organized and lack of hypoxia favors a more benign phenotype. Indeed, CMS2 subtype has the best overall survival among all CMS. We therefore suggest that WNT^{high} cancer stem cells, or the global degree of (de-) differentiation of the tumor²³³ would not profit from the adjunction of bevacizumab or any anti-VEGF analog to standard chemotherapy. We further propose to conduct a retrospective analysis of patients with metastatic colorectal cancer treated with bevacizumab and to correlate the consensus molecular subtypes with treatment response.

We described in several pre-clinical mouse models as well as in human samples how Wnt activation promoted Vegf-independent angiogenesis and resistance to Vegf-targeted therapies. We therefore wanted to decipher the molecular mechanisms by which cancer stem cells were able to regulate their blood vascular network. We thus performed a microarray analysis on FAC-sorted blood endothelial cells from the small intestine of wild type and *Apc*^{ΔIEC} mouse models. Among the ten most differentially regulated genes, *Apelin* and *Sema3F* were highly upregulated in BECs of *Apc*^{ΔIEC} mouse model (Fig.7A). Both proteins are secreted and exert unique angiogenic functions. Apelin has been shown to promote vascular enlargement and pericytes coverage, a phenotype commonly called vascular “normalization”¹³¹. In tumors, Apelin normalized the vasculature when overexpressed in Colon26 mouse colon cancer cell line decreased tumor growth and enhanced immune cell infiltration and anti-tumor immunity²⁰⁹. We confirmed tumor growth inhibition in MC38 overexpressing *Apelin* (Fig. 7C). Detailed analysis by immunohistochemistry is further required to assess blood vessel phenotype. I expect larger tumor vessels with increased mural cell coverage. Additionally, unlike in control MC38 tumors overexpressing GFP, homogeneous distribution of blood vessels might be observed when *Apelin* is overexpressed. Finally, *Apelin* overexpression in MC38 induced resistance to Vegfr-2 blocking antibody (Fig. 7G) and evaluation of vascular density in both control and

DC101 treatment would be needed. These observations need however to be confirmed with a larger cohort of mice but demonstrate a potentially important role of Apelin in WNT^{high} CRC-associated blood vasculature and response to anti-VEGF therapies. Indeed, Apelin expression was increased in patients with colorectal cancer non-responding to bevacizumab²³⁴ and we found that in MC38 overexpressing *Apelin*, mRNA expression was increased after DC101 treatment (data not shown).

Semaphorin 3F has axon guidance repulsive functions and anti-lymph-angiogenic properties^{204,235,236}. All class 3 Semaphorins and their cognate receptors are broadly known for their inhibition of tumor growth and tumor angiogenesis^{208,237–239}. Studies have shown that chromosomal regions often deleted in small cell lung cancer included *Sema3F* and therefore suggested *Sema3F* be a tumor-suppressor gene *in vitro* and *in vivo*. We found that *Sema3F* expression was increased in endothelial cells from *Apc-Vil-Cre*^{ERT2} intestine (Fig. 7A), but surprisingly as well in FAC-sorted Lgr5+ cells and AKP organoids cultured *in vitro* and *in vivo* in tumors (Fig. 7B and data not shown). Interestingly, high expression of *Sema3F* has been described in patients with Familial Adenomatous Polyposis (FAP) which all have *APC* mutations, as well as in the colon and small intestine from *Apc*^{min/+}-derived mouse adenomas²⁰⁶. This suggests a direct link between Wnt signaling and *Sema3F* expression. We found that Wnt^{high} intestinal and cancer stem cells were localized in a normoxic microenvironment (Fig. 1B, 4A-B). Hypoxia has been shown to suppress *Sema3F* receptor Neuropilin-2 (*Nrp2*) in tumor cells, preventing *Sema3F* signaling, F-actin depolymerization, inhibition of RhoA and thus cell migration²⁴⁰. Normoxic stem cell niche is therefore potentially needed for proper endothelial *Nrp2* expression and hence efficient vascular remodeling from stem cell-derived *Sema3F*.

Sema3F overexpression in cancer cells decreased tumor growth and vascular density¹³⁸. In MC38 tumors, we observed similar results (Fig. 7C) and overexpression of *Sema3F* drove

resistance to Vegf blockade (Fig. 7F). As for *Apelin* overexpressing tumors, detailed analysis of the blood vasculature by immunohistochemistry in MC38 overexpressing *Sema3F* is needed. In addition, results need to be confirmed with higher number of mice.

Despite the roles of Apelin and Sema3F in stem cell associated vasculature, we still don't know what triggers their expression in endothelial cells (Apelin) or in both endothelial and intestinal stem cells (Sema3F). *Apelin* expression has been mostly shown to be modulated by Vegf and hypoxia¹³⁰. However, Tie-2 activation by Ang-1 or Ang-2 similarly induced *Apelin in vitro*¹³¹ and Ang-2 has been described in the intestinal stem cell signature²⁴¹. Ang-2 being secreted, it is a good candidate for the modulation of stem cell-associated blood vessels. Co-culture experiment of AKP organoids with blood endothelial cells would eventually demonstrate induction of *Apelin* expression. We are also currently working on the generation of AKP organoids transduced with lentivirus CrispR-Cas9 KO for Ang-2. Similar co-culture experiment could be performed and absence of *Apelin* expression would demonstrate direct role of Ang-2 signaling in *Apelin* regulation. Generation of MC38 cells overexpressing *Ang-2* might be an interesting model as Ang-2 agonist functions on blood vessels are associated with poor response to Vegf blockade in pre-clinical tumor models. However, dual inhibition of Ang-2 and Vegf significantly hindered tumor growth²⁴²⁻²⁴⁴. This hypothesis opens new therapeutic strategies for WNT^{high} metastatic colorectal cancer. Finally, studies of Apelin have been hampered by the lack of specific antibodies that could be used for routine staining procedures. We therefore suggest using a reporter mouse to identify the expression patterns of Apelin within the intestine and in tumor models.

Antiangiogenic functions of Sema3F are well known, however the mechanisms regulating *Sema3F* expression remain elusive. Here we reported high levels Sema3F in Wnt^{high} cancer stem cells and analysis of human CRC corroborated these results²⁰⁶. *Sema3F* might therefore be a downstream target gene of Wnt signaling and our MC38 cancer cells, which

don't express any of the Wnt target genes (Fig. 3N), neither express *Sema3F*. Using pharmacologic approach, assessment of *Sema3F* expression in AKP organoids where Wnt signaling is inhibited could reinforce the link between stem cell phenotype and antiangiogenic factors. Similar to Ang-2, genetic deletion of *Sema3F* by CrispR-Cas9 technology in AKP organoids could determine its direct role in tumor angiogenesis and response to anti-Vegf targeted therapies.

Altogether, this work provides insight into organ- and tumor-specific regulation of blood vessels. It emphasizes that colorectal cancer is not a unique disease but rather is highly heterogeneous both histologically and transcriptionally. Indeed, previous molecular subtyping demonstrated different level of activation of the VEGF pathway. Our work suggests that colon cancer stem cells actively regulate their blood vasculature independently of the Vegf pathway. Interestingly, intestinal and cancer stem cells express high levels of *Sema3F*, a potent antiangiogenic secreted protein mostly synthesized by endothelial cells and often suppressed by cancer cells. It therefore highlights the need to study the regulation of blood vessel development and maintenance according to the context and the tissue of origin.

D. Materials & Methods

D.1. Cell lines and culture conditions

MC38 mouse colon cancer cells were provided by Dr. J. Schlom (NIH) and cultured in RPMI 1640 Medium (Gibco) supplemented with 10% (vol/vol) heat-inactivated Fetal Bovine Serum (FBS, Gibco) and 1mM Penicillin/Streptavidin (Gibco), here after cRPMI. Cells were split twice a week using Trypsin 0.05% EDTA 1X (Gibco). Human fibroblasts were isolated from human jejunum samples (CHUV). They were kept in DMEM (Gibco) supplemented with 10% (vol/vol) FBS and 1mM Penicillin/Streptavidin, hereafter cDMEM. MS-1 endothelial cells were provided by Prof. M. Gillet (NIH) and cultured in cDMEM. HEK-293T cells were purchased from ATCC and cultured in cDMEM.

All cells were kept as monolayers at +37°C and 5% CO₂ in a humidified incubator and were regularly tested for Mycoplasma contamination by qPCR.

D.2. Intestinal organoid culture

In order to obtain fresh intestinal tumorigenic organoids to culture *in vitro*,

Apc^{fl/fl};Kras^{LSI-G12D};Tp53^{fl/fl};villin-Cre^{ERT2} mice were injected daily with Tamoxifen 1mg/g of mouse diluted in sunflower oil (Sigma-Aldrich). 4 days after from the first injection, intestinal crypts were isolated and cultured in Matrigel (Corning, 356231) as described previously²⁴⁵. Briefly, intestinal organoids were dissolved in Cell recovery solution (Corning), centrifuged at 2000rpm at +4°C and suspended and incubated in TripLE Select 1X (Gibco) in a water bath at +37°C for 5min. TripLE was neutralized with FBS and cells were centrifuged at 2000rpm at +37°C. Cells were washed with ice-cold Phosphate Buffer Saline 1X (PBS, Sigma) and stained and counted with Trypan Blue in a Neubauer chamber (Hemocytometer). Desired number of cells were then mixed with Matrigel (Corning, 356231) and disks of 50µl were incubated in a 24-well plate with advanced DMEM F12 (Gibco) supplemented with

GlutaMAX 1X (Gibco), 1mM Penicillin/Streptavidin, HEPES buffer 0.01M (Gibco) and growth factors B-27 1X (Gibco) and N-2 1X (Gibco), hereafter caDMEM. All cells were kept at +37°C and 5% CO₂ in a humidified incubator and tested for Mycoplasma contamination by qPCR.

Prox1, *Lgr5*, *Ascl2*, *EpCAM* and *Krt20* RNA expression were assessed by RT-qPCR (see section RT-qPCR) in order to confirm expression of epithelial intestinal stem and differentiation markers. For all experiments, intestinal organoids were used from the same mouse at similar passages.

D.3. Human fibroblast isolation and purification

The biopsy was placed in physiological serum and opened in complete RPMI plus fungizone. 48h later, the epithelial cells were scraped off and the villi were cut in small pieces to enhance the digestion process. The latter consisted of 2 x 30 min digestion with CollagenaseA (1mg/ml), Dispase II (2mg/ml) and DnaseI (20 ug/ml) in RPMI. Cells were harvested, counted and plated in a fibronectin coated dish in EBM2 (Lonza). Dead cells were washed out. After 7 days, cells were detached with trypsin and marked with anti-CD44 antibody (Southern Biotech ; 9400-01) in EBM2 for 20 min, then centrifuged and resuspended in purification buffer (PBS 1X 0.1 % human serum albumin) with Sheep anti-mouse IgG linked beads (Dynal ; 110.02) for 30 min. The positive fraction of cells was then purified using Dynabeads magnet and were plated in a fibronectin coated dish in EBM2 (Lonza).

D.4. Vectors and Infection

GFP, Apelin and Sema3F vectors were generated by subcloning *Gfp* (pSD44-GFP vector, our lab), *Apelin* (SV40-Apelin vector, Origene) and *Sema3F* (pCMV6-Sema3F vector,

Origen) into a SFFV.OFP.WPRE vector²⁴⁶ using BamH1 and Sal1 (New England Biolabs). Lentiviral particles were produced in HEK-293T cells by transfecting the vectors of interest with pLVV01 (REV, Nature Technology Corp), pMD2.VSV.G (ENV, Nature Technology Corp), pMDLg/p.RRE (III Gen. Pack, Nature Technology Corp) and pAdvantage (Nature Technology Corp), using CaCl₂. Thirty hours after incubation, HEK-293T cells supernatants were collected, filtered with 0.22µm syringe-filters (TPP) and stored at -80°C until further use.

For MC38 or MS-1 transduction, 100'000 cells were seeded on a 6-well plate. After 24h of incubation, medium was replaced by cRPMI (MC38) or cDMEM (MS-1) and lentivirus-containing medium, in 1:1 proportion. After 12h of incubation, lentivirus-containing medium was changed for cRPMI (MC38) or cDMEM (MS-1) and cells were allowed to recover for 48h. Transfection efficiency was assessed using a Leica Stereomicroscope and by estimating GFP fluorescence in GFP transfected cells and. Only cells with >80% transduction efficiency were used for the experiments. .

D.5. 3D angiogenic assay in a microfluidic device

3D single-central channel microfluidic devices were kindly provided by Prof. Noo Li Jeon²⁰². Human jejunum fibroblasts and MS-1 GFP cells were used as previously described and at <80% confluency. Human jejunum fibroblasts (500'000 cells/ml) and MS-1 GFP (400'000 cells/ml) were mixed in a 2.5mg/ml Fibrin-based matrix (Fibrinogen, 90% clotting elements, Sigma-Aldrich) and seeded in the left channel and right medium chamber, respectively. Right channel was filled with an acellular 2.5mg/ml Fibrin-based matrix. In order to create a pro-angiogenic and prosurvival environment, human jejunum fibroblasts were seeded 24h before the MS-1 GFP. In addition, MS-1 GFP were seeded and incubated vertically for 30 min at +37°C and 5% CO₂ in a humidified incubator to allow endothelial cells sticking to the central channel. The latter was filled with a 2.5mg/ml fibrin-based matrix mixed in equal

proportion with 7.5mg/ml Matrigel (Corning, 356231) with or without AKP organoid single cell (140'000 cells/ml). AKP organoid cells were isolated, cultured and dissociated as previously described. Matrix clotting was obtained by mixing the Fibrin-based or Fibrin/Matrigel-based matrices with 16% Aprotinin 4U/ml (Sigma-Aldrich) and 2% Thrombin 50U/ml (Sigma-Aldrich). Final matrix volume was 50µl, and ~5µl was used per channel. Once inserted into the channels, matrices were allowed to clot for 5min at room temperature and then incubated with 130µl/reservoir of a mix of cDMEM and caDMEM (1:1 in proportion). Interstitial flow was generated in the direction of VEGF gradient to promote MS-1 GFP migration.

For each experiment, cells were treated with human recombinant VEGF-A (50ng/ml, gift of Kari Alitalo and Michael Jeltsch, Helsinki University) or Bovine Serum Albumin (BSA, 50ng/ml). Brightfield and fluorescent pictures were taken at 2, 3 and 4 days after MS-1 GFP seeding, with a cell Stereomicroscope (Leica). GFP images were exported and analysed in FIJI version 1.0. Alternatively, microfluidic devices were washed 2x with ice-cold PBS supplemented with MgCl₂ and CaCl₂ (PBSs, Sigma), fixed for 15min with paraformaldehyde 4% (PFA 4%, Sigma-Aldrich) at room temperature (RT), and permeabilized with 0.1% Triton X-100 (Sigma-Aldrich) for 15min at RT. Microfluidic devices were then blocked with a 3% BSA blocking buffer for 30min at RT, incubated in inclination with primary antibodies overnight (O/N) at +4°C, and then 3h in inclination with secondary antibodies at RT (Primary and secondary antibodies are listed in Table 5). Microfluidic devices were kept in PBSs until pictures were obtained. Fluorescent and bright field images were obtained using a Leica Cell Stereomicroscope DM13000B. Alternatively, confocal images were obtained using a Zeiss LSM 780. Images were analysed using Imaris (Bitplane) and FIJI version 1.0 (NIH).

D.6. Animals and tumor xenografts

Eight to 12 week-old female NOD-scid; IL-2R γ ^{-/-} mice (NSG, Jackson Lab) and C57BL/6J01aHsd mice (C57, Envigo) were used for tumor xenograft experiments. MC38 were split 48h prior subcutaneous implantation in order to achieve subconfluency. On day of injection, cells were harvested with 0.05% trypsin (Gibco), washed and suspended in ice-cold sterile PBS. Cells were counted with a Neubauer chamber and suspended in ice-cold sterile PBS to final cell concentration of 10⁷ cells/ml. 100 μ l of cell solution (1X10⁶cells/mouse) was injected subcutaneously in the right flank under isoflurane anesthesia. When tumor size reached 200mm³, mice were treated 2-3x a week with 40 μ g/g of mouse weight of an anti-Vegfr-2 monoclonal antibody (DC101, BE0060, BioXCell), or a control rat anti-horseradish peroxidase IgG (HRPN, BE0088, BioXCell). Tumor length and width were measured with a caliper (Sylvac) and the volume was calculated using the formula for an ellipsoid ((length*width²* π)/6). Mice were injected intraperitoneally (i.p.) with EdU (2mg/ml, Invitrogen) and Pimonidazole (12mg/ml, Hypoxyprobe) 1h and 30min prior sacrifice, respectively.

Apc^{fl/fl}, *p53*^{fl/fl}, *Kras*^{G12D}, *Apc*^{min/+}, *Lgr5-eGFP-Cre*^{ERT2} and *Villin-Cre*^{ERT2} mice were previously described^{190,247–250}. Cre-mediated deletion was induced in 8-12 week-old mice either by i.p. (50mg/ kg mouse) or subcutaneous injection (100mg/ kg mouse) of Tamoxifen diluted in sunflower oil (Sigma-Aldrich). DC101 and control IgG were delivered as previously described (BE0060 and BE0088, resp. BioXCell).

For intestinal organoid implantation and subsequent organoid tumor xenograft generation, organoids were dissociated and plated in 50 μ l-disks of Matrigel (Corning, 356231) at 10'000 cells/disk. After 72h in culture, Matrigel was dissolved by Cell recovery solution, spheroids were centrifuged at 600rpm at +4°C, washed in ice-cold PBS and suspended in Matrigel (Corning, 356234) and caDMEM, in a 1:1 proportion. Spheroids were then implanted s.c. in

the right flank of NSG mice with a 20G needle, under isoflurane anesthesia. When tumor size reached 200mm³, mice were treated with DC101 or a control IgG, as previously described. Mice were injected intraperitoneally (i.p.) with EdU (2mg/ml, Invitrogen) and Pimonidazole (12mg/ml, Hypoxyprobe) 1h and 30min prior sacrifice, respectively.

D.7. Mouse tissue and tumor xenografts collection, staining procedures and image acquisition

For subcutaneous tumor xenografts, experiments were stopped when sacrifice criterias were fulfilled according to the score sheet. Sacrifice was performed by general anesthesia with 10% Ketazol and 8% Xylazol followed by cardiac exsanguination with PBS 1X and tissue fixation with PFA 4%. Tumors were then fixed in PFA 4% overnight (O/N) at +4°C, washed with PBS 1X and weighted after removal of excessive skin on a Denver Instrument S-234. Tumors were finally embedded into paraffin.

Alternatively, small intestine whole-mount staining was performed as in Bernier-Latmani *et al.*, *JCI* 2015⁵. Briefly, after sacrifice was performed as previously described, small intestines were dissected in ice-cold PBS 1X, cleaned, cut longitudinally, and pinned on silicon plates. Intestines were then fixed overnight at +4°C in 15% picric acid, 0.5% PFA 4%, and 0.1M sodium phosphate. Samples were washed 3x in ice-cold PBS 1X for 5 minutes and subsequently washed 3 hours with 10% sucrose in PBS and overnight in 20% sucrose, 10% glycerol in PBS 1X. Samples were finally stored in 0.1% sodium azide in PBS 1X.

Immunohistochemistry was performed using TSA amplification Kit (Perkin Elmer) and DAB chromogen (Sigma), following manufacturer's protocol with minimal modifications. Briefly, 5- μ m paraffin-embedded sections were heated on a plate, deparaffinised in xylene and rehydrated in successive graded alcohol baths and dH₂O. Sections were subjected to heat-induced epitope retrieval (pH 9.0, Dako). Samples were washed in PBS 1X followed by a

solution of 100% Methanol (Reactolab) + 3% H₂O₂ (Panreac AppliChem) to block endogenous peroxidase activity. Sections were rinsed in dH₂O and in PBS 1X, blocked in TNB buffer (0.1M TrisHCl pH 7.5, 0.15M NaCl, 0.5% blocking reagent) and then incubated O/N with the primary antibody mixed in TNB. The list of primary antibodies and dilution factors are summarized in Table 5. After incubation, slides were washed in TNT washing buffer (0.1M TrisHCl pH 7.5, 0.15M NaCl, 0.05% Tween20) and incubated at RT with secondary biotinylated antibody mixed in TNB buffer. The list of secondary antibodies and dilution factors are summarized in Table 5. Slides were washed in TNT washing buffer and incubated at RT with Streptavidine-HRP (TSA™ Indirect Kit NEL700001KT, PerkinElmer®) mixed in TNB buffer. Slides were washed 3x 5min in TNT washing buffer and incubated 10 minutes at RT with Tyramide mixed in amplification diluent (TSA™ Indirect Kit NEL700001KT, PerkinElmer®; 1:100). Slides were washed in TNT, incubated with Streptavidine-HRP (TSA™ Indirect Kit NEL700001KT, PerkinElmer®) mixed in TNB and washed again in TNT and PBS 1X. Slides were incubated for in a solution of dH₂O + 0,5M TrisHCl pH 7.4 and again in that solution mixed with DAB pellet (10mg 3,3'-Diaminobenzidine tetra-hydrochloride, Sigma) and 30% H₂O₂. After convincing DAB revelation (according to control slide), slides were washed with the TrisHCl solution and then with dH₂O. Samples were counterstained for in Mayer's Hematoxylin (Bio System) and washed in flowing tap water. Finally, slides were mounted with Aquatex® (Merk®) mounting medium. Specificity of the antibodies immunopositivity was confirmed by staining tissue with and without primary antibodies.

For immunofluorescence staining, 5-µm paraffin-embedded sections were heated on a plate, deparaffinised in xylene and rehydrated in successive graded alcohol baths and dH₂O. Sections were subjected to heat-induced epitope retrieval (Dako® Cytomation pH 6.1 or 9.0). Samples were washed in PBS 1X, permeabilized with 0.3% Triton X-100 (Panreac AppliChem) and blocked with 5% donkey serum (AbD Serotec). Samples were then

incubated O/N with primary antibodies, washed with 0.3% Triton X-100 and incubated with Alexa Fluor 488, 555 and 647 fluorochrome-conjugated secondary antibodies (Invitrogen) for signal detection. Slides were washed and mounted with DAPI-containing Fluoromount-G (eBioscience) mounting medium on coverslip.

Immunostaining for hypoxia was performed either by Hif1a antibodies or by injecting mice with pimonidazole (HPI, Hypoxyprobe) 30 minutes prior sacrifice (12mg/ml, 5 μ l/g of weight). Tumor sections were then stained with mouse anti-HPI, according to manufacturer protocol. Immunostaining for proliferation was performed either by Ki67 antibodies or by perfusing mice one hour prior sacrifice with 5'-Ethylnyl-2'-deoxyuridine (2mg/ml, 5 μ l/gram of mouse, Santa Cruz). Tumors sections were then stained with a mix of H₂O, CuSO₄ 100mM, Azide (2mg/ml), Sodium Ascorbate 10mM and TBS pH 7.4 and incubated in the dark for 30 minutes.

Confocal images were obtained using Zeiss LSM 780, Zeiss LSM 510 META or Leica SP5 TANDEM microscopes and standard fluorescent images were obtained using a Zeiss Axio Imager Z1. Images were analysed using Imaris (Bitplane), FIJI version 1.0 (NIH) and Photoshop (Adobe) softwares.

D.8. Human tissue collection, staining procedures and image acquisition

Serial formalin-fixed paraffin embedded (FFPE) sections of human colon cancer with matched normal tissue samples (N = 48) were obtained from Vaud State University Hospital of Lausanne between 2013-2017 (CHUV, Lausanne, Switzerland). Immunohistochemistry was performed as previously described. Specificity of the antibodies immunopositivity was confirmed by staining for normal human jejunum tissue with and without primary antibodies. Standard bright field images were acquired using a Zeiss AxioScan Slidescanner Z1.

Histopathological classification and immunostaining analysis were performed by an expert pathologist (Prof. Christine Sempoux) and myself. Both investigators were blinded to the

clinicopathological datas at the time of scoring. Nuclear BCATENIN and PROX1 staining in cancer cells were scored for the whole tumour as similarly described²⁵¹. Briefly: 0 = negative, no staining in cancer cells; 1 = low, less than 20 glands throughout the tumour were strongly positive; 2 = moderate, 20-40 glands throughout the tumour were strongly positive; 3 = high, >40 glands throughout the tumour were strongly positive. Half-points were also attributed in case of doubts. Scoring was performed twice by each investigator. Of note, if only the invasive front was strongly positive, scoring never exceeded 2 as the invasive front represents a minor proportion of the tumor. Cancer samples were then divided into two groups according to BCATENIN and PROX1 expression: BCATENIN or PROX1 low groups comprised scores of 0-1. BCATENIN and PROX1 high groups comprised scores of 3-4. WNT scores were established by averaging BCATENIN and PROX1 scores for each sample. For the present study, a WNT^{neg} tumor was consider when both BCATENIN and PROX1 scores were 0. In WNT^{neg} tumors, intratumoral heterogeneity was assessed by differentiating the tumor bulk or luminal side of the tumor with the invasive front. When both BCATENIN and PROX1 scores were 3, tumor was considered WNT^{hi}. Within WNT^{hi} tumors, intratumoral heterogeneity was assessed by differentiating areas of strong BCATENIN/PROX1 signaling from BCATENIN/PROX1 low or negative areas (herafter WNT^{hi}-H and WNT^{hi}-L). Once WNT status for all samples was known, tumours were stained by IHC for CD31 (PECAM-1) and ESM-1 (Endocan). For quantifications, three representative images were obtained for each staining (serial sections) from both tumor compartments in each WNT^{neg} and WNT^{hi} tumors. CD31 and ESM-1 areas were quantified using the colour deconvolution H-DAB Plug-in in FIJI and were normalized to the stromal compartment. Percentage of ESM-1 coverage was calculated for each tumor quantified according to CD31 area. Evaluation of the microsatellite instability was analysed by IHC for MLH1 at IUP. In the case of positive IHC for MLH1 but high suspicion of MSI tumor, PCR using the mononucleotides loci BAT-25, BAT-26, NR-21, NR-24, NR-27 was performed²⁵².

D.9. Blood endothelial and intestinal epithelial cells isolation.

Mice were sacrificed and the intestine was dissected and flushed with ice-cold PBS. Intestine were cut into 1 cm pieces, which were put in a 10mM EDTA solution agitating at 37°C for 30min to remove epithelial cells. The remaining tissue was then digested with constant stirring at 37°C with Collagenase IV (3mg/mL, Worthington Biochemical) in cDMEM (Gibco) containing CaCl₂ (2mM) and 50ug/ml DNase I (Sigma-Aldrich) for 20 min and washed with medium. The cell suspension was incubated with labeled antibodies listed on Table 5. FACS sorting was performed on a BD FACSAria IIu (BD Biosciences). Blood endothelial cells were selected as being CD45neg, CD31pos, Lyve-1neg, Podoplanin neg. Cells were suspended in RLT buffer (RNeasy Plus Mini Kit, Qiagen) and kept at -80°C until further RNA extraction.

To isolate specifically *Lgr5*-expressing intestinal stem cells and differentiated epithelial cells, Cre-mediated recombination of *Lgr5-eGFP-Cre*^{ERT2} mice was obtained as previously described. After 3 injections, mice were sacrificed and the intestine was dissected as previously described. The cell suspension was incubated with labeled antibodies listed on Table 5. FACS sorting was performed on a BD FACSAria IIu (BD Biosciences). GFP⁺ (expressing *Lgr5*) and GFP⁻ (not expressing *Lgr5*) cells were obtained according to staining. GFP⁺ cells were CD45neg, EpCAMpos, CD31neg, GFPpos. GFP⁻ cells were CD45neg, EpCAMpos, CD31neg, GFPneg. Cells were suspended in RLT buffer (RNeasy Plus Mini Kit, Qiagen) and kept at -80°C until further RNA extraction (see next section).

D.10. RNA isolation and RT-qPCR

Cells or tumors were homogenized in Qiazol (Qiagen) and kept at -80°C. RNA extraction was performed with phenol/chloroform/isoamyl-alcohol (Biosolve) according to manufacturer protocol and RNA precipitation and elution with the RNeasy Plus Mini Kit (Qiagen). Alternatively, total cell RNA was isolated using the RNeasy Plus Micro Kit (Qiagen). Reverse transcription was performed from 500ng or 1µg of total RNA using Transcriptor First Strand cDNA Synthesis Kit (Roche Diagnostics), according to manufacturer protocol.

Real-time qPCR analyses were performed on StepOnePlus (Applied Biosystems) using SYBR Fast PCR Master Mix (KAPA) and SensiFast SYBR Hi-ROX Mix (Bioline). Analysis of gene expression was carried out using the comparative Ct ($\Delta\Delta Ct$) or the Standard Curve methods as described by the manufacturer (Fold change $2^{(-)\Delta\Delta Ct}$). Sequences of PCR primers are provided in Table 4. Gene expression was normalized to 18S ribosomal subunit (rRNA) or Cd31 (Pecam-1). All qPCR were repeated at least twice, using different samples for the standard curve calculation.

D.11. Primer design

Primers were designed using the Primer 3 software and all sequences were checked for self- or inter-molecular annealing with nucleic-acid-folding software (mfold and oligoAnalyzer 1.2). Alternatively, primers were selected on the Harvard PrimerBank website⁹. We performed local-alignment analyses with the BLAST program¹⁰ to confirm the specificity of the designed primers. Oligonucleotides were synthesized and purified on HPLC by Eurofins (Ebersberg, Germany) and quality control of the oligonucleotides was performed by MALDI TOF. The sequences of the selected primers are presented in the Table 4 .

D.12. Quantifications

All quantifications were performed in FIJI version 1.0 (NIH) using the original file format. Alternatively, human tumors acquired from the Zeiss AxioScan Slidescanner Z1 were

opened with a ZEN Blue 2.0 (Zeiss) and representative pictures were selected and exported as TIFFs. TIFFs were then quantified using FIJI. All quantifications were performed using 3-10 images per tissue or tumor, which were acquired with the same microscope settings and, if possible, on the same day. All the analysis were performed by calculating the ROIs using available algorithms in FIJI. The same algorithm was used for each specific channel of each specific quantification. ROIs were normalized to tumor area, stroma area or tissue area. For AKP organoid tumor xenografts quantification within a distance of 100µm, images were exported in FIJI, CD44^{high} areas were delineated and a 100µm-band was drawn. Only this band was used for quantifications. For cell number or vessel number, manual counting was performed on clear positive cell or vessel. Averages for each tissue/tumor were taken and grouped for graphic representation.

D.13. Statistical analyses

Two-tailed unpaired Student's t tests or one-way ANOVA were performed to determine statistical significance between ≥ 2 means, with Welch's correction to account for unequal variance. These tests were performed for scatter-plots and matched human tumour analysis. Tumour growth experiment between various tumour type and treatment assignment was analysed by a two-way ANOVA with repeated measures (mixed model) and Bonferroni post-tests to account for multiple testing. $P < 0.05$ were considered statistically significant. Inter-observer reliability was tested with the Coehn's Kappa test for 2 raters with equal weight. Data are shown as mean +/- Standard Deviation (S.D.). Each *in vitro* and *in vivo* experiment was repeated at least twice, independently.

All statistics were performed with GraphPad Prism 5.0 or R 3.3.1 for Mac OS X.

D.14. Study approval

Animal experiments were approved by the Animal Ethics Committee of Vaud, Switzerland.

D.15. Human tumors approval

Primary human tumor samples were collected with informed patient consent and with the approval of the Ethics Committee of the Canton de Vaud (project authorization n°2016/054).

Table 1: Clinico-pathological patient characteristics (part 1)

N°	Codage	N° Patient	Age	Sex	Primary Tumor Location	Microsatellite Status	T Stage	N Stage	M Stage	TNM Stage	Grade	Histologic WHO classification
1	R1600212	1A	75	F	Right	High	T3	N0	M0	IIA	2	mucinous adenocarcinoma
2	R1600212	1B	82	F	Right	High	T3	N0	M0	IIA	2	mucinous adenocarcinoma
3	R1600212	1C	88	F	Right	High	T3	N0	M0	IIA	3	mucinous adenocarcinoma
4	R1600212	1D	81	F	Right	High	T3	N1a	M0	IIIB	2	mucinous adenocarcinoma
5	R1600212	1E	79	F	Right	High	T4a	N2b	M1b	IVB	3	undifferentiated carcinoma
6	R1600212	1F	86	F	Right	High	T4b	N2b	M1b	IVB	3	undifferentiated carcinoma
7	R1600212	1G	68	F	Right	Stable	T3	N2b	M0	IIIC	3	adenocarcinoma
8	R1600212	1H	89	F	Left	Stable	T4a	N0	M0	IIB	2	mucinous adenocarcinoma
9	R1600212	1I	46	F	Left	Stable	T4a	N0	M1b	IVB	3	adenocarcinoma
10	R1600212	1J	62	F	Left	Stable	T4a	N0	M0	IIB	2	adenocarcinoma
11	R1600212	1K	79	F	Right	Stable	T4a	N1b	M0	IIIB	2	undifferentiated adenocarcinoma
12	R1600212	1L	53	F	Right	Stable	T4a	N1b	M1b	IVB	2	adenocarcinoma
13	R1600212	1M	41	F	Left	Stable	T4a	N2a	M1b	IVB	3	adenocarcinoma
14	R1600212	1N	68	F	Right	Stable	T4a	N2b	M0	IIIC	2	undifferentiated adenocarcinoma
15	R1600212	1O2	81	F	Left	Stable	T4b	N2b	M1b	IVB	3	mucinous adenocarcinoma
16	R1600212	2A	72	M	Right	High	T3	N0	M0	IIA	2	adenocarcinoma
17	R1600212	2B	55	M	Right	Stable	T2	N1b	M0	IIIA	2	adenocarcinoma
18	R1600212	2C1	43	M	Right	Stable	T3	N0	M0	IIA	2	adenocarcinoma
19	R1600212	2D	48	M	Right	Stable	T3	N0	M0	IIA	2	adenocarcinoma
20	R1600212	2E	65	M	Left	Stable	T3	N0	M0	IIA	2	mucinous adenocarcinoma
21	R1600212	2F	75	M	Left	Stable	T3	N0	M0	IIA	2	adenocarcinoma
22	R1600212	2G	79	M	Left	Stable	T3	N0	M0	IIA	3	mucinous adenocarcinoma
23	R1600212	2H	67	M	Right	Stable	T3	N1b	M0	IIIB	2	adenocarcinoma
24	R1600212	2I	73	M	Left	Stable	T3	N1a	M0	IIIB	2	adenocarcinoma

Table 2: Clinico-pathological patient characteristics (part 2)

N°	Codage	N° Patient	Age	Sex	Primary Tumor Location	Microsatellite Status	T Stage	N Stage	M Stage	TNM Stage	Grade	Histologic WHO classification
25	R1600212	2J	81	M	Left	Stable	T3	N1a	M0	IIIB	1	adenocarcinoma
26	R1600212	2K	80	M	Left	Stable	T3	N2a	M0	IIIB	2	adenocarcinoma
27	R1600212	2L	63	M	Left	Stable	T4a	N0	M0	IIB	2	adenocarcinoma
28	R1600212	2M	55	M	Left	High	T4a	N1a	M0	IIIB	1	mucinous adenocarcinoma on Lynch syndrome
29	R1600212	2N	66	M	Left	Stable	T4a	N1b	M0	IIIB	2	adenocarcinoma
30	R1600212	2O	73	M	Right	Stable	T4a	N2b	M1b	IVB	2	adenocarcinoma
31	R1600212	2P	77	M	Right	High	T4a	N2b	M0	IIIC	2	mucinous adenocarcinoma
32	R1700102	1A	62	M	Left	Stable	T4a	N2a	M1c	IVB	2	adenocarcinoma
33	R1700102	1B	60	F	Left	Stable	T2	N0	M0	I	2	adenocarcinoma
34	R1700102	1C	69	F	Right	Stable	T3	N0	M0	IIA	2	adenocarcinoma (<50% mucinous)
35	R1700102	1D	76	M	Left	Stable	T2/3	N0	M0	IIA	1	adenocarcinoma
36	R1700102	1E	50	M	Right	Stable	T3	N1b	M0	IIIB	2	adenocarcinoma
37	R1700102	1F	82	M	Left	Stable	T4a	N1a	M0	IIIB	1	adenocarcinoma
38	R1700102	1G	76	F	Right	High	T4b	N2a	M1c	IIIC	3	poorly differentiated carcinoma
39	R1700102	1H	88	M	Left	Stable	T4b	N1a	M0	IIIC	2	adenocarcinoma
40	R1700102	1I	56	M	Right	Stable	ypT3	N0	M0	IIA	2	adenocarcinoma
41	R1700102	1J	71	F	Left	Stable	T3	N0	M0	IIA	2	adenocarcinoma
42	R1700102	1K	76	M	Left	Stable	T4a	N0	M0	IIB	3	poorly differentiated carcinoma
43	R1700102	1L	80	M	Right	Stable	T3	N0	M0	IIA	2	adenocarcinoma (10% mucinous)
44	R1700102	1M	69	F	Right	Stable	T4a	N1a	M0	IIIB	2	adenocarcinoma
45	R1700102	1N	76	M	Right	Stable	T4a	N2b	M0	IIIC	3	poorly differentiated carcinoma (10% mucinous)
46	R1700102	1O	69	M	Left	Stable	T3	N1b	M0	IIIB	2	adenocarcinoma
47	R1700102	1P	64	M	Left	Stable	T3	N0	M0	IIA	2	adenocarcinoma
48	R1700102	1Q	61	M	Right	Stable	T3	N0	M0	IIB	2	adenocarcinoma

Table 3: Detailed human tumor characteristics

Characteristic	No.	(%)
MSS Tumors -- no. (%)		
Female	13	34.2
Men	25	65.8
Right	16	42.1
Left	22	57.9
WNT High	16	42.1
ESM1 High	21	55.3
MSI-H Tumors -- no. (%)		
Female	7	70.0
Men	3	30.0
Right	9	90.0
Left	1	10.0
WNT High	1	10.0
ESM1 High	6	60.0
Neoadjuvant Therapy -- no. (%)		
No	47	97.9
Yes	1	2.1
BCATENIN Status -- no. (%)		
Low	27	56.3
High	21	43.8
PROX1 Status -- no. (%)		
Low	30	62.5
High	18	37.5
WNT Status -- no. (%)		
Low	31	64.6
High	16	33.3
ESM1 Status -- no. (%)		
Low	27	56.3
High	21	43.8
WNT High -- no. (%)		
Right Tumors	4	25.0
MSI-H Tumors	1	6.3
ESM1 High	5	31.3
ESM1 High -- no. (%)		
Right Tumors	13	61.9
MSI-H Tumors	6	28.6
WNT High	5	23.8

Table 4: List of primers

	Name	Sequence
1	Sema3F Fwd	TGC TAC CCC TAT CCA GGA CC
2	Sema3F Rv	CTG TAG TCT GTA GTG TTG AGC AG
3	Apelin Fwd	TGC TGC TCT GGC TCT CCT TGA C
4	Apelin Rv	TTC TGG GCT TCA CCA GGT AGC G
5	CD31 Fwd	AAC AGA AAC CCG TGG AGA TG
6	CD31 Rv	GTC TCT GTG GCT CTC GTT CC
7	Krt20 Fwd	AGT TTT CAC CGA AGT CTG AGT
8	Krt20 Rv	GTA GCT CAT TAC GGC TTT GGA G
9	Lgr5 Fwd	GAC AAT GCT CTC ACA GAC
10	Lgr5 Rv	GGA GTG GAT TCT ATT ATT ATG G
11	18S Fwd	GCC TCA CTA AAC CAT CCA A
12	18S Rv	AGG AAT TCC CAG TAA GTG CG
13	MSGO	TGC ACC ATC TGT CAC TCT GTT AAC CTC
14	GPO-1	ACT CCT ACG GGA GGC AGC AGT A

Table 5: List of primary antibodies

	Antibody	Host	Reactivity	Company	Compagny number	Dilution	Staining
1	Cd31	rabbit	anti-mouse, human	Abcam	ab28364	300	paraffin
2	VE-cadherin	goat	anti-mouse	R&D	AF1002	300	paraffin
3	FoxO1	rabbit	anti-mouse	Cell Signaling	2880	250	paraffin
4	Esm1	goat	anti-human	Lunginnov	MEP08	500	paraffin
5	Esm1	mouse	anti-mouse	R&D	AF1999	300	paraffin
6	Hif1a	rabbit	anti-mouse	Chyman Chemical	10006421	300	paraffin
7	HPI	mouse	anti-mouse	Hypoxiprobe	HPI-100 Kit	200	paraffin
8	Glut1	mouse	anti-mouse	Thermo Scientific	MS-10637	300	paraffin
9	Prox1	goat	anti-mouse, human	R&D	AF2727	500	paraffin
10	Cd44	rat	anti-mouse	BD Pharmingen	550538	300	paraffin
11	Ki67	mouse	anti-mouse	BD Pharmingen	556003	500	paraffin
12	Erg	rabbit	anti-mouse	Abcam	Ab92513	300	paraffin
13	GFP	rabbit	-	Abcam	Ab290	200	paraffin
14	Vegfr-2	goat	anti-mouse	R&D	AF644	100	Wholemout
15	b-catenin	rabbit	anti-mouse, human	Merk-Millipore	06-734	200	paraffin
16	E-cadherin	rabbit	anti-mouse	Cell Signaling	3195S	400	Wholemout
17	Meca32	rat	anti-mouse	BD Pharmingen	550563	200	paraffin
18	Podocalyxin	rat	anti-mouse	R&D	MAB1556	200	paraffin
19	Claudin-5	rabbit	anti-mouse	Abcam	ab131259	300	paraffin
20	Aqua Live/Dead	-	anti-mouse	Thermo Scientific	C34967	1000	FACS
21	EpCAM-PB	rat	anti-mouse	BioLegend	118213	800	FACS
22	Cd31-PE	rat	anti-mouse	eBioscience	12-0311-82	1000	FACS
23	Gp38-A647		anti-mouse			1000	FACS
24	Cd45-PE/Cy7	rat	anti-mouse	eBioscience	25-0451-82	1000	FACS

E. Bibliography

1. Throckmorton, Z., Smilg, J. S., Zipfel, B. & Augustine, T. N. Earliest hominin cancer : 1 . 7-million-year- old osteosarcoma from Swartkrans Cave , South Africa. *S. Afr. J. Sci.* **112**, 7–11 (2016).
2. Bray, F., Jemal, A., Grey, N., Ferlay, J. & Forman, D. Global cancer transitions according to the Human Development Index (2008-2030): A population-based study. *Lancet Oncol.* **13**, 790–801 (2012).
3. Shetty, P. India faces growing breast cancer epidemic Breast cancer is set to overtake cervical cancer as the most common cancer in women in India in. *Lancet* **379**, 992–993 (2012).
4. Tackling the cancer epidemic Cancer. *Lancet Oncol.* **16**, 349 (2015).
5. Bernier-Latmani, J. *et al.* DLL4 promotes continuous adult intestinal lacteal regeneration and dietary fat transport. *J. Clin. Invest.* **125**, 0 (2015).
6. Lau, W. De, Peng, W. C., Gros, P. & Clevers, H. The R-spondin / Lgr5 / Rnf43 module : regulator of Wnt signal strength The R-spondin / Lgr5 / Rnf43 module : regulator of Wnt signal strength. *Genes Dev.* **28**, 305–316 (2014).
7. Yan, K., Chia, L. & Li, X. The intestinal stem cell markers Bmi1 and Lgr5 identify two functionally distinct populations. *PNAS* **109**, 466–471 (2012).
8. Tian, H. *et al.* A reserve stem cell population in small intestine renders Lgr5-positive cells dispensable. *Nature* **478**, 255–9 (2011).
9. Sato, T. *et al.* Paneth cells constitute the niche for Lgr5 stem cells in intestinal crypts. *Nature* **469**, 415–8 (2011).
10. Mowat, A. M. & Agace, W. W. Regional specialization within the intestinal immune system. *Nat. Rev. Immunol.* **14**, 667–685 (2014).
11. Velcich, A. Colorectal Cancer in Mice Genetically Deficient in the Mucin Muc2. *Science (80-.).* **295**, 1726–1729 (2002).
12. Van der Sluis, M. *et al.* Muc2-Deficient Mice Spontaneously Develop Colitis, Indicating That MUC2 Is Critical for Colonic Protection. *Gastroenterology* **131**, 117–129 (2006).
13. Boyle, P. & Langman, J. S. Epidemiology. *Br. J. Med.* **321**, 805–808 (2000).
14. Hagggar, F. A., Boushey, R. P. & Ph, D. Colorectal Cancer Epidemiology : Incidence , Mortality , Survival , and Risk Factors. *Clin. Colon Rectal Surg.* **22**, 191–197 (2009).
15. Siegel, R. L. *et al.* Colorectal Cancer Incidence Patterns in the United. *J Natl Cancer Inst* **109**, 27–32 (2017).
16. Kim, D. Colorectal Cancer Epidemic in Korea. *Ann. Coloproctol.* **29**, 1–4 (2013).
17. Park, S. *et al.* Association between screening and the thyroid cancer ‘ epidemic ’ in South Korea : evidence from a nationwide study. *Br. Med. J.* **355**, 1–8 (2009).
18. Junod, B., Zahl, P., Kaplan, R. M. & Olsen, J. An investigation of the apparent breast cancer epidemic in France : screening and incidence trends in birth cohorts. *BMC Cancer* **11**, 401 (2011).
19. Schröder, F. H. & Roobol, M. J. Prostate cancer epidemic in sight? *Eur. Urol.* **61**, 1093–1095 (2012).
20. López-Abente, G., García-Pérez, J., Fernández-Navarro, P., Boldo, E. & Ramis, R. Colorectal cancer mortality and industrial pollution in Spain. *BMC Public Health* **12**, 589 (2012).
21. Allemani, C. *et al.* Global surveillance of cancer survival 1995–2009: analysis of individual data for 25 676 887 patients from 279 population- based registries in 67 countries (CONCORD-2). *Lancet* **385**, 977–1010 (2016).
22. Ait Ouakrim, D. *et al.* Trends in colorectal cancer mortality in Europe: retrospective

- analysis of the WHO mortality database. *Br. Med. J.* **351**, h4970 (2015).
23. Labianca, R. *et al.* Early colon cancer: ESMO clinical practice guidelines for diagnosis, treatment and follow-up. *Ann. Oncol.* **24**, (2013).
 24. Brenner, H., Kloor, M. & Pox, C. P. Colorectal cancer. *Lancet* **383**, 1490–1502 (2014).
 25. Kinzler, K. W. & Vogelstein, B. Lessons from Hereditary Colorectal Cancer. *Cell* **87**, 159–170 (1996).
 26. Fodde, R. *et al.* Mutations in the APC tumour suppressor gene cause chromosomal instability. *Nat. Cell Biol.* **3**, 433–438 (2001).
 27. Fodde, R. *et al.* APC, signal transduction and genetic instability in colorectal cancer. *Nat. Rev. Cancer* **1**, 55–67 (2001).
 28. Nusse, R. & Clevers, H. Wnt/ β -Catenin Signaling, Disease, and Emerging Therapeutic Modalities. *Cell* **169**, 985–999 (2017).
 29. Markowitz, S. D. & Bertagnolli, M. Molecular basis of colorectal cancer. *N Engl J Med* **362**, 2449–2460 (2010).
 30. HT Lynch, PM Lynch, SJ Lanspa, CL Snyder, JF Lynch, and C. B. Review of the Lynch syndrome: history, molecular genetics, screening, differential diagnosis, and medicolegal ramifications. *Clin. Genet* **76**, 1–18 (2009).
 31. Rohlin, A. *et al.* A mutation in POLE predisposing to a multi-tumour phenotype. *Int. J. Oncol.* **45**, 77–81 (2014).
 32. Alexandrov, L. B. *et al.* Signatures of mutational processes in human cancer. *Nature* **500**, 415–421 (2013).
 33. Network, T. C. G. A. *et al.* Comprehensive molecular characterization of human colon and rectal cancer. *Nature* **487**, 330–337 (2012).
 34. Hsieh Peggy and Yamana Kazuhiko. DNA mismatch repair: Molecular mechanism, cancer and ageing. *Mech ageing Dev* **129**, 391–407 (2009).
 35. Goldstein, J. *et al.* Multicenter retrospective analysis of metastatic colorectal cancer (CRC) with high-level microsatellite instability (MSI-H). *Ann. Oncol.* **25**, 1032–1038 (2014).
 36. Van Cutsem, E. *et al.* ESMO consensus guidelines for the management of patients with metastatic colorectal cancer. *Ann. Oncol.* **27**, 1386–1422 (2016).
 37. Saridaki, Z., Souglakos, J. & Georgoulas, V. Prognostic and predictive significance of MSI in stages II/III colon cancer. *World J. Gastroenterol.* **20**, 6809–6814 (2014).
 38. Webber, E. M., Kauffman, T. L., O'Connor, E. & Goddard, K. A. Systematic review of the predictive effect of MSI status in colorectal cancer patients undergoing 5FU-based chemotherapy. *BMC Cancer* **15**, 156 (2015).
 39. Sargent, D. J. *et al.* Defective mismatch repair as a predictive marker for lack of efficacy of fluorouracil-based adjuvant therapy in colon cancer. *J. Clin. Oncol.* **28**, 3219–3226 (2010).
 40. Allis, C. D. & Jenuwein, T. The molecular hallmarks of epigenetic control. *Nat. Rev. Genet.* **17**, 487–500 (2016).
 41. Juo, Y. Y. *et al.* Prognostic value of CpG island methylator phenotype among colorectal cancer patients: A systematic review and meta-analysis. *Ann. Oncol.* **25**, 2314–2327 (2014).
 42. Tran, B. *et al.* Impact of BRAF Mutation and Microsatellite Instability on the Pattern of Metastatic Spread and Prognosis in Metastatic Colorectal Cancer. *Cancer* **117**, 4623–4632 (2011).
 43. Kopetz, S. *et al.* Phase II pilot study of vemurafenib in patients with metastatic BRAF-mutated colorectal cancer. *J. Clin. Oncol.* **33**, 4032–4038 (2015).
 44. Lee, Y. C., Lee, Y. L., Chuang, J. P. & Lee, J. C. Differences in survival between colon and rectal cancer from SEER data. *PLoS One* **8**, (2013).
 45. Tamas, K. *et al.* Rectal and colon cancer: Not just a different anatomic site. *Cancer Treat. Rev.* **41**, 671–679 (2015).

46. Loupakis, F. *et al.* Primary tumor location as a prognostic factor in metastatic colorectal cancer. *J. Natl. Cancer Inst.* **107**, (2015).
47. Missiaglia, E. *et al.* Distal and proximal colon cancers differ in terms of molecular, pathological, and clinical features. *Ann. Oncol.* **25**, 1995–2001 (2014).
48. Tejpar, S. *et al.* Prognostic and Predictive Relevance of Primary Tumor Location in Patients With RAS Wild-Type Metastatic Colorectal Cancer. *JAMA Oncol.* **3**, 194 (2017).
49. Demurtas, L. *et al.* The role of primary tumour sidedness, EGFR gene copy number and EGFR promoter methylation in RAS/BRAF wild-type colorectal cancer patients receiving irinotecan/cetuximab. *Br. J. Cancer* **117**, 315–321 (2017).
50. Roepman, P. *et al.* Colorectal cancer intrinsic subtypes predict chemotherapy benefit, deficient mismatch repair and epithelial-to-mesenchymal transition. *Int. J. Cancer* **134**, 552–562 (2013).
51. Salazar, R. *et al.* Gene expression signature to improve prognosis prediction of stage II and III colorectal cancer. *J. Clin. Oncol.* **29**, 17–24 (2011).
52. Sadanandam, a *et al.* A colorectal cancer classification system that associates cellular phenotype and responses to therapy. *Nat. Med.* **19**, 619–625 (2013).
53. Budinska, E. *et al.* Gene expression patterns unveil a new level of molecular heterogeneity in colorectal cancer. *J. Pathol.* **231**, 63–76 (2013).
54. Marisa, L. *et al.* Gene Expression Classification of Colon Cancer into Molecular Subtypes: Characterization, Validation, and Prognostic Value. *PLoS Med.* **10**, (2013).
55. Schlicker, A. *et al.* Subtypes of primary colorectal tumors correlate with response to targeted treatment in colorectal cell lines. *BMC Med. Genomics* **5**, 66 (2012).
56. Sadanandam, A. *et al.* Reconciliation of classification systems defining molecular subtypes of colorectal cancer. *Cell Cycle* **13**, 353–357 (2014).
57. Del Rio, M. *et al.* Gene expression signature in advanced colorectal cancer patients select drugs and response for the use of leucovorin, fluorouracil, and irinotecan. *J. Clin. Oncol.* **25**, 773–780 (2007).
58. Guinney, J. *et al.* The consensus molecular subtypes of colorectal cancer. *Nat. Med.* **21**, 1350–1356 (2015).
59. Batlle, E. & Clevers, H. Cancer stem cells revisited. *Nat. Med.* **23**, 1124–1134 (2017).
60. Kreso, A. & Dick, J. E. Evolution of the cancer stem cell model. *Cell Stem Cell* **14**, 275–291 (2014).
61. Bonnet, D. & Dick, J. E. Human acute myeloid leukemia is organized as a hierarchy that originates from a primitive hematopoietic cell. *Nat. Med.* **3**, 730–737 (1997).
62. Vermeulen, L. & Snippert, H. J. Stem cell dynamics in homeostasis and cancer of the intestine. *Nat. Rev. Cancer* **14**, 468–80 (2014).
63. Barker, N. *et al.* Crypt stem cells as the cells-of-origin of intestinal cancer. *Nature* **457**, 608–611 (2009).
64. Schepers, A. G. *et al.* Lineage Tracing Reveals Lgr5+ Stem Cell Activity in Mouse Intestinal Adenomas. *Science (80-.)*. **337**, 730–735 (2012).
65. Shimokawa, M. *et al.* Visualization and targeting of LGR5+ human colon cancer stem cells. *Nature* **545**, 187–192 (2017).
66. Melo, F. de S. e *et al.* A distinct role for Lgr5+ stem cells in primary and metastatic colon cancer. *Nature* **543**, 676–680 (2017).
67. Vermeulen, L. *et al.* Wnt activity defines colon cancer stem cells and is regulated by the microenvironment. *Nat. Cell Biol.* **12**, 468–476 (2010).
68. Sottoriva, A., Vermeulen, L. & Tavaré, S. Modeling Evolutionary Dynamics of Epigenetic Mutations in Hierarchically Organized Tumors. *PLoS Comput. Biol.* **7**, (2011).
69. Lu, J. *et al.* Endothelial Cells Promote the Colorectal Cancer Stem Cell Phenotype through a Soluble Form of Jagged-1. *Cancer Cell* **23**, 171–185 (2013).

70. Todaro, M. *et al.* CD44v6 is a marker of constitutive and reprogrammed cancer stem cells driving colon cancer metastasis. *Cell Stem Cell* **14**, 342–356 (2014).
71. Li, H.-J., Reinhardt, F., Herschman, H. R. & Weinberg, R. A. Cancer-stimulated mesenchymal stem cells create a carcinoma stem-cell niche via Prostaglandin E2 signaling. *Cancer Discov.* **2**, (2012).
72. Kryczek, I. *et al.* IL-22+ CD4+ T cells promote colorectal cancer stemness via STAT3 transcription factor activation and induction of the methyltransferase DOT1L. *Immunity* **40**, (2014).
73. Lotti, F. *et al.* Chemotherapy activates cancer-associated fibroblasts to maintain colorectal cancer-initiating cells by IL-17A. *J. Exp. Med.* **210**, 2851–2872 (2013).
74. Zeuner, A., Todaro, M., Stassi, G. & De Maria, R. Colorectal cancer stem cells: From the crypt to the clinic. *Cell Stem Cell* **15**, 692–705 (2014).
75. Shaikat, A. *et al.* Long-Term Mortality after Screening for Colorectal Cancer. *N. Engl. J. Med.* **369**, 1106–1114 (2013).
76. Lansdorp-Vogelaar, I., Van Ballegooijen, M., Zauber, A. G., Habbema, J. D. F. & Kuipers, E. J. Effect of rising chemotherapy costs on the cost savings of colorectal cancer screening. *J. Natl. Cancer Inst.* **101**, 1412–1422 (2009).
77. Winawer, S. J. Colorectal Cancer Screening Comes Of Age. *N Engl J Med* **328**, 1416–1417 (1993).
78. Auer, R. *et al.* Programme cantonal vaudois de dépistage du cancer colorectal information et décision partagée. *Rev. Med. Suisse* **11**, 2209–2215 (2015).
79. Allegra, C. J. *et al.* Phase III trial assessing bevacizumab in stages II and III carcinoma of the colon: Results of NSABP protocol C-08. *J. Clin. Oncol.* **29**, 11–16 (2011).
80. De Gramont, A. & Van Cutsem, E. Investigating the potential of bevacizumab in other indications: Metastatic renal cell, non-small cell lung, pancreatic and breast cancer. *Oncology* **69**, 46–56 (2005).
81. Alberts, S. R. *et al.* Effect of Oxaliplatin, Fluorouracil, and Leucovorin With or Without Cetuximab on Survival Among Patients With Resected Stage III Colon Cancer. *JAMA* **307**, 1383–1393 (2012).
82. Taieb, J. *et al.* Oxaliplatin, fluorouracil, and leucovorin with or without cetuximab in patients with resected stage III colon cancer (PETACC-8): An open-label, randomised phase 3 trial. *Lancet Oncol.* **15**, 862–873 (2014).
83. Glynne-Jones, R. *et al.* Rectal cancer: ESMO Clinical Practice Guidelines for diagnosis, treatment and follow-up. *Ann. Oncol.* **28**, iv22–iv40 (2017).
84. Schmoll, H. J. *et al.* Esmo consensus guidelines for management of patients with colon and rectal cancer. A personalized approach to clinical decision making. *Ann. Oncol.* **23**, 2479–2516 (2012).
85. Peeters, C. F. J. M. *et al.* Vascular density in colorectal liver metastases increases after removal of the primary tumor in human cancer patients. *Int. J. Cancer* **112**, 554–559 (2004).
86. Ghiringhelli, F. *et al.* Bevacizumab Efficacy in Metastatic Colorectal Cancer is Dependent on Primary Tumor Resection. *Ann. Surg. Oncol.* **21**, 1632–1640 (2014).
87. Bardelli, A. & Siena, S. Molecular mechanisms of resistance to cetuximab and panitumumab in colorectal cancer. *J. Clin. Oncol.* **28**, 1254–1261 (2010).
88. Pozzi, C. *et al.* The EGFR-specific antibody cetuximab combined with chemotherapy triggers immunogenic cell death. *Nat. Med.* **22**, 624–631 (2016).
89. Potente, M. & Mäkinen, T. Vascular heterogeneity and specialization in development and disease. *Nat. Rev. Mol. Cell Biol.* **18**, 477–494 (2017).
90. Stappenbeck, T. S., Hooper, L. V. & Gordon, J. I. Nonlinear partial differential equations and applications: Developmental regulation of intestinal angiogenesis by indigenous microbes via Paneth cells. *Proc. Natl. Acad. Sci.* **99**, 15451–15455

- (2002).
91. Blanco, R. & Gerhardt, H. VEGF and Notch in tip and stalk cell selection. *Cold Spring Harb. Perspect. Med.* **3**, 1–19 (2013).
 92. Ricard, N. & Simons, M. When It Is Better to Regress: Dynamics of Vascular Pruning. *PLoS Biol.* **13**, 1–6 (2015).
 93. Korn, C. & Augustin, H. G. Mechanisms of Vessel Pruning and Regression. *Dev. Cell* **34**, 5–17 (2015).
 94. Sang, Q. X. A. Complex role of matrix metalloproteinases in angiogenesis. *Cell Res.* **8**, 171–177 (1998).
 95. Patterson, B. C. & Sang, Q. A. Angiostatin-converting Enzyme Activities of Human Matrilysin (MMP-7) and Gelatinase B / Type. *Biochemistry* **272**, 28823–28825 (1997).
 96. Rundhaug, J. E. Matrix metalloproteinases and angiogenesis. *J. Cell. Mol. Med.* **9**, 267–285 (2005).
 97. DR Senger, S., Galli, AM Dvorak, CA Perruzzi, V. H. & HDvorak, F. Tumor cells secrete a vascular permeability factor that promotes accumulation of ascites fluid. *Science (80-)*. **219**, 983–986 (1981).
 98. Ferrara, N. & Henzel, W. Pituitary follicular cells secrete a novel heparin-binding growth factor specific for vascular endothelial cells. *Biochem. Biophys. Res. Commun.* **161**, 851–858 (1989).
 99. Kivelä, R. *et al.* VEGF-B-induced vascular growth leads to metabolic reprogramming and ischemia resistance in the heart. *EMBO Mol. Med.* **6**, 307–321 (2014).
 100. Olofsson, B., Jeltsch, M., Eriksson, U. & Alitalo, K. Current biology of VEGF-B and VEGF-C. *Curr. Opin. Biotechnol.* **10**, 528–535 (1999).
 101. Aspelund, A., Robciuc, M. R., Karaman, S., Makinen, T. & Alitalo, K. Lymphatic System in Cardiovascular Medicine. *Circ. Res.* **118**, 515–530 (2016).
 102. Carmeliet, P. *et al.* Abnormal blood vessel development and lethality in embryos lacking a single VEGF allele. *Nature* **380**, 435–439 (1996).
 103. Shalaby, F. *et al.* Failure of blood-island formation and vasculogenesis in Flk-1-deficient mice. *Nature* **376**, 62–66 (1995).
 104. Neufeld, G., Tessler, S., Gitay-Goren, H., Cohen, T. & Levi, B. Z. Vascular endothelial growth factor and its receptors. *FASEB J.* **13**, 9–22 (1999).
 105. Simons, M., Gordon, E. & Claesson-Welsh, L. Mechanisms and regulation of endothelial VEGF receptor signalling. *Nat. Rev. Mol. Cell Biol.* **17**, 611–625 (2016).
 106. Yuan, L. *et al.* Abnormal lymphatic vessel development in neuropilin 2 mutant mice. *Development* **129**, 4797–4806 (2002).
 107. Cheng, N. *et al.* Blockade of EphA Receptor Tyrosine Kinase Activation Inhibits Vascular Endothelial Cell Growth Factor-Induced Angiogenesis. *Mol.Cancer Res.* **1**, 2–11 (2002).
 108. Pitulescu, M. E., Adams, R. H., Pitulescu, M. E. & Adams, R. H. Regulation of signaling interactions and receptor endocytosis in growing blood vessels Regulation of signaling interactions and receptor endocytosis in growing blood vessels. *Cell Adh. Migr.* **8**, 366–377 (2014).
 109. Limbourg, A. *et al.* Notch ligand delta-like 1 is essential for postnatal arteriogenesis. *Circ. Res.* **100**, 363–371 (2007).
 110. Wang, G., Jacquet, L., Karamariti, E. & Xu, Q. Origin and differentiation of vascular smooth muscle cells. *J. Physiol.* **593**, 3013–3030 (2015).
 111. Mellgren, A. M. *et al.* Platelet-Derived Growth Factor Receptor β Signaling Is Required for Efficient Epicardial Cell Migration and Development of Two Distinct Coronary Vascular Smooth Muscle Cell Populations. *Circ Res* **103**, 1393–1401 (2008).
 112. Lindahl, P., Johansson, B. R., Levéen, P. & Betsholtz, C. Pericyte Loss and

- Microaneurysm Formation in PDGF-B-Deficient Mice. *Science (80-.)*. **277**, 242–245 (1997).
113. Bergers, G. & Song, S. The role of pericytes in blood-vessel formation and maintenance. *Neuro. Oncol.* **7**, 452–464 (2005).
 114. Foo, S. S. *et al.* Ephrin-B2 controls cell motility and adhesion during blood-vessel-wall assembly. *Cell* **124**, 161–173 (2006).
 115. Suri, C. *et al.* Requisite role of angiopoietin-1, a ligand for the TIE2 receptor, during embryonic angiogenesis. *Cell* **87**, 1171–1180 (1996).
 116. Maisonpierre, P. C. *et al.* Angiopoietin-2, a natural antagonist for Tie2 that disrupts in vivo angiogenesis. *Science (80-.)*. **277**, 55–60 (1997).
 117. Lobov, I. B., Brooks, P. C. & Lang, R. A. Angiopoietin-2 displays VEGF-dependent modulation of capillary structure and endothelial cell survival in vivo. *Proc. Natl. Acad. Sci.* **99**, 11205–11210 (2002).
 118. Fiedler, U. *et al.* The Tie-2 ligand Angiopoietin-2 is stored in and rapidly released upon stimulation from endothelial cell Weibel-Palade bodies. *Blood* **103**, 4150–4156 (2004).
 119. Pietilä, R. *et al.* Ligand oligomerization state controls Tie2 receptor trafficking and angiopoietin-2-specific responses. *J. Cell Sci.* **125**, 2212–2223 (2012).
 120. Han, S. *et al.* Amelioration of sepsis by TIE2 activation-induced vascular protection. *Sci. Transl. Med.* **8**, 335ra55-335ra55 (2016).
 121. Gavard, J., Patel, V. & Gutkind, J. S. Angiopoietin-1 Prevents VEGF-Induced Endothelial Permeability by Sequestering Src through mDia. *Dev. Cell* **14**, 25–36 (2008).
 122. Taddei, A. *et al.* Endothelial adherens junctions control tight junctions by VE-cadherin-mediated upregulation of claudin-5. *Nat. Cell Biol.* **10**, 923–934 (2008).
 123. Shen, J. *et al.* Targeting VE-PTP activates TIE2 and stabilizes the ocular vasculature. *J. Clin. Invest.* **124**, 4564–4576 (2014).
 124. Fong, G.-H. & Takeda, K. Role and regulation of prolyl hydroxylase domain proteins. *Cell Death Differ.* **15**, 635–641 (2008).
 125. Jin, Z.-G. Ligand-Independent Activation of Vascular Endothelial Growth Factor Receptor 2 by Fluid Shear Stress Regulates Activation of Endothelial Nitric Oxide Synthase. *Circ. Res.* **93**, 354–363 (2003).
 126. Ruan, G. X. & Kazlauskas, A. Lactate engages receptor tyrosine kinases Axl, Tie2, and vascular endothelial growth factor receptor 2 to activate phosphoinositide 3-kinase/AKT and promote angiogenesis. *J. Biol. Chem.* **288**, 21161–21172 (2013).
 127. Jia, Y. X. *et al.* Apelin activates l-arginine/nitric oxide synthase/nitric oxide pathway in rat aortas. *Peptides* **28**, 2023–2029 (2007).
 128. Bertrand, C., Valet, P. & Castan-Laurell, I. Apelin and energy metabolism. *Front. Physiol.* **6**, 1–5 (2015).
 129. Kasai, A. *et al.* Apelin is a crucial factor for hypoxia-induced retinal angiogenesis. *Arterioscler. Thromb. Vasc. Biol.* **30**, 2182–2187 (2010).
 130. Kidoya, H., Naito, H. & Takakura, N. Apelin induces enlarged and nonleaky blood vessels for functional recovery from ischemia. *Blood* **115**, 3166–3174 (2010).
 131. Kidoya, H. *et al.* Spatial and temporal role of the apelin/APJ system in the caliber size regulation of blood vessels during angiogenesis. *EMBO J.* **27**, 522–534 (2008).
 132. Kidoya, H. *et al.* APJ Regulates Parallel Alignment of Arteries and Veins in the Skin. *Dev. Cell* **33**, 247–259 (2015).
 133. Liu, Q. *et al.* Genetic targeting of sprouting angiogenesis using Apln-CreER. *Nat. Commun.* **6**, 6020 (2015).
 134. Kruger, R. P., Aurandt, J. & Guan, K.-L. Semaphorins command cells to move. *Nat. Rev. Mol. Cell Biol.* **6**, 789–800 (2005).
 135. Miao, H. *et al.* Vascular Endothelial Growth Factor-165. *J. Cell Biol.* **146**, 233–241

- (1999).
136. Kessler, O. *et al.* Semaphorin-3F Is an Inhibitor of Tumor Angiogenesis. *Cancer Res.* **64**, 1008–1015 (2004).
 137. Guttman-Raviv, N. *et al.* Semaphorin-3A and semaphorin-3F work together to repel endothelial cells and to inhibit their survival by induction of apoptosis. *J. Biol. Chem.* **282**, 26294–26305 (2007).
 138. Kigel, B., Varshavsky, A., Kessler, O. & Neufeld, G. Successful inhibition of tumor development by specific class-3 semaphorins is associated with expression of appropriate semaphorin receptors by tumor cells. *PLoS One* **3**, (2008).
 139. Baluk, P., Morikawa, S., Haskell, A., Mancuso, M. & McDonald, D. M. Abnormalities of Basement Membrane on Blood Vessels and Endothelial Sprouts in Tumors. *Am. J. Pathol.* **163**, 1801–1815 (2003).
 140. Facciabene, A. *et al.* Tumour hypoxia promotes tolerance and angiogenesis via CCL28 and Treg cells. *Nature* **475**, 226–230 (2011).
 141. Hanahan, D. & Folkman, J. Patterns and emerging mechanisms of the angiogenic switch during tumorigenesis. *Cell* **86**, 353–364 (1996).
 142. Shibuya, M. Involvement of Flt-1 (VEGF receptor-1) in cancer and preeclampsia. *Proc. Jpn. Acad. Ser. B. Phys. Biol. Sci.* **87**, 167–78 (2011).
 143. Kim, K. J. *et al.* Inhibition of vascular endothelial growth factor-induced angiogenesis suppresses tumour growth in vivo. *Nature* **362**, 841–844 (1993).
 144. Ferrara, N., Hillan, K. J. & Novotny, W. Bevacizumab (Avastin), a humanized anti-VEGF monoclonal antibody for cancer therapy. *Biochem. Biophys. Res. Commun.* **333**, 328–335 (2005).
 145. De Palma, M., Biziato, D. & Petrova, T. V. Microenvironmental regulation of tumour angiogenesis. *Nat. Rev. Cancer* **17**, 457–474 (2017).
 146. MacDonald, K. P. A. *et al.* An antibody against the colony-stimulating factor 1 receptor depletes the resident subset of monocytes and tissue- and tumor-associated macrophages but does not inhibit inflammation. *Blood* **116**, 3955–3963 (2010).
 147. Bingle, L. *et al.* The role of tumor-associated macrophages in tumor progression : implications for new anticancer therapies [J] The role of tumour-associated macrophages in tumour progression : implications for new anticancer therapies. *J. Pathol.* **196**, 254–265 (2002).
 148. De Palma, M. & Lewis, C. E. Macrophage regulation of tumor responses to anticancer therapies. *Cancer Cell* **23**, 277–286 (2013).
 149. De Palma, M. *et al.* Tie2 identifies a hematopoietic lineage of proangiogenic monocytes required for tumor vessel formation and a mesenchymal population of pericyte progenitors. *Cancer Cell* **8**, 211–226 (2005).
 150. Coffelt, S. B. *et al.* Angiopoietin 2 Stimulates TIE2-Expressing Monocytes To Suppress T Cell Activation and To Promote Regulatory T Cell Expansion. *J. Immunol.* **186**, 4183–4190 (2011).
 151. Gabrilovich, D. I., Ostrand-Rosenberg, S. & Bronte, V. Coordinated regulation of myeloid cells by tumours. *Nat. Rev. Immunol.* **12**, 253–268 (2012).
 152. Shojaei, F. & Ferrara, N. Refractoriness to antivascular endothelial growth factor treatment: Role of myeloid cells. *Cancer Res.* **68**, 5501–5504 (2008).
 153. Shojaei, F., Singh, M., Thompson, J. D. & Ferrara, N. Role of Bv8 in neutrophil-dependent angiogenesis in a transgenic model of cancer progression. *Proc Natl Acad Sci USA* **105**, 2640–5 (2008).
 154. Xing, F., Saidou, J. & Watabe, K. Cancer associated fibroblasts (CAFs) in tumor microenvironment. *Front Biosci* **15**, 166–179 (2011).
 155. Crawford, Y. *et al.* PDGF-C Mediates the Angiogenic and Tumorigenic Properties of Fibroblasts Associated with Tumors Refractory to Anti-VEGF Treatment. *Cancer*

- Cell* **15**, 21–34 (2009).
156. Hurwitz, H., Fehrenbacher, L., Novotny, W. & F, K. Bevacizumab plus Irinotecan, Fluorouracil, and Leucovorin for Metastatic Colorectal Cancer. *N. Engl. J. Med.* 609–619 (2004). doi:10.1056/NEJMoa1109071
 157. Sandler, A. *et al.* Paclitaxel–Carboplatin Alone or with Bevacizumab for Non–Small-Cell Lung Cancer. *N. Engl. J. Med.* **355**, 2542–2550 (2006).
 158. Friedman, H. S. *et al.* Bevacizumab alone and in combination with irinotecan in recurrent glioblastoma. *J. Clin. Oncol.* **27**, 4733–4740 (2009).
 159. Yang, J. C. *et al.* A randomized trial of bevacizumab, an anti-vascular endothelial growth factor antibody, for metastatic renal cancer. *N Engl J Med* **349**, 427–434 (2003).
 160. Miller, K. *et al.* Paclitaxel plus Bevacizumab versus Paclitaxel Alone for Metastatic Breast Cancer. *N. Engl. J. Med.* **357**, 2666–2676 (2007).
 161. Van Cutsem, E. *et al.* Addition of aflibercept to fluorouracil, leucovorin, and irinotecan improves survival in a phase III randomized trial in patients with metastatic colorectal cancer previously treated with an oxaliplatin-based regimen. *J. Clin. Oncol.* **30**, 3499–3506 (2012).
 162. Grothey, A. *et al.* Regorafenib monotherapy for previously treated metastatic colorectal cancer (CORRECT): An international, multicentre, randomised, placebo-controlled, phase 3 trial. *Lancet* **381**, 303–312 (2013).
 163. Motzer, R. J. *et al.* Sunitinib versus Interferon Alfa in Metastatic Renal-Cell Carcinoma. *N. Engl. J. Med.* **356**, 115–124 (2007).
 164. Llovet, J. M. *et al.* Sorafenib in advanced hepatocellular carcinoma. *N. Engl. J. Med.* **359**, 378–390 (2008).
 165. Escudier, B. *et al.* Sorafenib in Advanced Clear-Cell Renal-Cell Carcinoma. *N. Engl. J. Med.* **356**, 125–134 (2007).
 166. Park, J. S. *et al.* Normalization of Tumor Vessels by Tie2 Activation and Ang2 Inhibition Enhances Drug Delivery and Produces a Favorable Tumor Microenvironment. *Cancer Cell* **31**, 157–158 (2017).
 167. Jain, R. K. Normalization of tumor vasculature: an emerging concept in antiangiogenic therapy. *Science (80-.).* **307**, 58–62 (2005).
 168. Winkler, F. *et al.* Kinetics of vascular normalization by VEGFR2 blockade governs brain tumor response to radiation: Role of oxygenation, angiopoietin-1, and matrix metalloproteinases. *Cancer Cell* **6**, 553–563 (2004).
 169. Goel, S. *et al.* Normalization of the Vasculature for Treatment of Cancer and Other Diseases. *Physiol. Rev.* **91**, 1071–1121 (2011).
 170. Bergers, G. & Hanahan, D. Modes of resistance to anti-angiogenic therapy. *Nat. Rev. Cancer* **8**, 592–603 (2008).
 171. Rigamonti, N. *et al.* Role of angiopoietin-2 in adaptive tumor resistance to VEGF signaling blockade. *Cell Rep.* **8**, 696–706 (2014).
 172. Cascone, T. *et al.* Upregulated stromal EGFR and vascular remodeling in mouse xenograft models of angiogenesis inhibitor – resistant human lung adenocarcinoma. *J. Clin. Invest.* **121**, 1313–1328 (2011).
 173. Olive, K. P. *et al.* Inhibition of Hedgehog Signaling a Mouse Model of Pancreatic Cancer. *Science (80-.).* **324**, 1457–1461 (2009).
 174. Yang, Z. F. & Poon, R. T. P. Vascular Changes in Hepatocellular Carcinoma. *Anat. Rec.* **291**, 721–734 (2008).
 175. Vermeulen, P. B. *et al.* Liver metastases from colorectal adenocarcinomas grow in three patterns with different angiogenesis and desmoplasia. *J. Pathol.* **195**, 336–342 (2001).
 176. Bridgeman, V. L. *et al.* Vessel co-option is common in human lung metastases and mediates resistance to anti-angiogenic therapy in preclinical lung metastasis

- models. *J. Pathol.* **241**, 362–374 (2017).
177. Frentzas, S. *et al.* Vessel co-option mediates resistance to anti-angiogenic therapy in liver metastases. *Nat. Med.* **22**, 1294–1302 (2016).
 178. Oberg, K. *et al.* Molecular pathogenesis of neuroendocrine tumors: Implications for current and future therapeutic approaches. *Clin. Cancer Res.* **19**, 2842–2849 (2013).
 179. Gerhardt, H. *et al.* VEGF guides angiogenic sprouting utilizing endothelial tip cell filopodia. *J. Cell Biol.* **161**, 1163–1177 (2003).
 180. Barker, N. *et al.* Identification of stem cells in small intestine and colon by marker gene *Lgr5*. *Nature* **449**, 1003–1007 (2007).
 181. Siekmann, A. F., Affolter, M. & Belting, H. G. The tip cell concept 10 years after: New players tune in for a common theme. *Exp. Cell Res.* **319**, 1255–1263 (2013).
 182. Potente, M. *et al.* Involvement of Foxo transcription factors in angiogenesis and postnatal neovascularization. *J. Clin. Invest.* **115**, 2382–2392 (2005).
 183. Laakkonen, J. P. *et al.* Differential regulation of angiogenic cellular processes and claudin-5 by histamine and VEGF via PI3K-signaling, transcription factor SNAI2 and interleukin-8. *Angiogenesis* **20**, 109–124 (2017).
 184. Koto, T. *et al.* Hypoxia disrupts the barrier function of neural blood vessels through changes in the expression of claudin-5 in endothelial cells. *Am. J. Pathol.* **170**, 1389–97 (2007).
 185. Wilhelm, K. *et al.* FOXO1 couples metabolic activity and growth state in the vascular endothelium. *Nature* **529**, 1–18 (2016).
 186. Rocha, S. F. *et al.* *Esm1* modulates endothelial tip cell behavior and vascular permeability by enhancing VEGF bioavailability. *Circ. Res.* **115**, 581–590 (2014).
 187. Forsythe, J. A. *et al.* Activation of vascular endothelial growth factor gene transcription by hypoxia-inducible factor 1. *Mol. Cell. Biol.* **16**, 4604–13 (1996).
 188. Kizaka-Kondoh, S. & Konse-Nagasawa, H. Significance of nitroimidazole compounds and hypoxia-inducible factor-1 for imaging tumor hypoxia. *Cancer Sci.* **100**, 1366–1373 (2009).
 189. Witte, L. *et al.* Monoclonal antibodies targeting the VEGF receptor-2 (Flk1/KDR) as an anti-angiogenic therapeutic strategy. *Cancer Metastasis Rev.* **17**, 155–161 (1998).
 190. Shibata, H., Toyama, K., Shioya, H. & Ito, M. Rapid Colorectal Adenoma Formation Initiated by Conditional Targeting of the *Apc* Gene. *Science (80-.)*. **278**, 120–124 (1997).
 191. Huels, D. J. & Sansom, O. J. Stem vs non-stem cell origin of colorectal cancer. *Br. J. Cancer* **113**, 1–5 (2015).
 192. Sansom, O. J. *et al.* Loss of *Apc* in vivo immediately perturbs Wnt signaling, differentiation, and migration. *Genes Dev.* **18**, 1385–1390 (2004).
 193. Sato, T. *et al.* Single *Lgr5* stem cells build crypt-villus structures in vitro without a mesenchymal niche. *Nature* **459**, 262–5 (2009).
 194. Zeilstra, J. *et al.* Stem cell CD44v isoforms promote intestinal cancer formation in *Apc(min)* mice downstream of Wnt signaling. *Oncogene* **33**, 665–670 (2014).
 195. Ragusa, S. *et al.* PROX1 promotes metabolic adaptation and fuels outgrowth of Wnhigh metastatic colon cancer cells. *Cell Rep.* **8**, 1957–1973 (2014).
 196. Fodde, R., Smits, R. & Clevers, H. APC, Signal transduction and genetic instability in colorectal cancer. *Nat. Rev. Cancer* **1**, 55–67 (2001).
 197. Prewett, M. *et al.* Antivascular Endothelial Growth Factor Receptor (Fetal Liver Kinase 1) Monoclonal Antibody Inhibits Tumor Angiogenesis and Growth of Several Mouse and Human Tumors. *Cancer Res.* **59**, 5209–5218 (1999).
 198. Reya, T., Morrison, S. J., Clarke, M. F. & Weissman, I. L. Stem cells, cancer, and cancer stem cells. *Nature* **414**, 105–111 (2001).
 199. Vermeulen, L., de Sousa e Melo, F., Richel, D. J. & Medema, J. P. The developing cancer stem-cell model: Clinical challenges and opportunities. *Lancet Oncol.* **13**,

- e83–e89 (2012).
200. De Smedt, L. *et al.* Microsatellite instable vs stable colon carcinomas: analysis of tumour heterogeneity, inflammation and angiogenesis. *Br. J. Cancer* **113**, 500–509 (2015).
 201. Horst, D. *et al.* The intratumoral distribution of nuclear b-catenin is a prognostic marker in colon cancer. *Cancer* **115**, 2063–2070 (2009).
 202. Kim, S., Chung, M. & Jeon, N. L. Three-dimensional biomimetic model to reconstitute sprouting lymphangiogenesis in vitro. *Biomaterials* **78**, 115–128 (2016).
 203. Nakayama, H. *et al.* Regulation of mTOR Signaling by Semaphorin 3F-Neuropilin 2 Interactions In Vitro and In Vivo. *Sci. Rep.* **5**, 11789 (2015).
 204. Buehler, A. *et al.* Semaphorin 3F forms an anti-angiogenic barrier in outer retina. *FEBS Lett.* **587**, 1650–1655 (2013).
 205. Xiang, R. H. *et al.* Semaphorin 3F Gene from Human 3p21 . 3 Suppresses Tumor Formation in Nude Mice. *Cancer Res.* **62**, 2637 (2002).
 206. Segditsas, S. *et al.* Putative direct and indirect Wnt targets identified through consistent gene expression changes in APC-mutant intestinal adenomas from humans and mice. *Hum. Mol. Genet.* **17**, 3864–3875 (2008).
 207. George, M. D. *et al.* In vivo gene expression profiling of human intestinal epithelial cells: analysis by laser microdissection of formalin fixed tissues. *BMC Genomics* **9**, 209 (2008).
 208. Serini, G., Bussolino, F., Maione, F. & Giraudo, E. Class 3 semaphorins: Physiological vascular normalizing agents for anti-cancer therapy. *J. Intern. Med.* **273**, 138–155 (2013).
 209. Kidoya, H. *et al.* The apelin/APJ system induces maturation of the tumor vasculature and improves the efficiency of immune therapy. *Oncogene* **31**, 3254–3264 (2012).
 210. Kasai, A. *et al.* Apelin is a novel angiogenic factor in retinal endothelial cells. *Biochem. Biophys. Res. Commun.* **325**, 395–400 (2004).
 211. Kusumbe, A. P., Ramasamy, S. K. & Adams, R. H. Coupling of angiogenesis and osteogenesis by a specific vessel subtype in bone. *Nature* **507**, 323–328 (2014).
 212. Parmar, K., Mauch, P., Vergilio, J.-A., Sackstein, R. & Down, J. D. Distribution of hematopoietic stem cells in the bone marrow according to regional hypoxia. *Proc. Natl. Acad. Sci.* **104**, 5431–5436 (2007).
 213. Ellis, S. L. *et al.* The relationship between bone , hemopoietic stem cells , and vasculature. *Blood* **118**, 1–3 (2016).
 214. Yoshida, S., Sueno, M. & Nabeshima, Y. -i. A Vasculature-Associated Niche for Undifferentiated Spermatogonia in the Mouse Testis. *Science (80-.).* **317**, 1722–1726 (2007).
 215. Shen, Q. *et al.* Adult SVZ Stem Cells Lie in a Vascular Niche: A Quantitative Analysis of Niche Cell-Cell Interactions. *Cell Stem Cell* **3**, 289–300 (2008).
 216. Rodríguez-Colman, M. J. *et al.* Interplay between metabolic identities in the intestinal crypt supports stem cell function. *Nature* **543**, 424–427 (2017).
 217. Kamba, T. *et al.* VEGF-dependent plasticity of fenestrated capillaries in the normal adult microvasculature. *Am. J. Physiol. Heart Circ. Physiol.* **290**, H560–H576 (2006).
 218. Yang, Y. *et al.* Anti-VEGF- and anti-VEGF receptor-induced vascular alteration in mouse healthy tissues. *Arch. Gen. Psychiatry* **110**, 12018–12023 (2013).
 219. Yamasaki, T. *et al.* Tumor microvasculature with endothelial fenestrations in VHL null clear cell renal cell carcinomas as a potent target of anti-angiogenic therapy. *Cancer Sci.* **103**, 2027–2037 (2012).
 220. Esser, S. *et al.* Vascular endothelial growth factor induces endothelial fenestrations in vitro. *J. Cell Biol.* **140**, 947–959 (1998).
 221. Koliarakis, V., Pallangyo, C. K., Gretchen, F. R. & Kollias, G. Mesenchymal Cells in Colon

- Cancer. *Gastroenterology* **152**, 964–979 (2017).
222. Coussens, L. M. *et al.* Inflammatory mast cells up-regulate angiogenesis during squamous epithelial carcinogenesis. *Genes Dev.* **13**, 1382–1397 (1999).
 223. Tazzyman, S., Lewis, C. E. & Murdoch, C. Neutrophils: Key mediators of tumour angiogenesis. *Int. J. Exp. Pathol.* **90**, 222–231 (2009).
 224. Sato, T. & Clevers, H. Growing Self-Organizing Mini-Guts from a Single Intestinal Stem Cell: Mechanism and Applications. *Science (80-.).* **340**, 1190–1194 (2013).
 225. Hansen, T. F. *et al.* The relationship between serum vascular endothelial growth factor A and microsatellite instability in colorectal cancer. *Color. Dis* **13**, 984–988 (2011).
 226. Sandmann, T. *et al.* Patients with proneural glioblastoma may derive overall survival benefit from the addition of bevacizumab to first-line radiotherapy and temozolomide: Retrospective analysis of the AVAglio trial. *J. Clin. Oncol.* **33**, 2735–2744 (2015).
 227. Yin, X. *et al.* A VEGF-dependent gene signature enriched in mesenchymal ovarian cancer predicts patient prognosis. *Sci. Rep.* **6**, 31079 (2016).
 228. Li, Y. *et al.* Evidence that transgenes encoding components of the Wnt signaling pathway preferentially induce mammary cancers from progenitor cells. *Proc. Natl. Acad. Sci. U. S. A.* **100**, 15853–8 (2003).
 229. Geyer, F. C. *et al.* β -Catenin pathway activation in breast cancer is associated with triple-negative phenotype but not with CTNNB1 mutation. *Mod. Pathol.* **24**, 209–231 (2011).
 230. Bell, R. *et al.* Final efficacy and updated safety results of the randomized phase III BEATRICE trial evaluating adjuvant bevacizumab-containing therapy in triplenegative early breast cancer. *Ann. Oncol.* **28**, 754–760 (2017).
 231. Van Den Eynden, G. G. *et al.* The histological growth pattern of colorectal cancer liver metastases has prognostic value. *Clin. Exp. Metastasis* **29**, 541–549 (2012).
 232. Smith, N. R. *et al.* Tumor stromal architecture can define the intrinsic tumor response to VEGF-targeted therapy. *Clin. Cancer Res.* **19**, 6943–6956 (2013).
 233. De Sousa E Melo, F. *et al.* Methylation of cancer-stem-cell-associated wnt target genes predicts poor prognosis in colorectal cancer patients. *Cell Stem Cell* **9**, 476–485 (2011).
 234. Zuurbier, L. *et al.* Apelin: A putative novel predictive biomarker for bevacizumab response in colorectal cancer. *Oncotarget* **8**, 42949–42961 (2017).
 235. Maden, C. H. *et al.* NRP1 and NRP2 cooperate to regulate gangliogenesis, axon guidance and target innervation in the sympathetic nervous system. *Dev. Biol.* **369**, 277–285 (2012).
 236. Sakurai, A., Doci, C. & Gutkind, J. S. Semaphorin signaling in angiogenesis, lymphangiogenesis and cancer. *Cell Res.* **22**, 23–32 (2012).
 237. Gaur, P. *et al.* Role of class 3 semaphorins and their receptors in tumor growth and angiogenesis. *Clin. Cancer Res.* **15**, 6763–6770 (2009).
 238. Guo, H. F. *et al.* Mechanistic basis for the potent anti-angiogenic activity of Semaphorin 3f. *Biochemistry* **52**, 7551–7558 (2013).
 239. Bielenberg, D. R. & Klagsbrun, M. Targeting endothelial and tumor cells with semaphorins. *Cancer Metastasis Rev.* **26**, 421–431 (2007).
 240. Coma, S., Shimizu, A. & Klagsbrun, M. Hypoxia induces tumor and endothelial cell migration in a semaphorin 3F- and VEGF-dependent manner via transcriptional repression of their common receptor neuropilin 2. *Cell Adh. Migr.* **5**, 266–275 (2011).
 241. Muñoz, J. *et al.* The Lgr5 intestinal stem cell signature: robust expression of proposed quiescent '+4' cell markers. *EMBO J.* **31**, 3079–3091 (2012).
 242. Daly, C. *et al.* Angiopoietin-1 modulates endothelial cell function and gene

- expression via the transcription factor FKHR (FOXO1). *Genes Dev.* **18**, 1060–71 (2004).
243. Kienast, Y. *et al.* Ang-2-VEGF-A crossmab, a novel bispecific human IgG1 antibody Blocking VEGF-A and Ang-2 functions simultaneously, mediates potent antitumor, antiangiogenic, and antimetastatic efficacy. *Clin. Cancer Res.* **19**, 6730–6740 (2013).
 244. Kloepper, J. *et al.* Ang-2/VEGF bispecific antibody reprograms macrophages and resident microglia to anti-tumor phenotype and prolongs glioblastoma survival. *Proc. Natl. Acad. Sci. U. S. A.* **113**, 4476–81 (2016).
 245. Sato, T. *et al.* Long-term expansion of epithelial organoids from human colon, adenoma, adenocarcinoma, and Barrett's epithelium. *Gastroenterology* **141**, 1762–1772 (2011).
 246. Squadrito, M. L. *et al.* Article miR-511-3p Modulates Genetic Programs of Tumor-Associated Macrophages. *Cell Rep.* **1**, 141–154 (2012).
 247. Marino, S. *et al.* Induction of medulloblastomas in p53 -null mutant mice by somatic inactivation of Rb in the external granular layer cells of the cerebellum. *Genes Dev.* **14**, 994–1004 (2000).
 248. Jackson, E. L. *et al.* Analysis of lung tumor initiation and progression using conditional expression of oncogenic K-ras. *Genes Dev.* **15**, 3243–3248 (2001).
 249. Marjou, F. El *et al.* Tissue-Specific and Inducible Cre-Mediated Recombination in the Gut Epithelium. *Genesis* **39**, 186–193 (2004).
 250. Moser, A. R., Pitot, H. C. & Dove, W. F. A Dominant Mutation That Predisposes to Multiple Intestinal Neoplasia in the Mouse. *Science (80-)*. **247**, 322–324 (2016).
 251. Skog, M. *et al.* Expression and prognostic value of transcription factor PROX1 in colorectal cancer. *Br. J. Cancer* **105**, 1346–1351 (2011).
 252. Bacher, J. W. *et al.* Development of a fluorescent multiplex assay for detection of MSI-High tumors. *Dis. Markers* **20**, 237–50 (2004).